Proceedings of the

ARGE Sensorik PhD-Summit 2011

June 29-30, 2011

Johannes Kepler University Linz,
Science Park, Room MT 226/1

Edited by Bernhard Jakoby (Johannes Kepler University Linz)

Chairmen of the Workshop:

Bernhard Jakoby (Johannes Kepler University Linz),
Michiel Vellekoop (Vienna University of Technology),
Franz Kohl (Austrian Academy of Sciences)

Proceedings Editor:

Bernhard Jakoby (Johannes Kepler University Linz)

Contact:

Bernhard Jakoby
Institute for Microelectronics and Microsensors
Johannes Kepler University Linz
Altenberger Strasse 69
A4040 Linz, Austria

Published electronically in September 2011

ISBN: 978-3-9502856-1-1 (Online-Publication)

Content

Note: Page numbers in arabic numerals refer to the page numbers given at the bottom of the respective pages (in red color if you view or print in color) - these were electronically imprinted on the documents provided by the authors (some contributions use independent page numbering)

Preface

The Austrian Working Group on Sensors (ARGE Sensorik) was founded in 2006 aiming at the optimization of the joint utilization of sensor know-how and associated technology distributed over Austria. One major goal of the ARGE Sensorik is the initiation of joint research networks also involving industrial partners. The ARGE now serves as platform representing various facets of interdisciplinary sensor research in Austria. Its members are research institutes and centers of competence working on sensors or dealing with problems where sensors play a major role. The activities of the ARGE have been stimulated and financially supported by the Austrian Research Association (Österreichische Forschungsgemeinschaft, ÖFG) from the very beginning.

One of the main activities of the ARGE is the organization of workshops featuring the presentation of current research topics by major Austrian players in sensor research and leading to scientific exchange among them. This is done in plenary workshops but also in topically focuses small groups. For more information on the ARGE and current activities, please visit www.arge-sensorik.at .

In 2009 the ARGE steering committee decided to have a plenary meeting where young researchers, in particularly those who are about to or have recently finished their PhD theses present their work. Due to the success of that event (held in Vienna) we decided to continue with another young researcher meeting in 2011, this time in Linz. The ARGE Sensorik Award was also presented at this occasion where the jury selection was based on the presentations at the workshop and one journal publication per participant submitted before the workshop. The award was presented to Roman Bruck and two special awards have been given to Norbert Reitinger and Thomas Voglhuber-Brunnmaier.

A selection of the contributions is presented in this electronic Proceedings volume.

At this occasion I would like to thank all individuals who helped to organize this event (in particular staff at the Institute of Microelectronics and Microsensors), our financial sponsors (Johannes Kepler University Linz, Austrian Center of Competence in Mechatronics ACCM, Österreichische Forschungsgemeinschaft ÖFG), and of course the contributors for presenting and discussing their work!

Linz, September 2011 Bernhard Jakoby

Workshop Program

Time	Name	Affiliation	Topic*
09:00	*B. Jakoby*	*JKU*	*Welcome and Introduction*
09:15	Roman Bruck	AIT	Integrated polymer-based Mach-Zehnder interferometer label-free streptavidin biosensor compatible with injection molding
09:35	Norbert Reitinger	UG	Radiationless energy transfer in CdSe/ZnS quantum dot aggregates embedded in PMMA
09:55	Thomas Voglhuber	JKU	Modeling of an LFE piezoelectric fluid sensor as layered structure in the spectral domain
10:15	Wolfgang Buchegger	TUW	A highly uniform lamination micromixer with wedge shaped inlet channels for time resolved infrared spectroscopy
10:35			*Coffee Break*
11:00	Dominik Samson	TUW	Wireless sensor node powered by aircraft specific thermoelectric energy harvesting
11:20	Lukas Richter	AIT	Monitoring Cellular Stress Responses to Nanoparticles using a Lab-on-a-Chip
11:40	Michael Moser	TUG	Strong and Weak Electric Fields Interfering: Capacitive Icing Detection and Capacitive Energy Harvesting on a 220 kV High-Voltage Overhead Power Line
12:00			*Lunch Break*
13:00	Michael Rosenauer (ARGE Sensorik Award Winner 2010)	Osram	Introduces his research associated with the ARGE Sensorik Award 2010 and his current work with OSRAM
13:20	Moritz Eggeling	AIT	Low spin current-driven dynamic excitations and metastability in spin-valve nanocontacts with unpinned artificial antiferromagnet
13:40	Thomas Lederer	JKU	Utilizing a high fundamental frequency quartz crystal resonator as a biosensor in a digital microfluidic platform
14:00	Sander van den Driesche	TUW	A label-free indicator for tumor cells based on the CH2-stretch ratio
14:20			*Coffee Break*
14:40	Johannes Sell	ACCM, JKU	Real-time monitoring of a high pressure reactor using a gas density sensor
15:00	Markus Neumayer	TUG	Accelerated Markov Chain Monte Carlo Sampling in Electrical Capacitance Tomography
15:20	Nicola Moscelli	TUW	An Imaging System for Real-Time Monitoring of Adherently Grown Cells
15:40	Alexander Niedermayer	ACCM, JKU	Yet another precision impedance analyzer (YAPIA)—Readout electronics for resonating sensors
16:00			*Short Break (Jury Meeting)*
16:15	B. Jakoby, M.J. Vellekoop, F. Kohl	JKU, TUW,ÖAW	Presentation of the ARGE Sensorik Awards 2010 (M. Rosenauer) and 2011 (to be announced at this moment)
16:30	*B Jakoby*	*JKU*	*Closing Discussion*

*indicated topics are titles of papers submitted for the ARGE Sensorik Award 2011, topics of talks may vary.

Selected Contributions

Notes:

In this electronic compilation, the page format has not been unified but has been kept as provided by the individual authors. Thus in the remainder of this document the page format (size) varies, which may have to be kept in mind when printing selected contributions.

In the following, page numbers are given at the bottom of the respective pages (in red color if you view or print in color) - these were electronically imprinted on the documents provided by the authors (some contributions use independent page numbering).

Polymer-based photonic label-free biosensor

R. Bruck[a], E. Melnik[a], P. Muellner[a], R. Hainberger[a],
M. Lämmerhofer[b]

[a] AIT Austrian Institute of Technology GmbH, Health & Environment Department, Nano Systems
[b] University of Vienna, Department of Analytical Chemistry

AIT Austrian Institute of Technology GmbH
Donau-City-Straße 1 | 1220 Vienna | Austria
T +43(0) 50550-4309 | F +43(0) 50550-4399
roman.bruck@ait.ac.at
www.ait.ac.at

30.6.2010– Roman Bruck

Polymer-based photonic label-free biosensor

Polymer-based photonic label-free biosensor

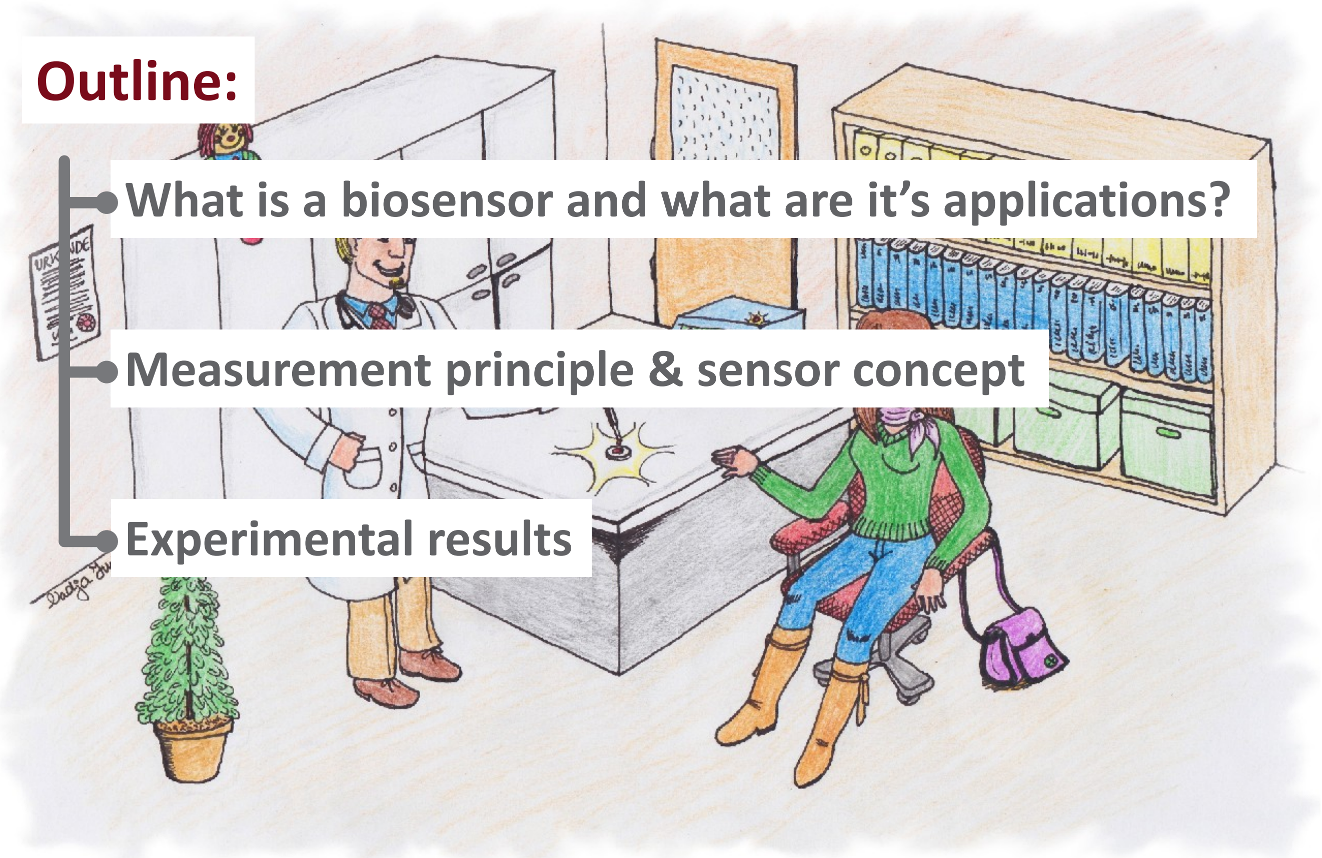

Outline:

- What is a biosensor and what are it's applications?
- Measurement principle & sensor concept
- Experimental results

Polymer-based photonic label-free **biosensor**

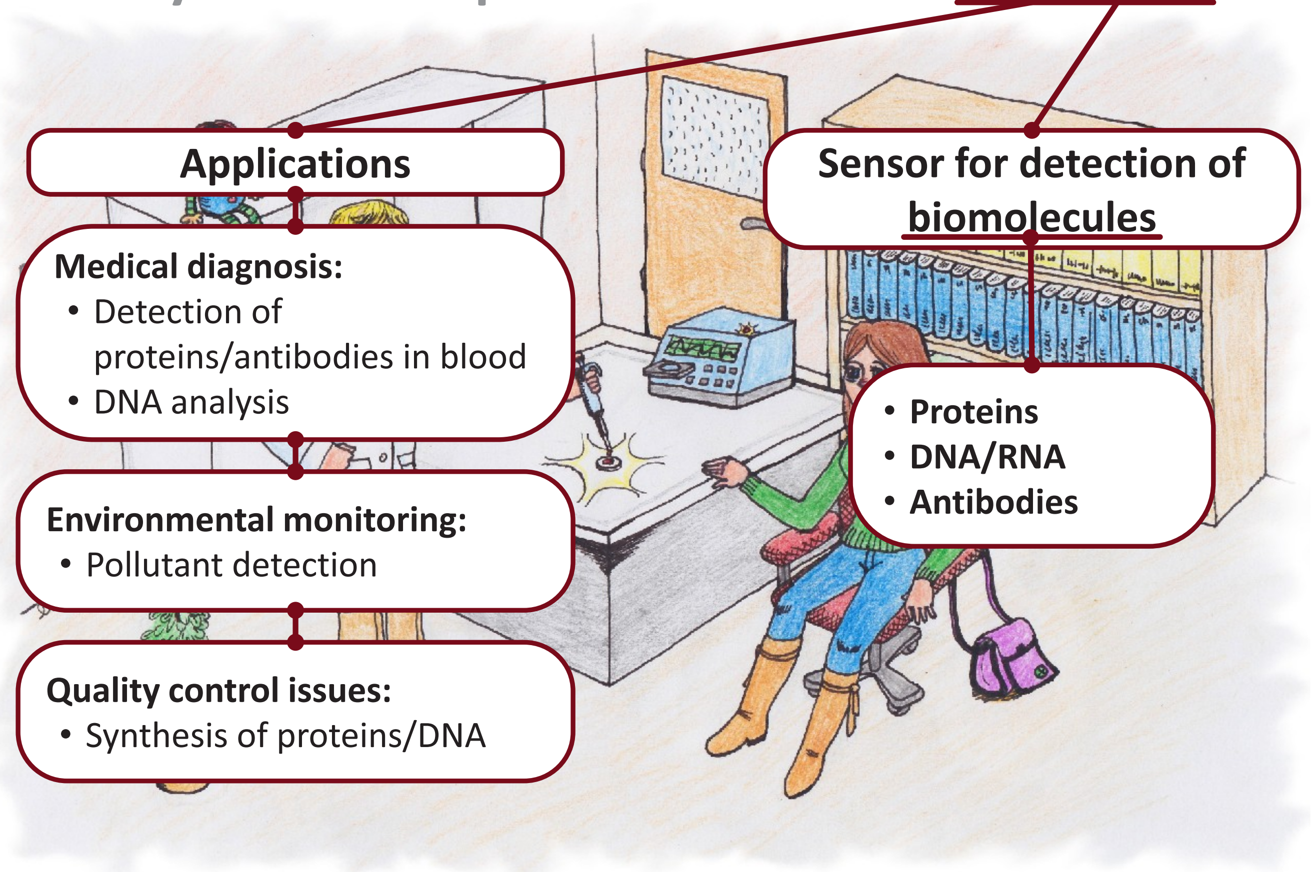

Polymer-based photonic label-free biosensor

Polymer-based photonic **label-free** biosensor

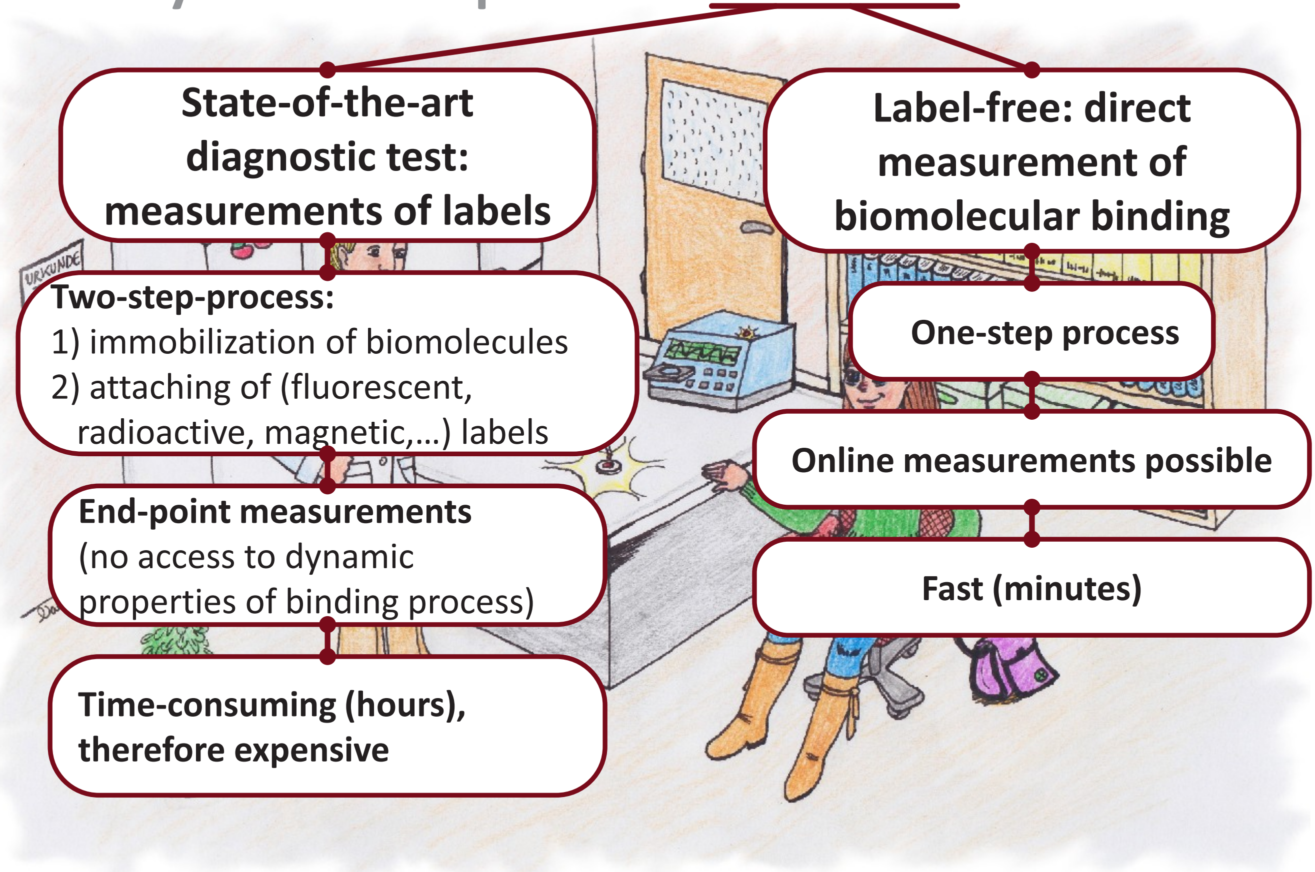

Polymer-based **photonic** label-free biosensor

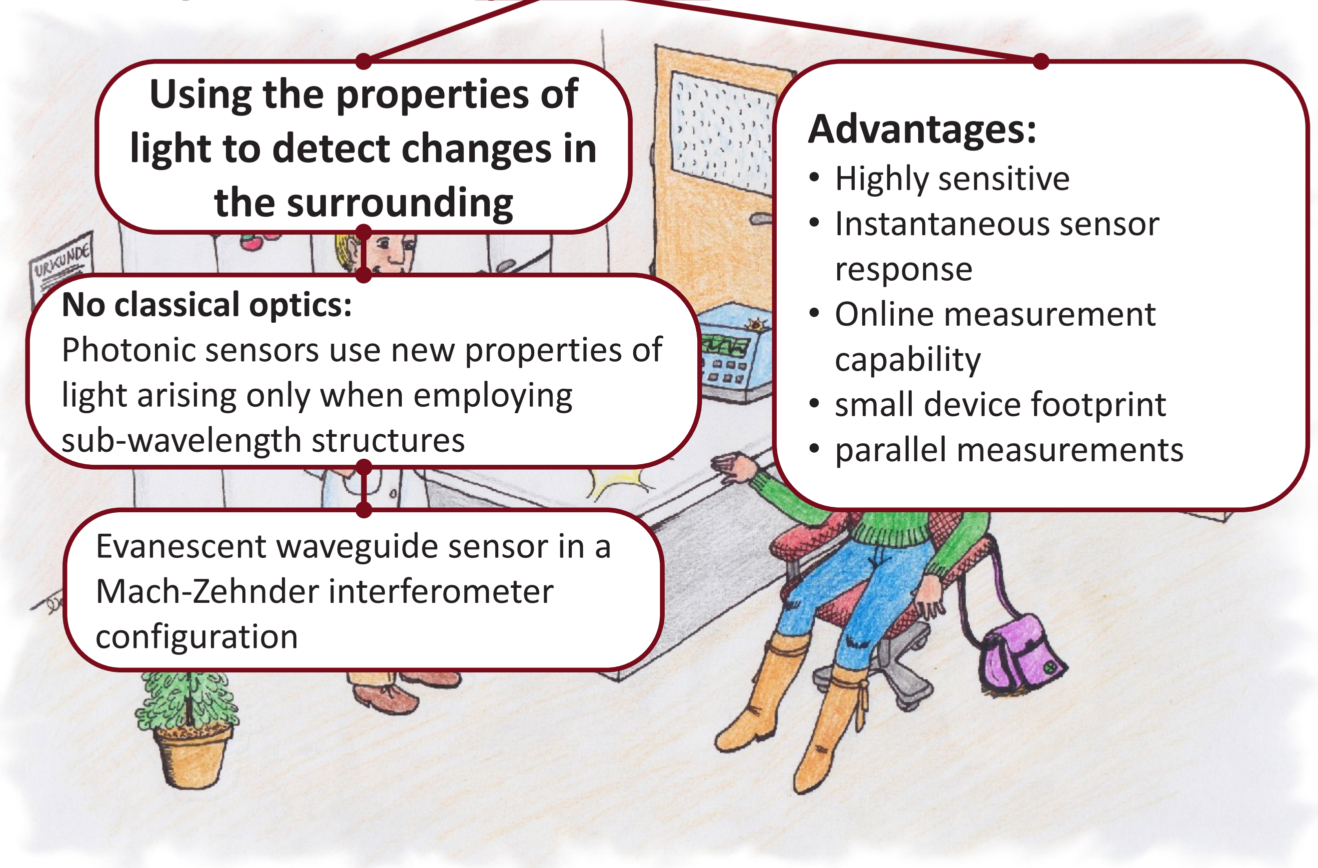

Polymer-based photonic label-free biosensor

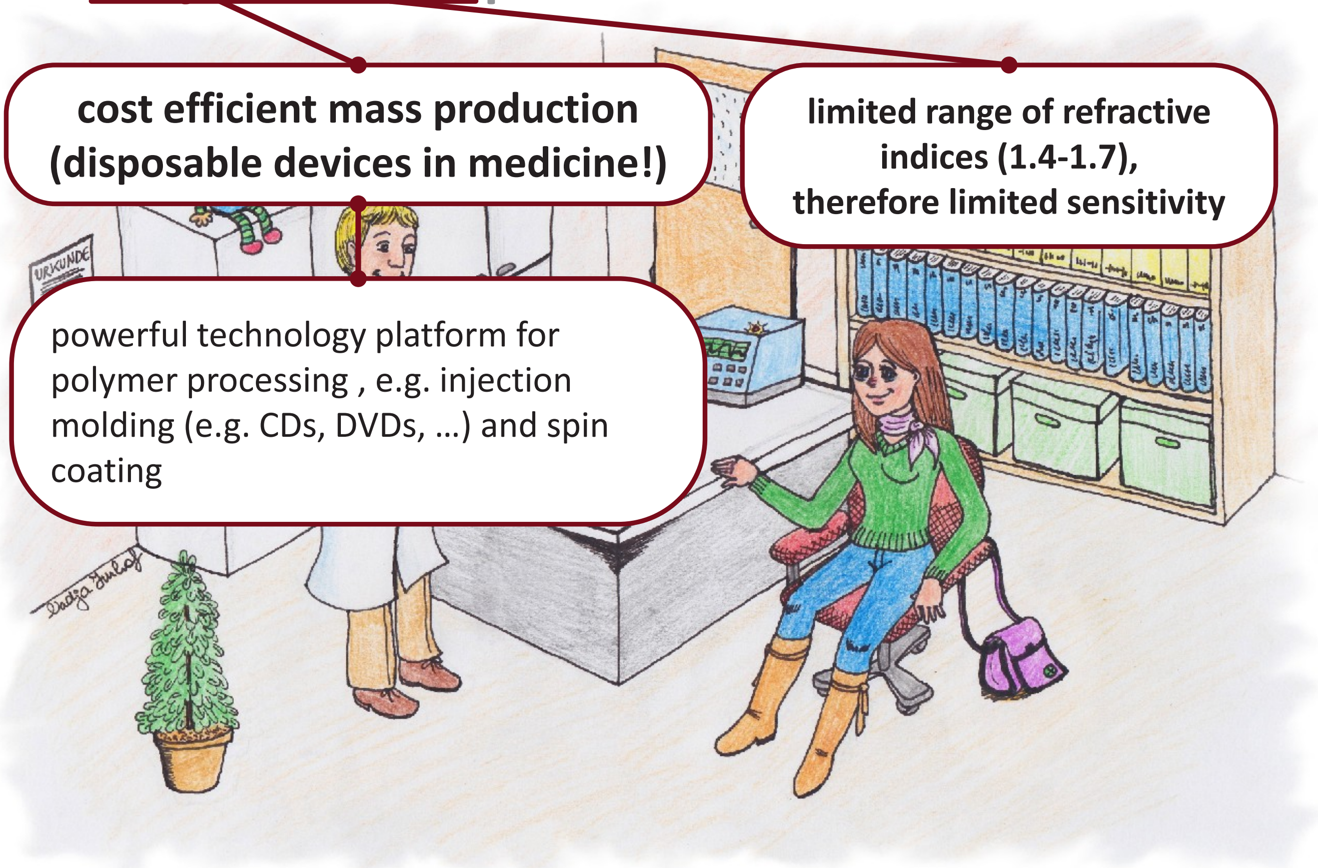

Measurement principle:

waveguide side view:

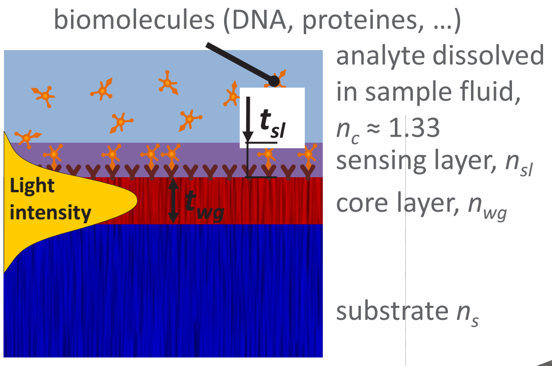

Biosensitive layer on top of waveguide provides **selective binding** and an **enrichment** of biomolecules on the sensor surface.

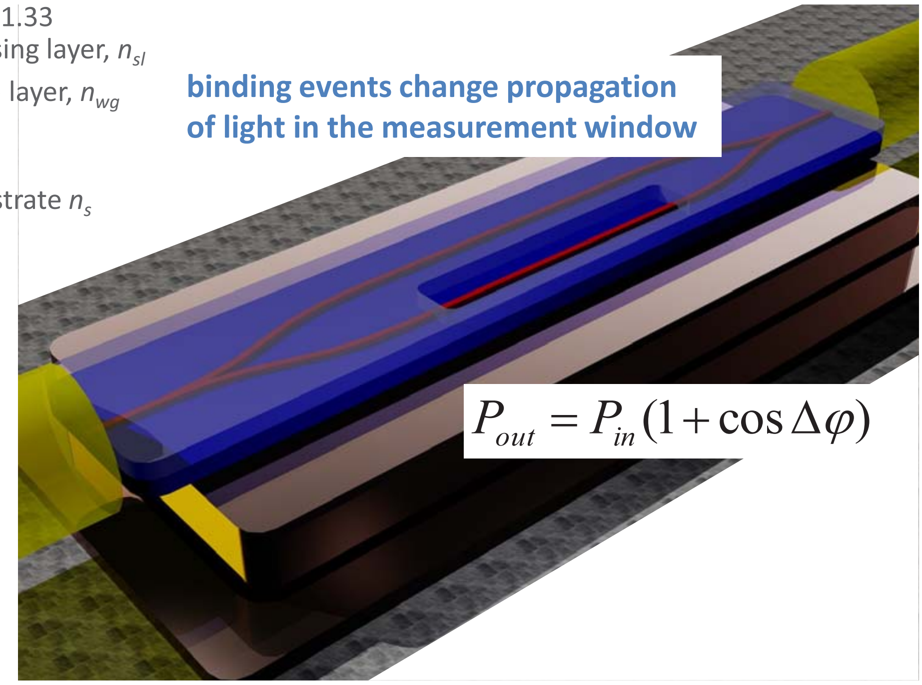

- Highly sensitive
- Simple & low-priced read-out system

Device design:

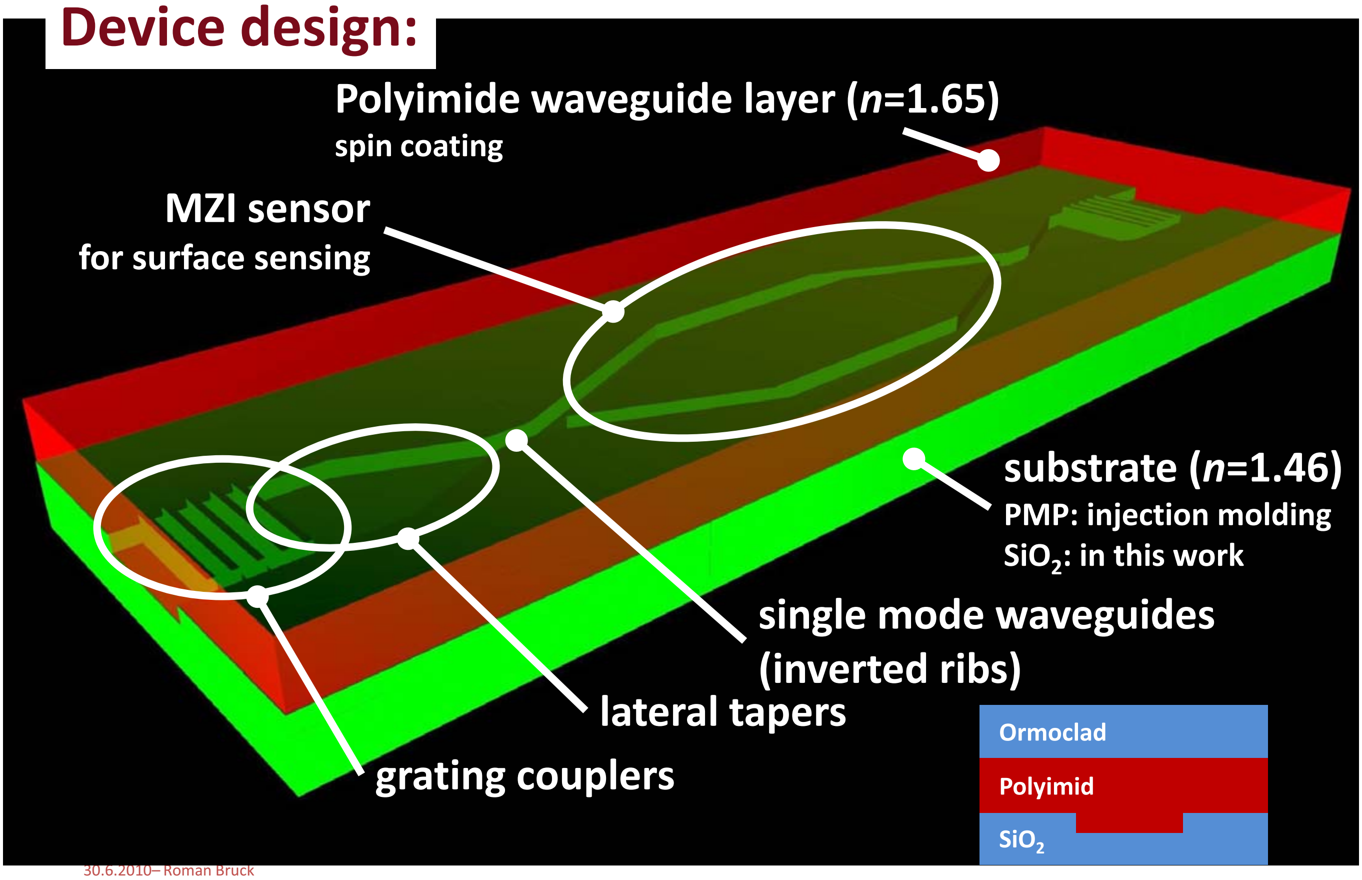

MZI – measurement setup:

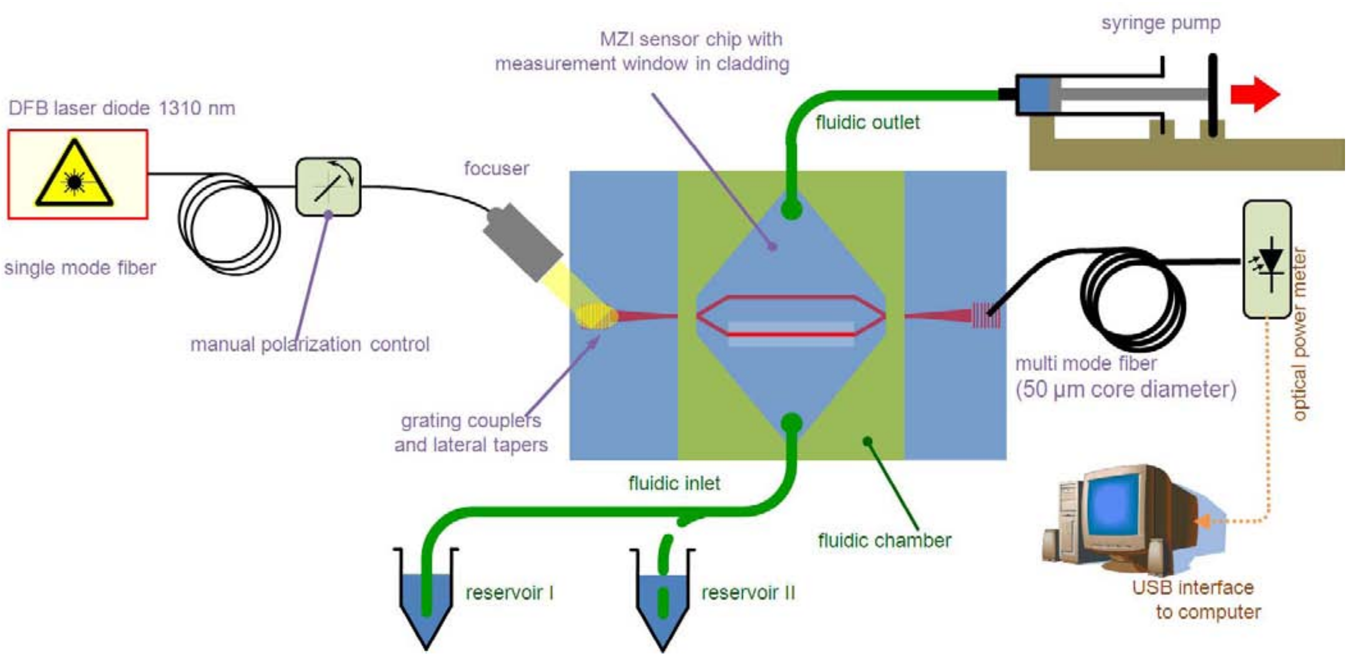

Biotin-streptavidin measurements:

Biotin – streptavidin binding on non-blocked surfaces

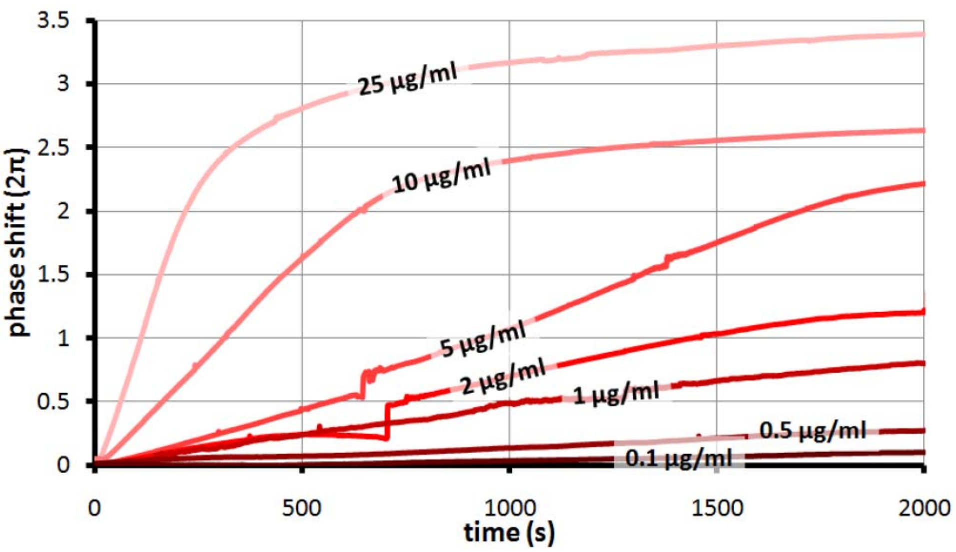

smallest concentration measured:
0.1 µg/ml = 1.6 nMol = 30 ppb

Biotin-streptavidin measurements:

Reproducability – blocking – specificity

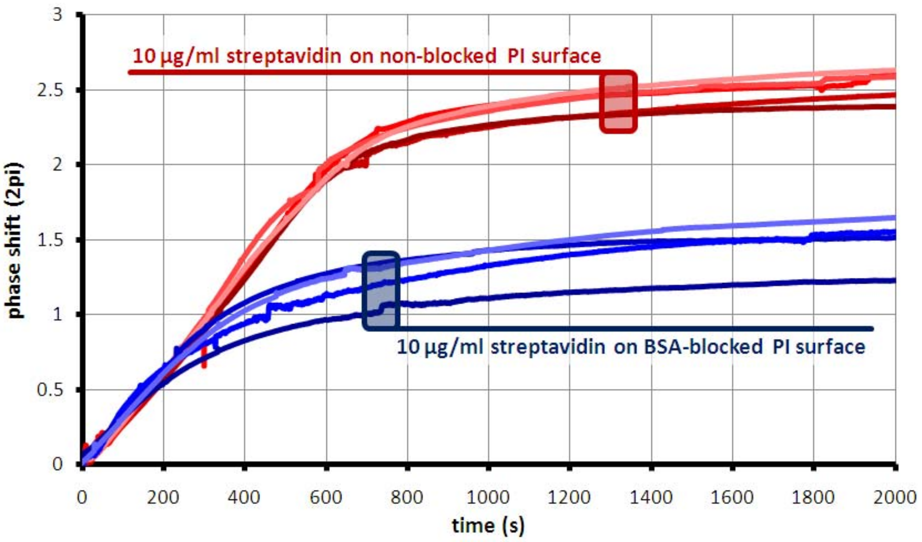

- Standard deviation ~ 5%
  Sensor sensitivity varies max. 2%
- Blocking:
  Signal reduced by about 40%
  BUT:
  No non-specific binding!

A vision:

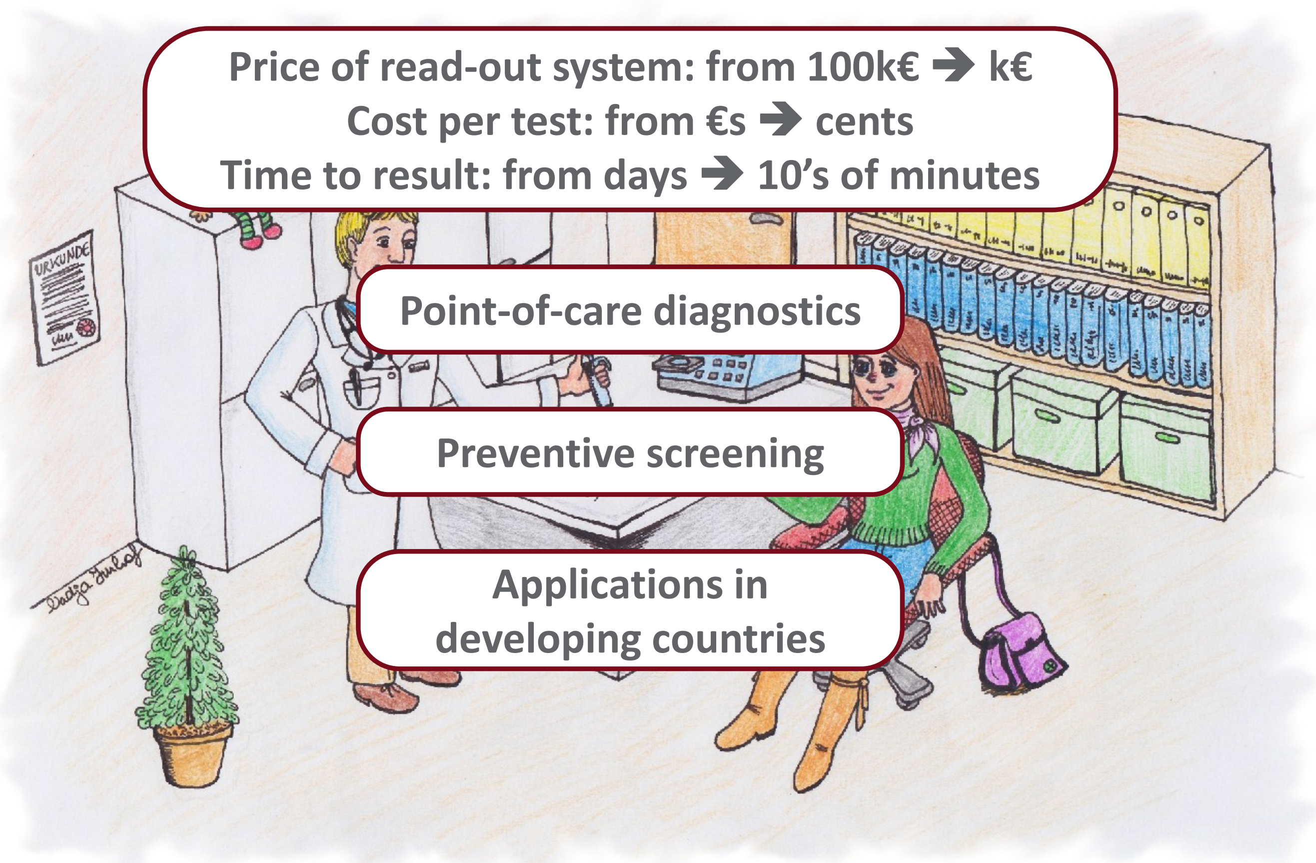

Quantum Dots in plasmonic systems for optochemical sensors

Norbert Reitinger

Nano-Optics Group

nanooptics.uni-graz.at

ARGE Sensorik – PhD Summit 2011
June 30, 2011

ISOTEC Research Cluster

ISOTEC Integrated Organic Sensor and Optoelectronic Technologies

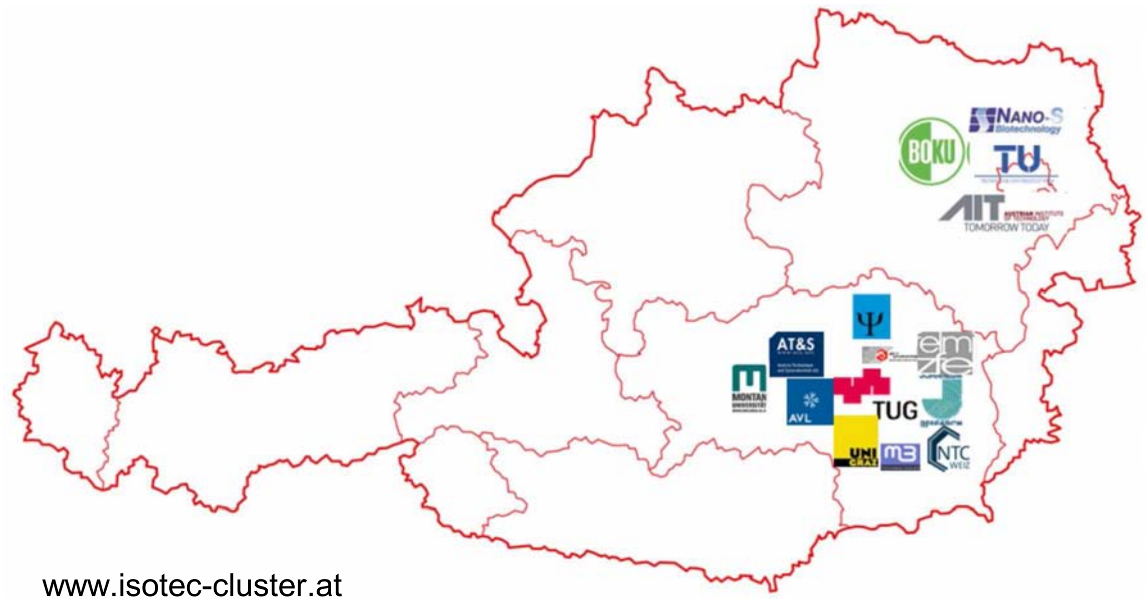

www.isotec-cluster.at

ISOTEC Research Cluster

ISOTEC Integrated Organic Sensor and Optoelectronic Technologies

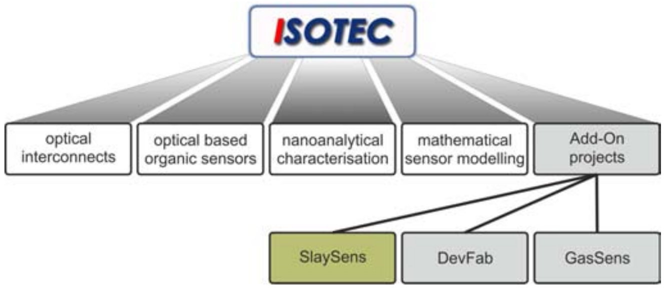

SLAYSENS Optochemical sensors based on S-layer membranes (**S**-**lay**er based **sens**ors)

Contents

Introduction	Experiments	Conclusion
SlaySens - sensor principle quantum dots	QD characterisation energy transfer emitter metal interaction	summary outlook & applications

Sensor Working Principle

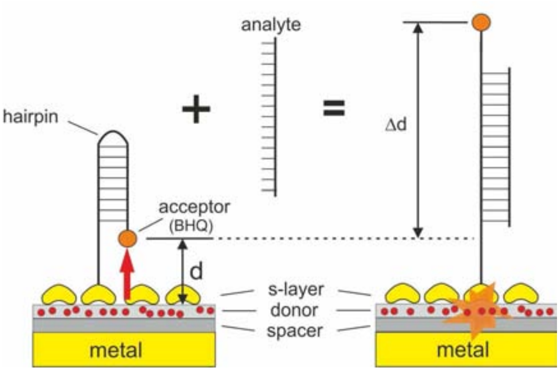

Scanning-force-microscope-surface-relief reconstruction of a crystalline protein S-layer from Bacillus sphaericus

Quantum Dots

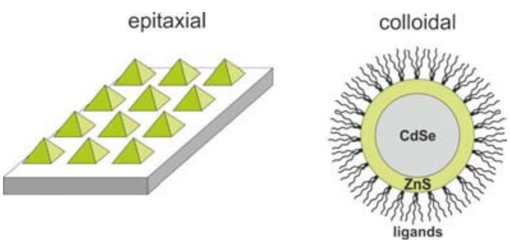

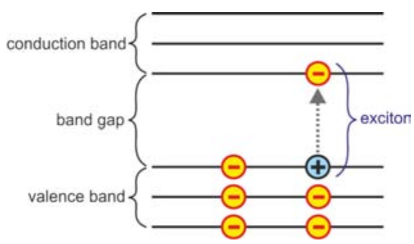

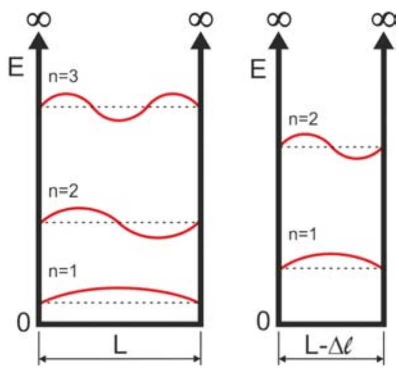

QD characterization

QD-ensemble spectrum

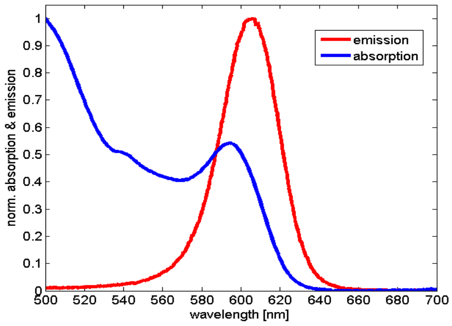

fluorescence decay and intensity time trace

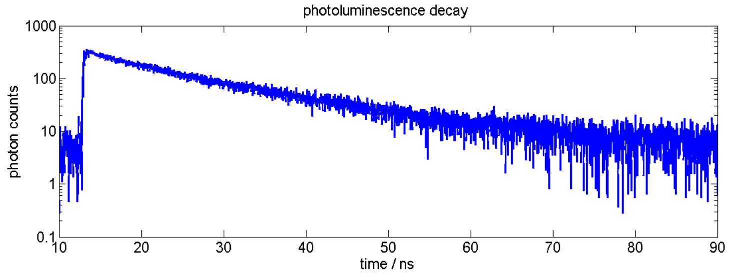

single QD spectra

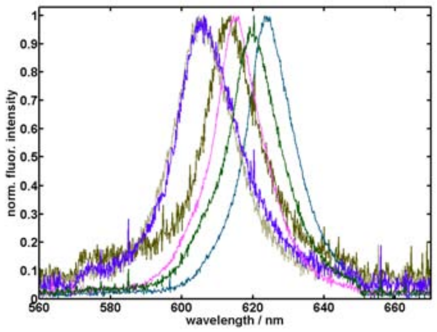

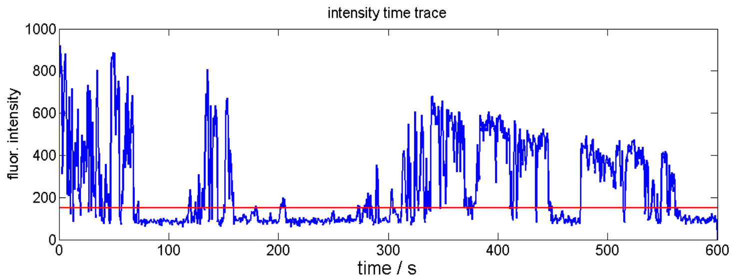

τ = 15ns, time channel width = 24.4ps resp. 0.5s,
integration time = 600s

FRET between Quantum Dots

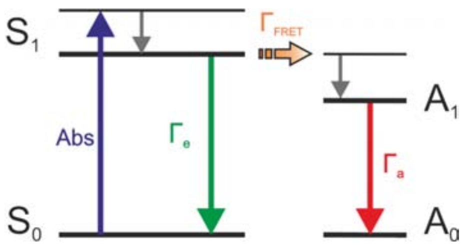

$$\Gamma_{ET}(r) = \frac{1}{\tau_D}\left(\frac{R_0}{r}\right)^6 = \Gamma_D\left(\frac{R_0}{r}\right)^6$$

$$R_0^6 = 0.529\,\frac{\kappa^2 Q_D}{n^4 N} J(\lambda)$$

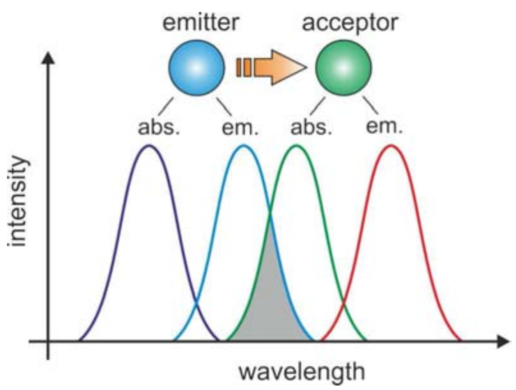

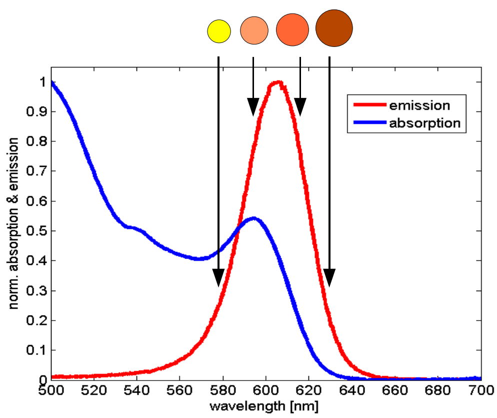

FRET between Quantum Dots

QDs in a PMMA layer

QDs in toluene solution

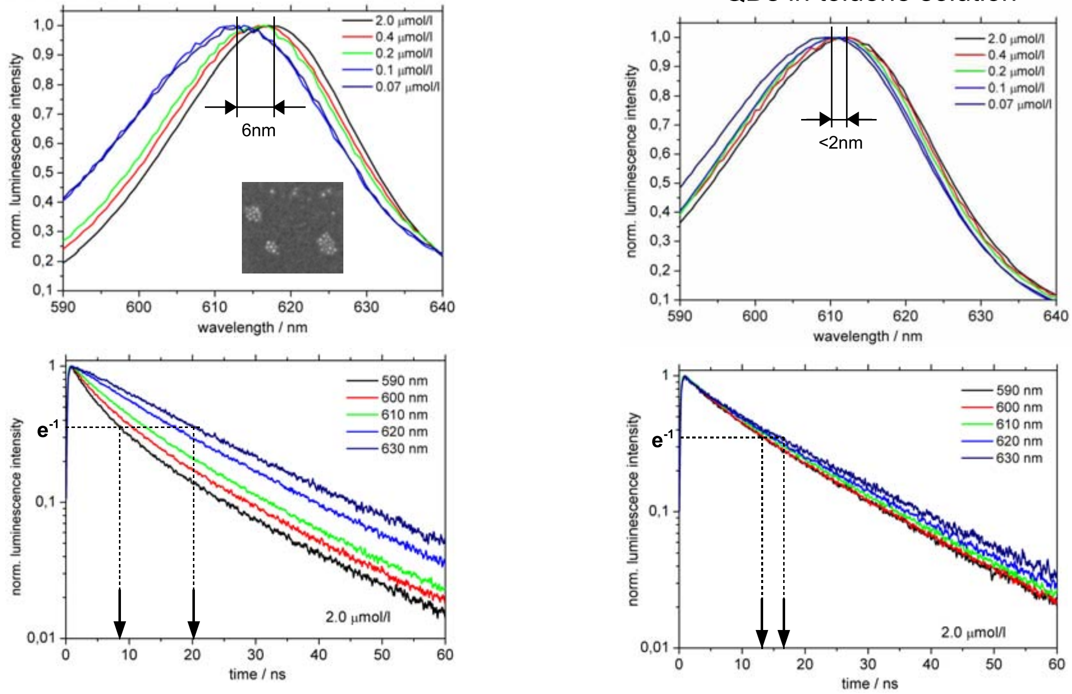

N. Reitinger et al., Phys. Stat. Sol. A **208**, 710 (2011)

QD's and a flat metal film

water-soluble CdTe QDs (EWL =630nm) (Prof. Dr. Xinhua Zhong, Department of Chemistry, East China University of Science and Technology, Shanghai)

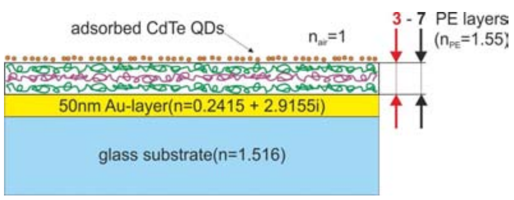

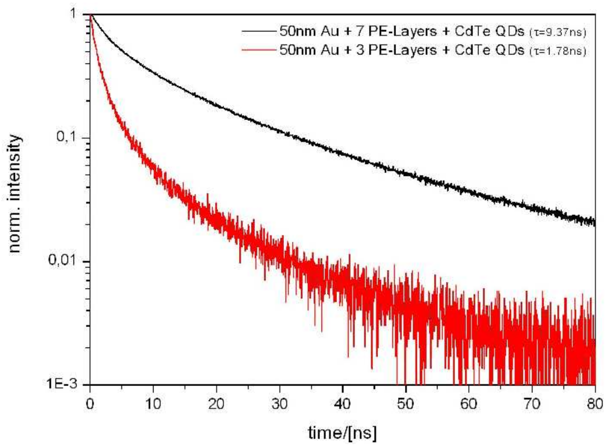

$$I(t) = I_0 \cdot e^{-(t/\tau)^\beta}, \quad 0 < \beta \leq 1$$

QD – MNP interaction

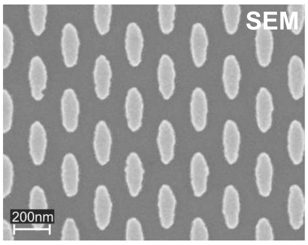

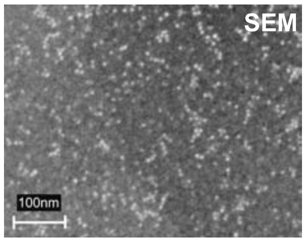

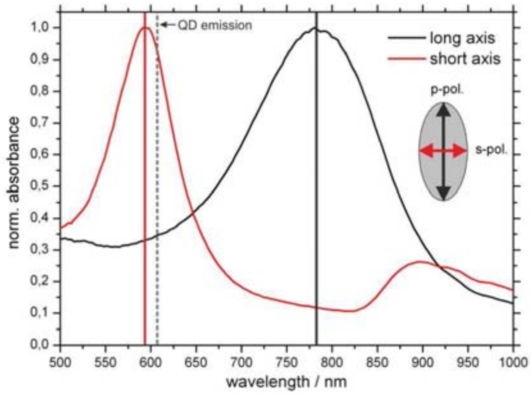

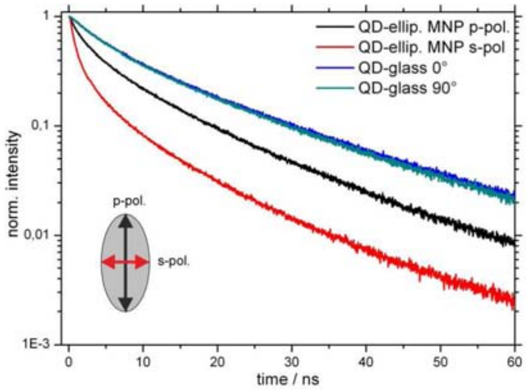

Summary

- fluorescence lifetime is suitable as sensor quantity
- but interpretation of decay curves can be difficult
- investigation of energy transfer between QD's
- interaction between QD's and metal

Outlook

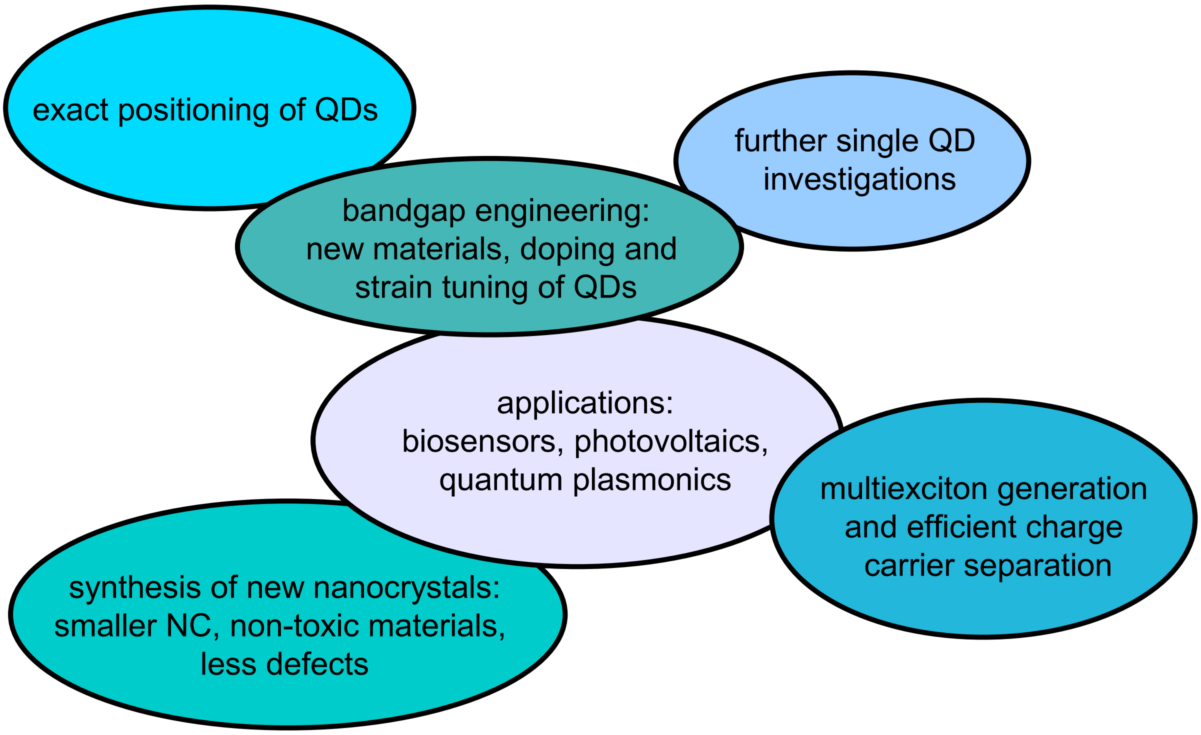

Acknowledgements / Financial Support

Partners:

A. Hohenau, H. Ditlbacher, K. Rumpf, P. Granitzer, N. Galler, P. Kusar, J.-C. Tinguely, C. Gruber, V. Häfele, F. Aussenegg, A. Leitner, J. Krenn (Nano-Optics, Graz)

S. Scheicher, S. Köstler, V. Ribitsch (Joanneum Research & IfC, Graz)

B. Kainz, D. Pum (Boku, Vienna)

Financial support:

Austrian NANO Initiative

Austrian Research Promotion Agency (FFG)

Federal Ministry for Transport, Innovation and Technology (BMVIT)

Modeling of an LFE piezoelectric fluid sensor as layered structure in the spectral domain

Thomas Voglhuber-Brunnmaier
Institute for Microelectronics and Microsensors,
Johannes Kepler University, Linz, Austria

Liquid sensing

- Measure the parameters of a fluid
  E.g.: density, viscosity, permittivity, conductivity
- Thickness field excitation (TFE) vs. lateral field excitation (LFE)
- Modeled utilizing a semi-numeric spectral method

Sensing utilizing piezoelectric structures

Sauerbrey (1959) (mass loading)

$$\Delta f = -\frac{2f_0^2}{A\sqrt{\rho c}}\Delta m$$

A...face area
ρ...density

Δm…mass loading
c…shear modulus

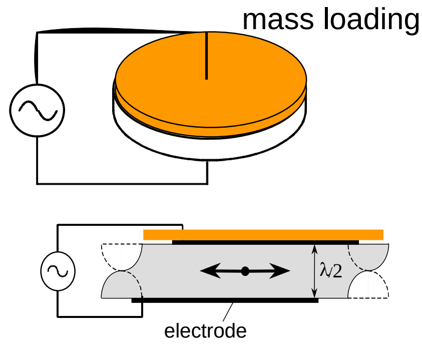

Kanazawa, Gordon (1985) (viscous fluid loading)

$$\Delta f = -f_0^{3/2}\sqrt{\frac{\rho'\mu}{\pi\rho c}}$$

ρ'...liquid density
μ…shear viscosity

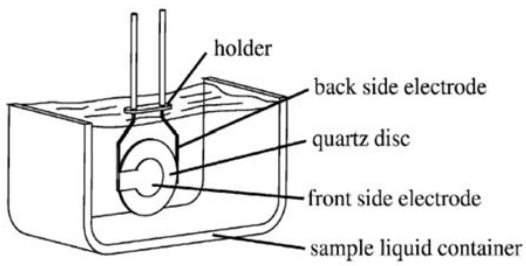

Thickness **F**ield vs. **L**ateral **F**ield **E**xcitation

TFE:

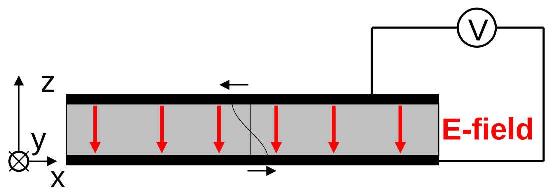

stresses: piezoelectricity (Quartz): E-field:

$$\begin{bmatrix} T_{xx} \\ T_{yy} \\ T_{zz} \\ T_{yz} \\ T_{xz} \\ T_{xy} \end{bmatrix} = \begin{bmatrix} e_{11} & 0 & 0 \\ e_{12} & 0 & 0 \\ e_{13} & 0 & 0 \\ e_{14} & 0 & 0 \\ 0 & e_{25} & e_{35} \\ 0 & e_{26} & e_{36} \end{bmatrix} \cdot \begin{bmatrix} E_x \\ E_y \\ E_z \end{bmatrix}$$

LFE:

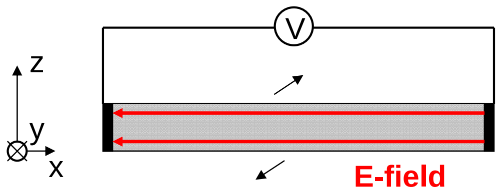

$$\begin{bmatrix} T_{xx} \\ T_{yy} \\ T_{zz} \\ T_{yz} \\ T_{xz} \\ T_{xy} \end{bmatrix} = \begin{bmatrix} e_{11} & 0 & 0 \\ e_{12} & 0 & 0 \\ e_{13} & 0 & 0 \\ e_{14} & 0 & 0 \\ 0 & e_{25} & e_{35} \\ 0 & e_{26} & e_{36} \end{bmatrix} \cdot \begin{bmatrix} E_x \\ E_y \\ E_z \end{bmatrix}$$

Couplingfactors 330µm AT-Cut quartz :

		k_{TE} in %	$k_{LE,0}$ in %	$k_{LE,90}$ in %	v in m/s	f_0 in MHz
extensional	a	0	6.48	0	7009	10.619
fast shear	b	0	6.17	0	3801	5.759
slow shear	c	8.74	0	6.26	3326	5.034

(i.e., coupling strength between electrical and mechanical fields)

Thickness Field vs. Lateral Field Excitation

TFE:

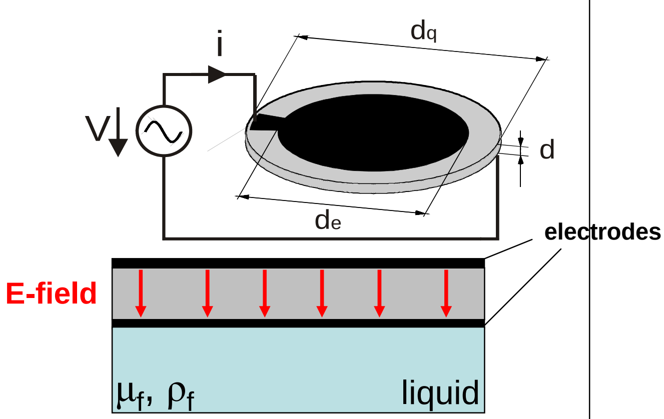

- only TFE - modes excited
- electric field confined in the piezo
- sensitivity to viscosity and density

LFE:

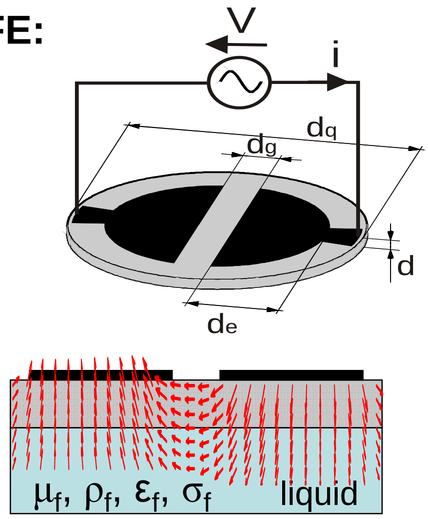

- also LFE modes excited
- electric field propagates into liquid
- sensitivity also to permittivity and conductivity

Modeling of the physical domains

piezoelectric equations + quasistatic approximation + equation of motion

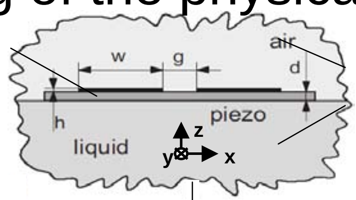

linearized Navier Stokes + electrostatic Maxwell Eqn.

piezo equations:
$\rho\ddot{\boldsymbol{u}} = \nabla\cdot\boldsymbol{c}^E : \nabla_s\boldsymbol{u} + \nabla\cdot\boldsymbol{e}\nabla\varphi$ $\nabla\cdot\boldsymbol{e} : \nabla_s\boldsymbol{u} = \nabla\cdot\boldsymbol{\varepsilon}^S\cdot\nabla\varphi$
$\boldsymbol{u}$... displacement vector, φ... electric potential ρ... mass density, $\boldsymbol{c}^E$ ... elastic stiffness tensor $\boldsymbol{e}$... piezoelectric stress tensor , $\boldsymbol{\varepsilon}$... permittivity tensor ∇... gradient operator, ∇_s... symmetric gradient operator

TABLE I

EQUATIONS DESCRIBING THE PIEZO MATERIAL AND DENOTATION OF THE INCLUDED QUANTITIES.

equations for liquid and air:
$\rho\ddot{\boldsymbol{u}} = \frac{1}{\zeta}\nabla(\nabla\cdot\boldsymbol{u}) + \mu\nabla\dot{\boldsymbol{u}} + (\lambda+\mu)\nabla(\nabla\cdot\dot{\boldsymbol{u}})$ $\nabla\cdot\left(\frac{\sigma}{\varepsilon}\,\boldsymbol{D} + \dot{\boldsymbol{D}}\right) = 0$
$\boldsymbol{D}$... electric displacement vector, ζ... compressibility coefficient μ... shear viscosity coefficient, λ... volume viscosity coefficient σ... electrical conductivity, ε... isotropic permittivity

TABLE II

EQUATIONS DESCRIBING LIQUID AND AIR AND DENOTATION OF INCLUDED QUANTITIES.

time-harmonic, layered structure:

$$\frac{\partial}{\partial t} \circ\!\!-\!\!\bullet \cdot \mathrm{i}\omega,\; \frac{\partial}{\partial x} \circ\!\!-\!\!\bullet \cdot(-\mathrm{i}k_x),\; \frac{\partial}{\partial y} \circ\!\!-\!\!\bullet \cdot(-\mathrm{i}k_y)$$

spectral domain method

3 systems of ODEs of 1st order of dim 8:

$$\frac{\partial}{\partial z}\tilde{\boldsymbol{\psi}}_{a,p,l}(k_x,k_y,z,\omega) = \tilde{\boldsymbol{A}}_{a,p,l}\cdot\tilde{\boldsymbol{\psi}}_{a,p,l}(k_x,k_y,z,\omega)$$

$$\tilde{\boldsymbol{\psi}}_{a,p,l} = \left[\tilde{u}_x, \tilde{u}_y, \tilde{u}_z, \tilde{\varphi}, \tilde{T}_{xz}, \tilde{T}_{yz}, \tilde{T}_{zz}, \tilde{D}_z\right]^T_{a,p,l}$$

air piezo liquid

Modeling of the electrodes: Green's function

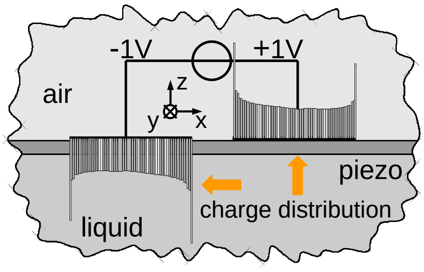

- electrodes modeled as purely electrical (mechanic loading of electrodes is neglected)
- determine the charge distribution necessary to produce the prescribed potential.
- Green's function (G) is potential response due to point charge (G obtained from coupled ODEs in the spectral domain)

Green's function

$$\varphi(x,y,d/2,\omega) = \int_{\Omega(x',y')} G(x-x',y-y',\omega)\varrho(x',y',d/2,\omega)\mathrm{d}x'\mathrm{d}y'$$

electric potential — charge distribution

deconvolution (Method of Moments)

$$\varrho(x,y,d/2,\omega)$$

admittance spectrum

$$I(\omega) = \frac{d}{dt}\int_{\Omega_e} \varrho(x,y,\omega)dA$$

$$Y(\omega) = I(\omega)/V$$

field variables

$$\psi(x,y,z) = [u_x, u_y, u_z, \varphi, T_{xz}, T_{yz}, T_{zz}, D_z]^T$$

displacements, el. potential, stresses, el. displacement

Results for AT-cut quartz (ZXwlt 0°/54.75°/0°):

slow thickness-shear-mode (c-mode)

TFE-mode k=8.8%

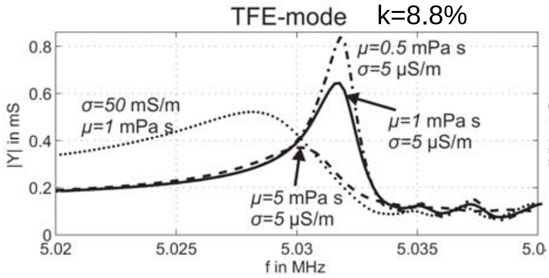

fast thickness-shear-mode (b-mode)

LFE-mode k=6.2%

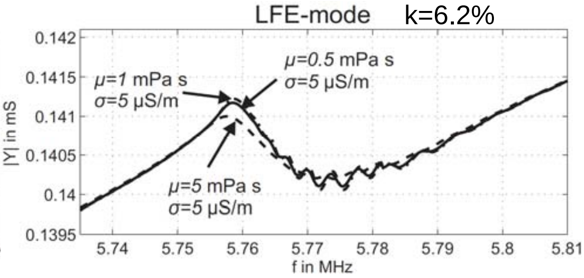

piezoelectric disc: *330* µm AT-cut quartz *5* MHz, shear displacement in x
sample liquid: pure (σ = *5* µS/m) and tap water (σ = *50* mS/m). Shear viscosity of water (μ = *1* mPa s) varied to μ = *0.5* mPa s and μ = *5* mPa s.

- slow shear mode shows good sensitivity to viscosity changes
- high cross-sensitivity to conductivity
- extensional and fast shear mode not useable
- **Coupling factors are not sufficient! Also geometry has to be considered!**

Results for AT-cut quartz

	k_{TE} in %	$k_{LE,0}$ in %	$k_{LE,90}$ in %	v in m/s	f_0 in MHz	
a	0	6.48	0	7009	10.619	very weak
b	0	6.17	0	3801	5.759	weak
c	8.74	0	6.26	3326	5.034	strong

COUPLING FACTORS FOR a, b, c-MODES FOR TFE AND LFE, WAVE VELOCITIES, AND RESONANCE FREQUENCIES FOR A $330\mu m$ DISC.

For AT-quartz only TFE mode is usable: **PSEUDO-LFE**

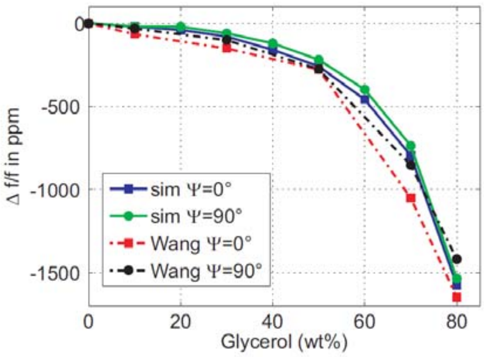

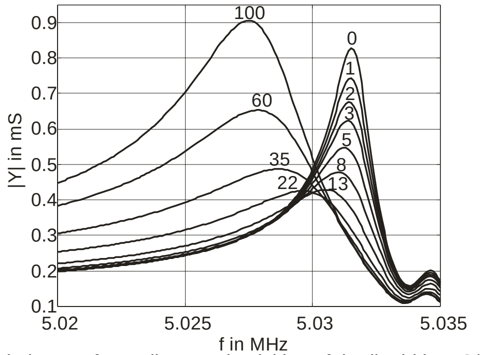

Admittance for variing conductivities of the liquid in mS/m.

Experimental data from:

Wang, W.; Zhang, Z.; Zhang, C.; Liu, Y.; Feng, G. & Jing, G. Pseudo-LFE study in AT-cut quartz for sensing applications *Proc. IEEE Sensors,* **2008**, 1548-1551

A pure LFE sensor: lithium niobate (YXwl 60°/58°)

	k_{TE} in %	$k_{LE,0}$ in %	$k_{LE,90}$ in %	v in m/s	f_0 in MHz
lithium niobate:					
a	31.9	0	7.8	7217	10.934
b	2.74	0	19.15	3993	6.050
c	0	92.51	0	3481	5.274

TABLE III

COUPLING FACTORS FOR a, b, c-MODES FOR TFE AND LFE, WAVE VELOCITIES, AND RESONANCE FREQUENCIES FOR A $330\mu m$ DISC.

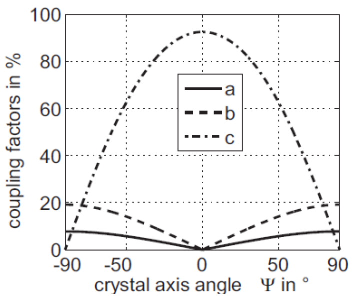

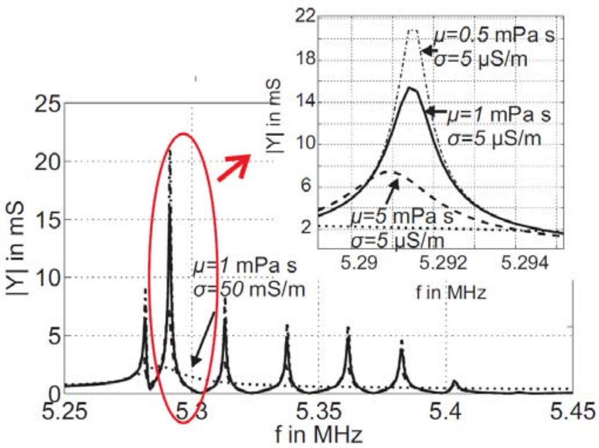

Summary

+ Method yields reasonable admittance spectra and fields

+ Fluid-structure interaction is fully modeled.
  - mechanical and electrical loading

+ Additional material layers can be applied easily
  - e.g. shielding electrode at bottom

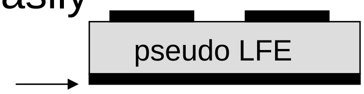

+ Arbitrary piezoelectric materials and fluids can be simulated

A Highly Uniform Lamination Micromixer with Wedge Shaped Inlet Channels for Time Resolved Infrared Spectroscopy

W. Buchegger[1], C. Wagner[2], B. Lendl[2],
M.Kraft[3], M. Vellekoop[1]
[1]Institute of Sensor and Actuator Systems
[2]Institute of Chemical Technologies and Analytics
Vienna University of Technology
[3]CTR Carinthian Tech Research AG

Outline

- Background
- Motivation
- Micromixer requirements
- Mixer designs and simulation
- Material and fabrication
- Measurement results
- Conclusion

ARGE Sensorik PhD Summit 30. Juni 2011 Wolfgang Buchegger isas

TU WIEN TECHNISCHE UNIVERSITÄT WIEN Vienna University of Technology

Background

- Many chemical and bio-chemical reactions have so far unknown transition states or kinetics (e.g. protein folding)
- Infrared Spectroscopy is a powerful method for time resolved analysis
- Current technologies
  - Step-Scan
  - Rapid-Scan

CTA ARGE Sensorik PhD Summit 30. Juni 2011 Wolfgang Buchegger

isas

TU WIEN TECHNISCHE UNIVERSITÄT WIEN Vienna University of Technology

Background

- Step Scan
  - Precise external trigger
  - Cyclic reactions
- Rapid Scan
  - Limited mirror velocity
  - Resolution 10ms

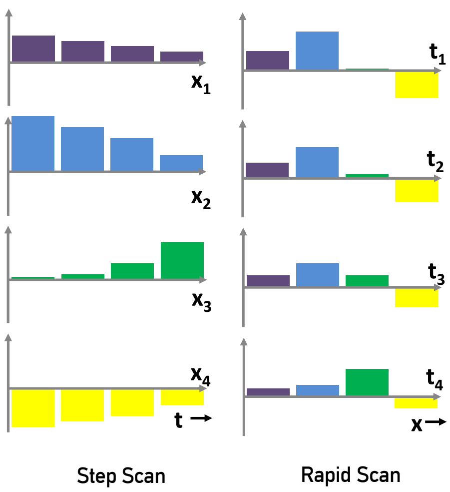

CTA ARGE Sensorik PhD Summit 30. Juni 2011 Wolfgang Buchegger

Motivation

- Continuous flow micromixer to observe chemical reactions
- Mixing by diffusion (passive) in the low millisecond range
- Real-time information about reaction mechanisms and conformation changes of an analyte

Micromixer requirements

- IR Spectroscopy requires shallow channels for aqueous solutions (about 10µm)
- Measurement spot of about 150x150µm²
- Strictly laminar flow

$$\text{Reynolds number}: Re \leq 1$$

- Mixing strongly depends on diffusion length

$$t_{mix} \propto \frac{l^2_{diff}}{D}$$

D... diffusion coefficient

l_{diff}... diffusion length

- Materials for mid-infrared wavelength

Micromixer design

- Two fluid channels
- Mixing channel on top
- Transparent cover
  - Two fluid layers are formed
  - Mixing times 5-10 ms

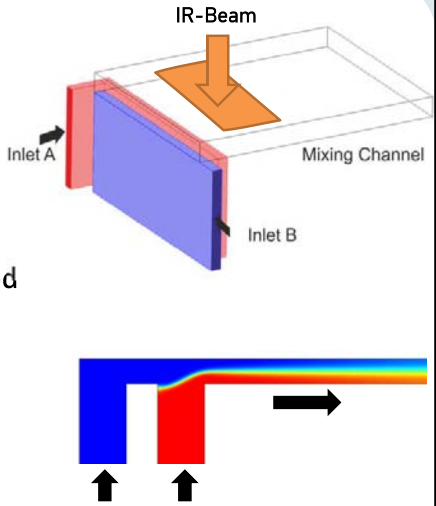

TECHNISCHE UNIVERSITÄT WIEN Vienna University of Technology

Micromixer design

- Distribution network splits 2 liquid feeds into 4 streams
- Velocity optimized for each stream
  - Resulting in layers with different thickness
  - Accounts for diffusion layers

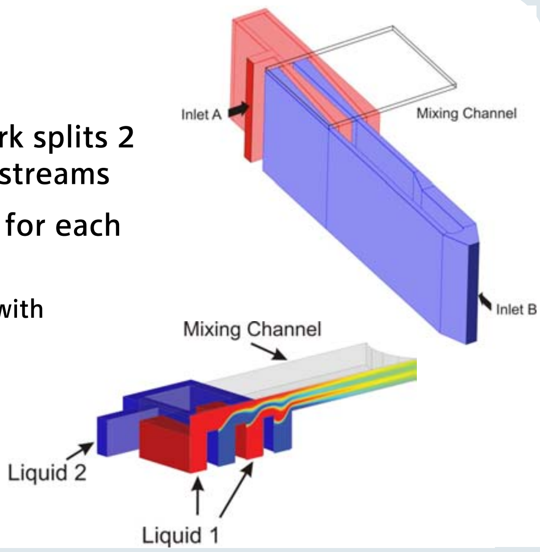

Simulation results

Straight shaped inlets create non-uniform fluid layers

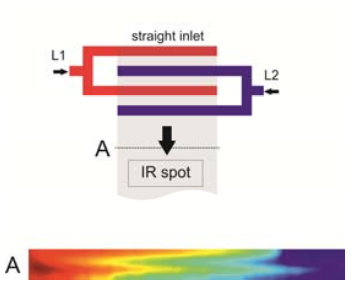

Wedge shaped inlets form uniform layers, shortening the diffusion length

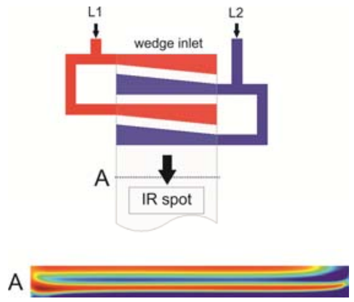

Materials and Fabrication

- Channel structures on silicon wafer by DRIE (20:1 aspect ratio)
- Mixing channel in WL5150 (8µm)
- Optical and IR transparent Cover for microscopic analysis: CaF_2 (1mm)

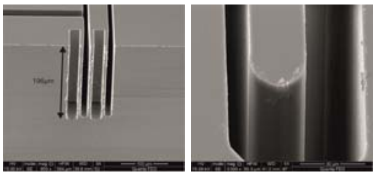

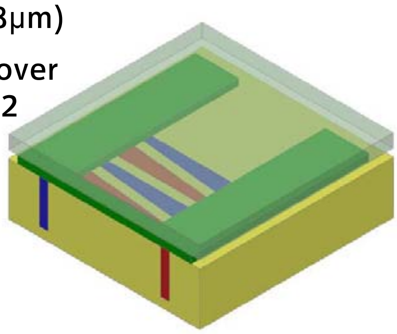

Measurement principle

- Each measurement spot equals a time stamp
- Spot size about 150x150 µm²
- Flow rate determines the time between spots and the overall time range

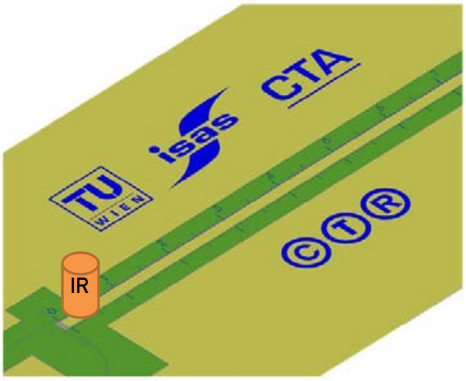

Characterization

- Wedge shape
  - Mixing times of <1ms
- Testreaction:
  - Iron (III) [Fe3+] and thiocyanate [SCN–] form a dark complex
- Flow rates ranging from 1-30µl/min

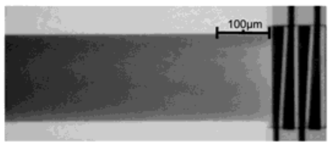

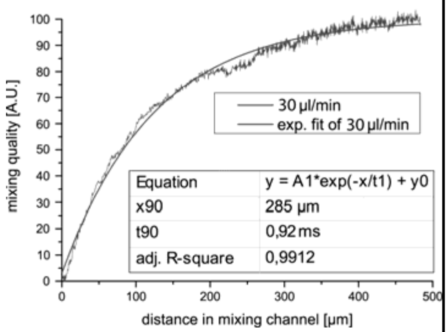

Characterization

- Straight shape
  - Mixing times of >3.5ms
- Testreaction:
  - Iron (III) [Fe^{3+}] and thiocyanate [SCN^-] form a dark complex
- Flow rates ranging from 1-30µl/min

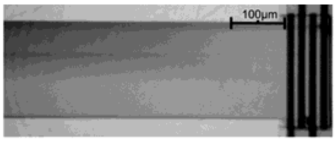

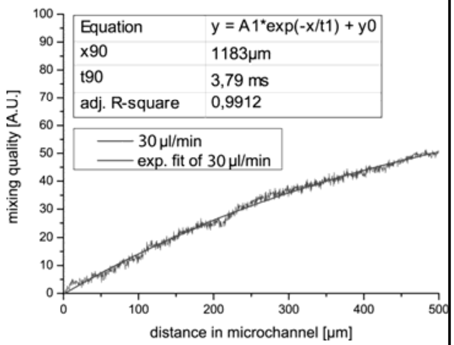

Characterization

- Testreactions:
  - Fluorescent dyes to visualize the individual fluid layers
- Micromixer with a 25µm channel height
- Formation of fluid layers equals simulation results

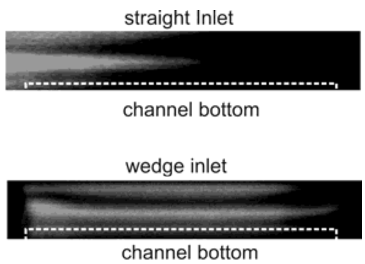

Time resolved FTIR Measurement

- Sodium sulfite Na_2SO_3 and formaldehyde solution HCHO
- Three changing bands
  - ($942 cm^{-1}$, $1025 cm^{-1}$, $1180 cm^{-1}$)
- 86 recorded spectra in about 80 milliseconds

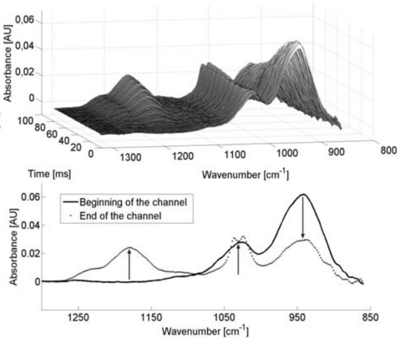

Wolfgang Buchegger

Conclusion

- Passive mixing device applicable for IR-Spectroscopy enables continuous spectral analysis
- Short mixing times due to individual fluid layers formed by the distribution network and the wedge shaped inlets
- Mixing times in low millisecond range for aqueous solutions enable investigation of many chemical reactions

Wolfgang Buchegger

isas

TECHNISCHE UNIVERSITÄT WIEN
Vienna University of Technology

Acknowledgements

Dr. Artur Jachimowicz
Dr. Hannes Schalko
Edda Svasek
Peter Svasek
Ewald Pirker
Andreas Rigler

COMET Competence Center Program

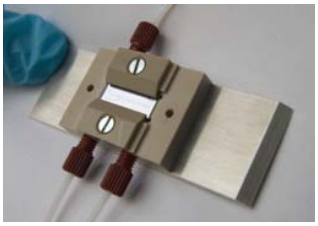

Thank you for your attention!

CTA ARGE Sensorik PhD Summit 30. Juni 2011 Wolfgang Buchegger

Thermoelectric energy harvesting in aircraft for wireless sensors

Dominik Samson (EADS),
Thomas Becker (EADS),
Ulrich Schmid (TU Wien)

Linz, Austria 30/06/2011

TECHNISCHE UNIVERSITÄT WIEN Vienna University of Technology

EADS

Scenario

Maintenance check by wireless sensor

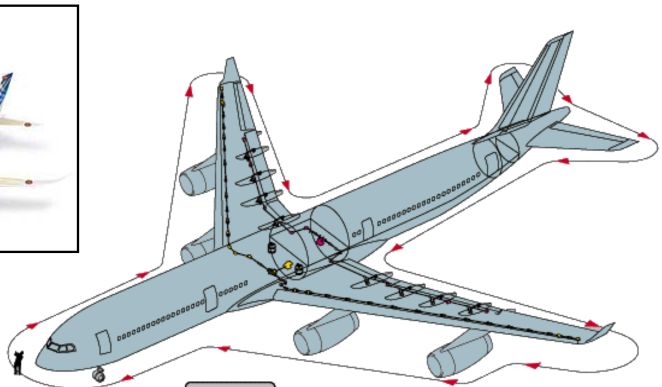

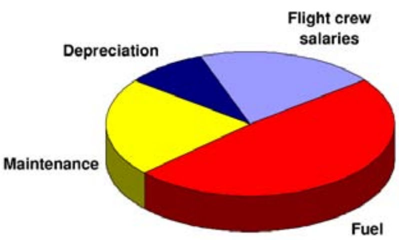

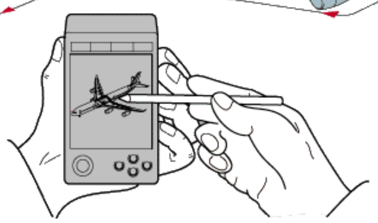

EADS

Scenario

How does Energy come to the sensor?

By cable:
- heavy
- difficult to install
- expensive to plan

By batterie:
- may not always work
- maintenance

Solution:
local power production at the sensor
= **energy harvesting**

[2]

Content

EADS and IW

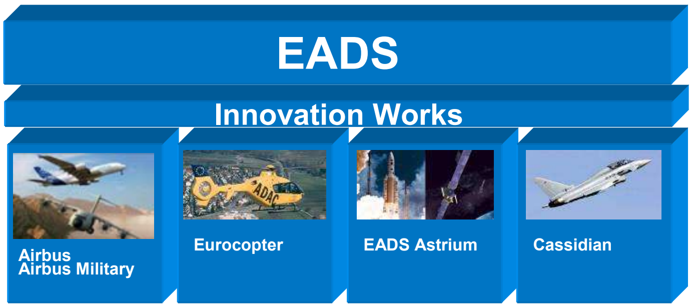

TECHNISCHE UNIVERSITÄT WIEN
Vienna University of Technology

Prof. Schmid

IW Staff (2009)
Headcount : 524
PhD/Thesis : 62

EADS

Energy harvesting

Possibilities for energy harvesting

Solar cell

- Sunlight
- External

Vibration Harvester

- vibrations
- in aircraft not large

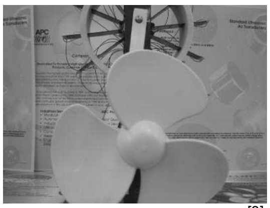

[3]

Windmill

- Airflow
- External

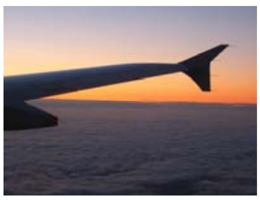

Triboelectricity

- Airflow
- Fixed

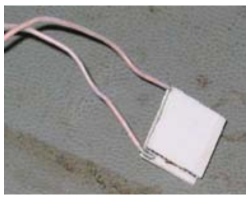

Thermoelectric generator

- In/outside ΔT

EADS

Thermoelectric theory

Origin of the thermoelectricity

Seebeck effect: $U = Q \cdot \Delta T$

Thermoelectric Generator (TEG):

$$U = (Q_B - Q_A) \cdot \Delta T$$

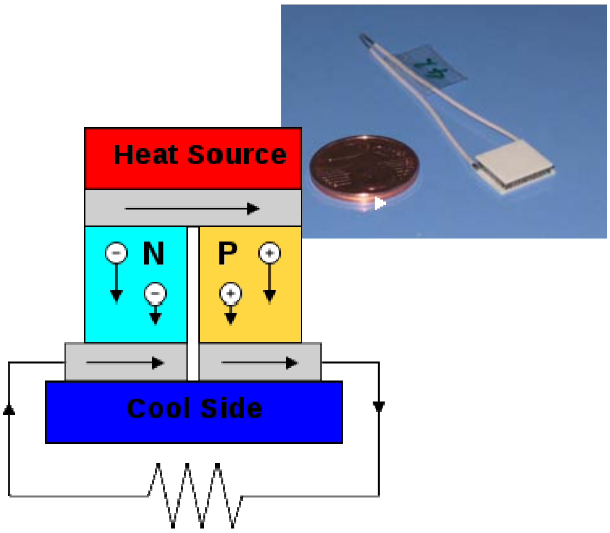

Thermoelectric theory

Model of Thermodiffusion:

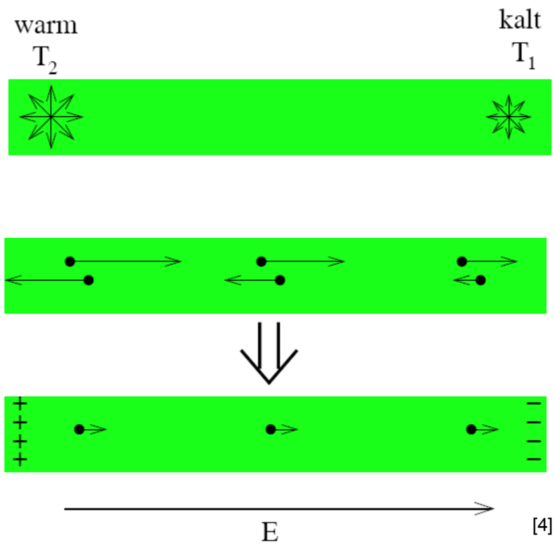

[4]

!!Source of thermoelectricity is the thermodiffusion!!

Thermoelectric Energy Harvesting

Static harvesting
inside: 24℃
outside: -20℃
+ constant energy output
- difficult to install

Dynamic harvesting
ground: 20℃
cruise: -20℃
- peaked energy output
+ easy to install

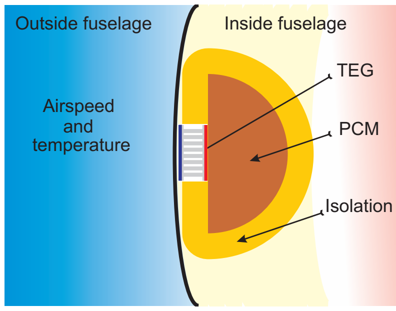

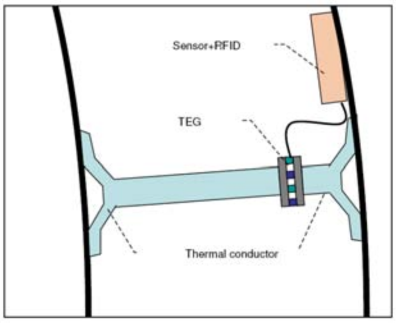

[6]

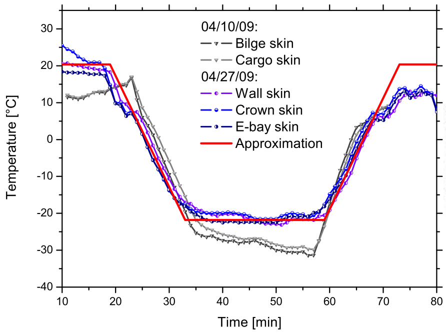

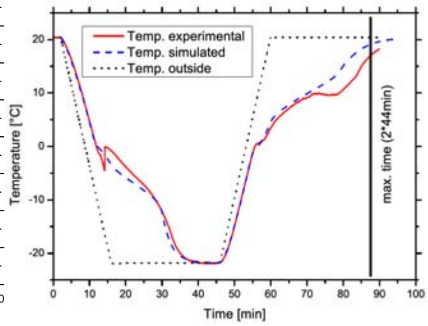

Thermoelectric phase changer

COMSOL FEM simulations for design parameters and energy output using general heat equation

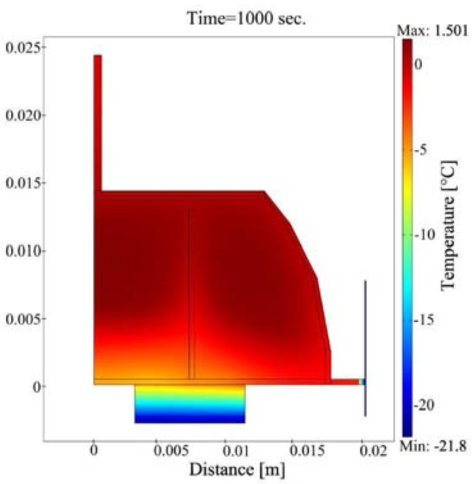

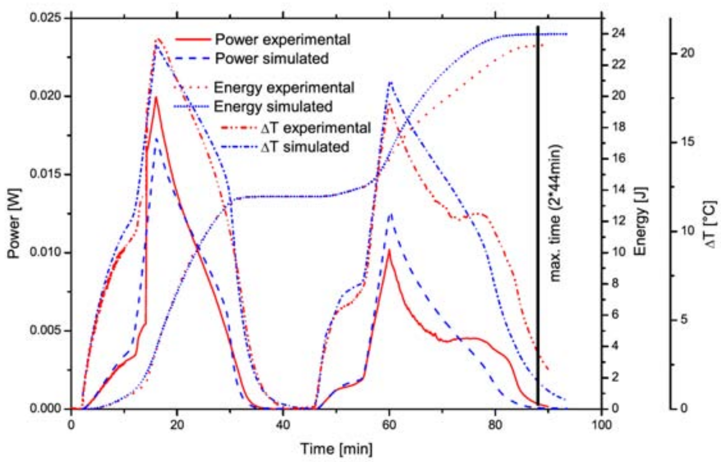

Energy output from 10g H_2O ~ 6.5 mWh

Thermoelectric phase changer

Optimization of the TEG heat conductivity

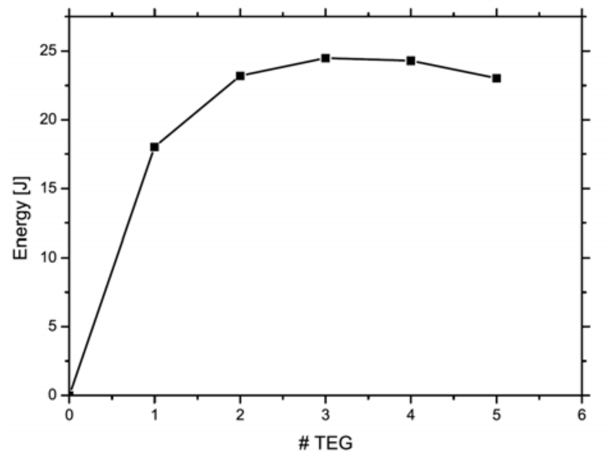

Thermoelectric phase changer

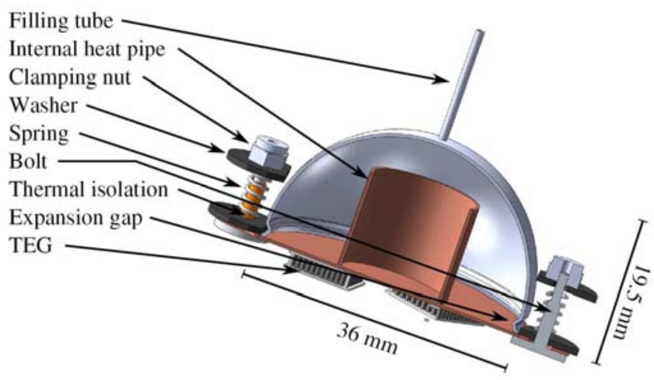

N^o	Short description	Energy output $[J]$ | Weight (PCM + containment, no TEG) $[g]$	PtW-ratio ($t = 88min$) $[W \cdot kg^{-1}]$
1	Double-walled, _no_ internal heat pipe, 3 mounting bolts, simulation results	20.9 | 30.85	0.128
2	Double-walled, with internal heat pipe, 3 mounting bolts, experimental results	22.1 | 33.19	0.128
2b	Double-walled, with internal heat pipe, 3 mounting bolts, _with_ vacuum isolation; experimental results	23.2 | 33.19	0.131
3	Double-walled, with internal heat pipe, 3 mounting bolts, **20 ml** H_2O, 8 TEGs, $R_l = 75\Omega$, experimental results	60.5 | 57.5	0.199
4	Single-walled, with heat pipe, 2 mounting bolts, $\approx 10mm$ PU foam isolation; experimental results	30.9 | 27.9	0.210
4b	Single-walled, with heat pipe, 2 mounting bolts, $\approx 100mm$ PU foam isolation; experimental results	35 | 60	0.110
4c	N^o 4 with Marlow TEG, simulated data	35.5 | 27.9	0.241

Power management & Sensor node

Sucessful test in climate chamber, from one flight cycle sensor worked 2.5h @ 189 µW

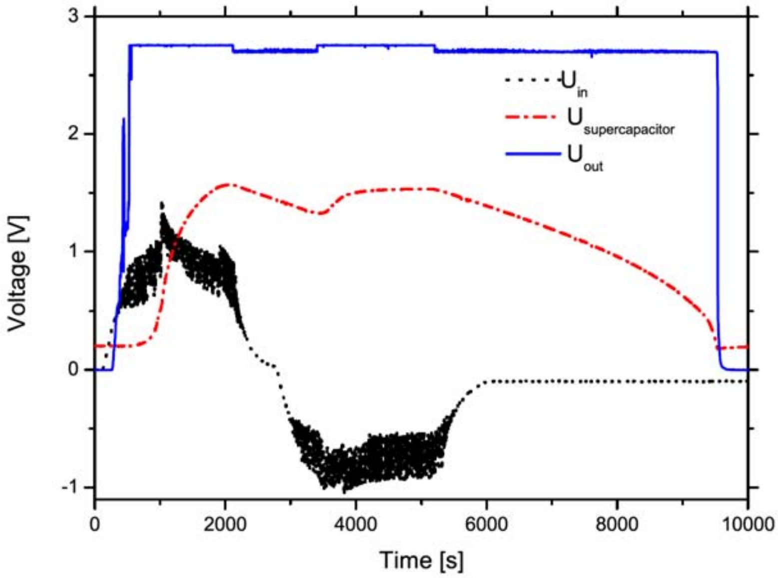

EADS

Power management & Sensor node

Ciruit to store and provide the power is necessary:

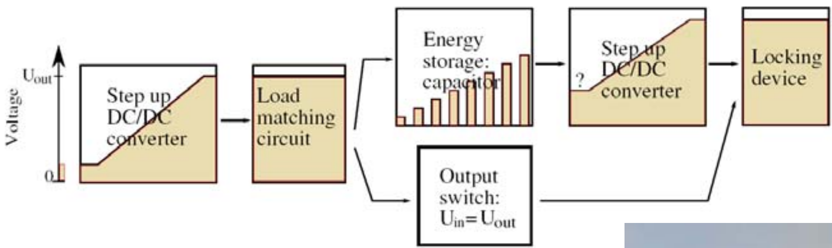

⇒ conversion efficiency up to 55%

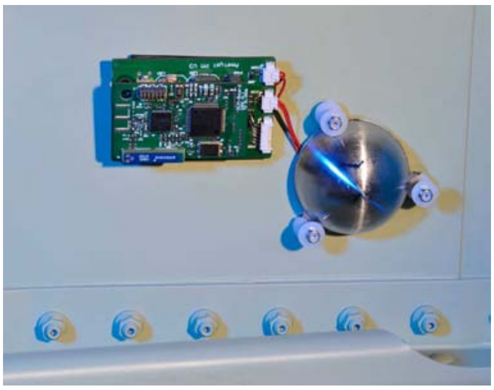

EADS

Flight test

Flight test of the harvester:

Flight test

Flight test of the harvester:

Flight test

Flight test of the harvester:

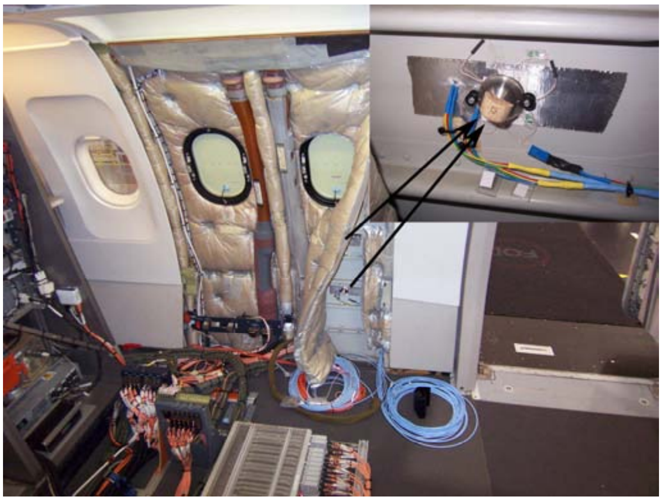

Conclusion

- energy harvesting in aircraft is possible
- thermoelectricity is the most promising candidate
- efficient power management is needed
- flight test proved the concept

References

[1] Airline financial detail report.
[2] Wiring tips up A380 schedule. International Herald Tribune, June,14th 2006.
[3] Darren FYE Shashank PRIYA, Chih-Ta CHEN and Jeff ZAHND. Piezoelectric windmill: A novel solution to remote sensing. Japanese Journal of Applied Physics, 44(3):104–107, 2005.
[4] Ingo Hüttl Rolf Pelster, Reinhard Pieper. Thermospannungen - Vielgenutzt und fast immer falsch erklärt! Physik und Didaktik in der Schule und Hochschule PhyDid, 1/4:10–22, 2005.
[6] http://www.ametyst-projekt.de/

Capacitive Icing Detection and Capacitive Energy Harvesting on a 220kV HV Overhead Power Line

Institute of Electrical Measurement
and Measurement Signal Processing

Head of the Institute & Supervisor: Univ.-Prof. DI Dr. Georg Brasseur

in collaboration with APG

Institute of Electrical Measurement and Measurement Signal Processing

Introduction

What is „Icing of Overhead Power Lines"?

- atmospheric icing (aggregation of ice and/or snow)
- onto the surface of overhead conductors
- posing additional weight load (up to several kg/m) to the supporting towers

Source: NOAA, WRH, http://www.wrh.noaa.gov

Michael J. Moser PhD Summit 2011, Linz, 30.6.2011

Countermeasures


Source: Hydro Quebec
http://www.hydroquebec.com


Source: Manitoba Hydro,
www.hydro.mb.ca


Source: http://www.lopour.cz

Further measures:
- AC and DC currents
- dielectric coatings, hydrophobic coatings (CIGRÈ)

How to detect icing?

- Weather monitoring on OHL towers
- Optical, ultrasonic, microwave thickness or line sag measurement:
- Conductor weight measurement
- Optical inspection

- **Aims for a new approach:**
  - **Measurement on the surface of the conductor**
  - **Measurement of minimal quantities of ice**
  - **Autonomous, versatile device**
  - **Idea: Capacitive Measurement?**

Field Simulation for a Capacitive Measurement Setup

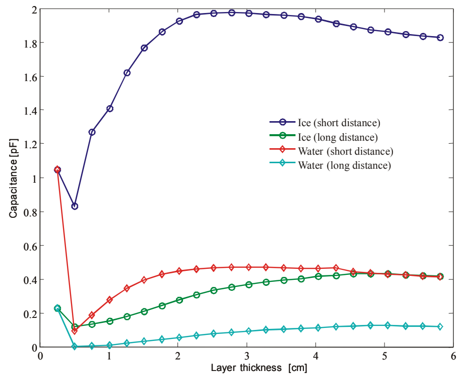

Source: M.J. Moser, B. George, H. Zangl and G. Brasseur: „Icing Detector for Overhead Power Transmission Lines“, Proceedings of the 2009 IEEE Instrumentation and Measurement Technology Conference, pp. 1105-1109

Challenges with capacitive measurement

In general:

- Large offset + small signal changes
- Disturbers/EMC
- Ambiguities (Shielding and Coupling effects)
- Presence of metal (surfaces) adds additional offsets

Here:

- All of the above!
- Field Gradient: measurement of fF in an AC kV environment!

Laboratory Testbed

Melting of clear ice

Icing from droplets

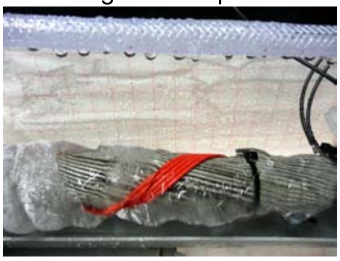

Clear ice layer

Institute of Electrical Measurement and Measurement Signal Processing

Laboratory Results

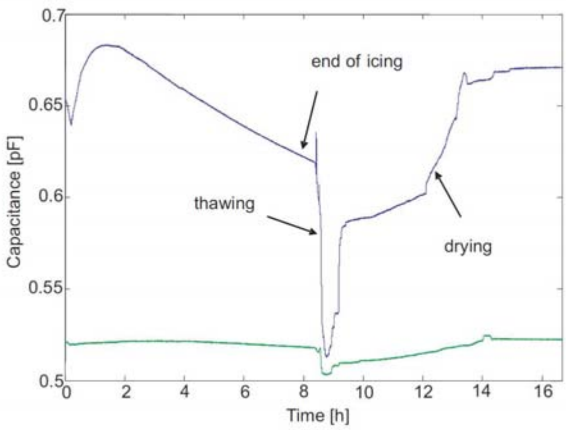

M.J. Moser, B. George, H. Zangl and G. Brasseur:, „Icing Detector for Overhead Power Transmission Lines", Proceedings of the 2009 IEEE Instrumentation and Measurement Technology Conference, pp. 1105-1109

Michael J. Moser PhD Summit 2011, Linz, 30.6.2011

Energy Harvesting

How to get energy for autonomous operation?

- *Batteries.* Only for lowest power demands.
- *Current Transformer*. Depends on a minimum current in the line.
- *Solar panels.* Depend on sunlight, need much space, are comparatively inefficient. Suffer from pollution.

- *Capacitive Energy Harvesting?*

Capacitive Energy Harvester

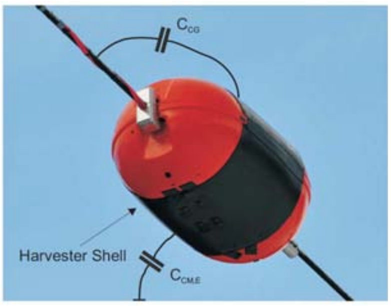

Source:

This device just needs a live power line but the line does not need to transport power (compared with current transformers).

Power Demand

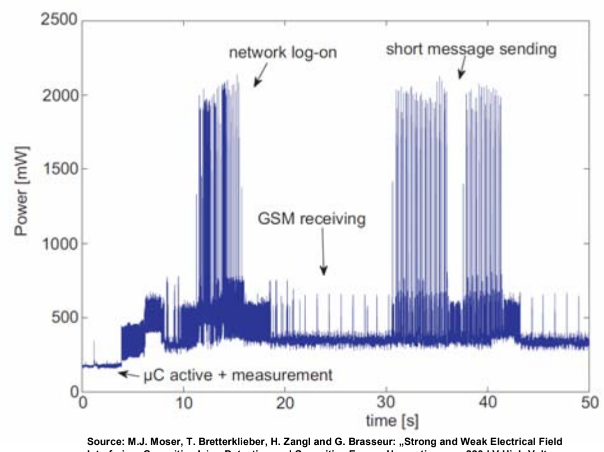

Source: M.J. Moser, T. Bretterklieber, H. Zangl and G. Brasseur: „Strong and Weak Electrical Field Interfering: Capacitive Icing Detection and Capacitive Energy Harvesting on a 220-kV High-Voltage Overhead Power Line“, IEEE Transactions on Industrial Electronics, Vol. 58, No. 7, July 2011, pp. 2597-2604

HV Laboratory Test Setup

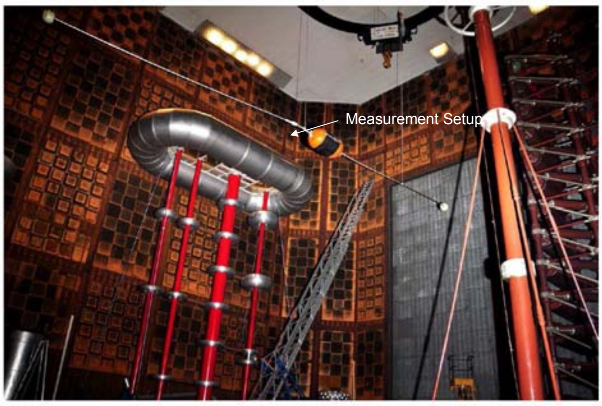

Institute of Electrical Measurement and Measurement Signal Processing

HV Laboratory Test Setup (cont'd)

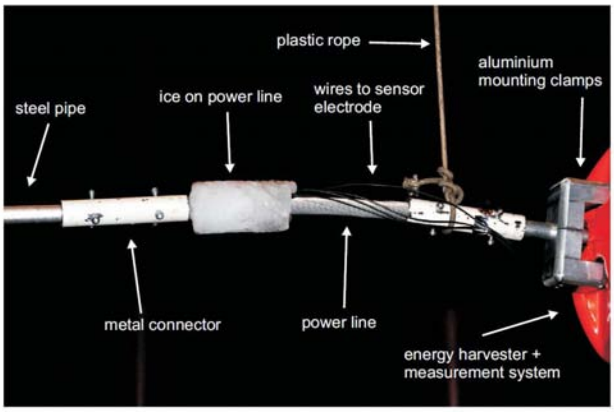

Michael J. Moser | PhD Summit 2011, Linz, 30.6.2011

Institute of Electrical Measurement and Measurement Signal Processing

Field Test on a 220 kV Line

Michael J. Moser | PhD Summit 2011, Linz, 30.6.2011

Results

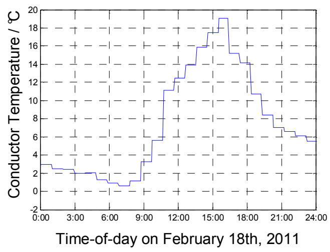

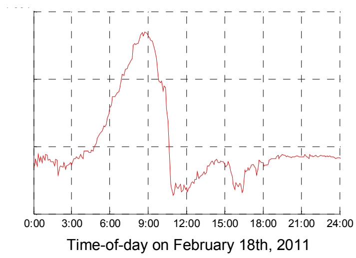

-> Conductor temperature is around 0°C for a short period of time

-> A thin layer of soft rime is forming @ 3 a.m. and melts again @ 9 a.m.

Summary

- Approach is feasible, icing events were successfully detected.
- Evaluation of multiple capacitances allows estimation of the thickness of the ice layer.
- High sensitivity occurs for thin layers of ice – good for timely application of comparatively simple counter measures.
- Field Test until 05/2011
- Industrialization, first installations planned in winter 2011/12

Acknowledgment

Thank you for your valuable support:

- Herbert Lugschitz & Gerhard Bernhard
- Hubert Zangl, Thomas Bretterklieber & the Sensors&Instrumentation Working Group

Sensor Integration in digital microfluidic systems

PhD Summit ARGE Sensorik
Thomas Lederer

JOHANNES KEPLER UNIVERSITY LINZ | JKU

Outline

- **Microfluidics**
- **EWOD**
- **QCM**
- **Results (+Outlook)**
- **Impedance spectroscopy**
- **Results (+Outlook)**

Micro fluidics

Microfluidics

Investigation of Properties as well as manipulations of small amounts of fluids (<nl)

Digital Microfluidics

Electro wetting on Dielectrics (EWOD)

Key Advantages

-short reaction times
-reduced consumption of reagents and sample materials
-high achievable level of automation

Sensor Principles

-Functionalized resonant sensor
-Impedance spectroscopy

Electrowetting on Dielectrics (EWOD)

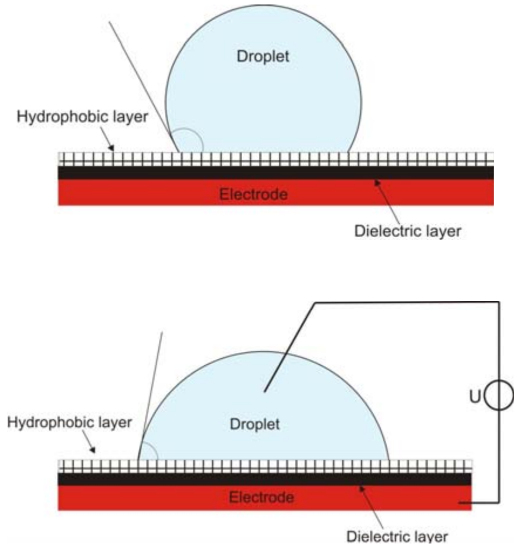

Lippmann-Young equation:

$$(\cos\theta) = \cos(\theta_0) + \frac{cV^2}{2\gamma_{LG}}$$

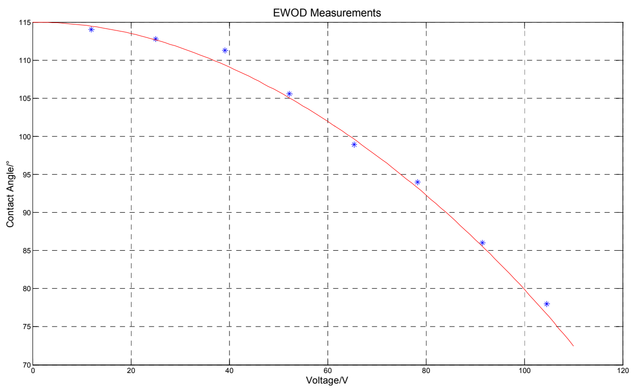

EWOD Realisation

EWOD Translation

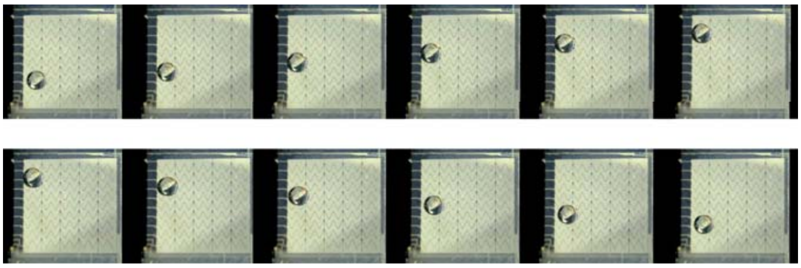

Sensor integration

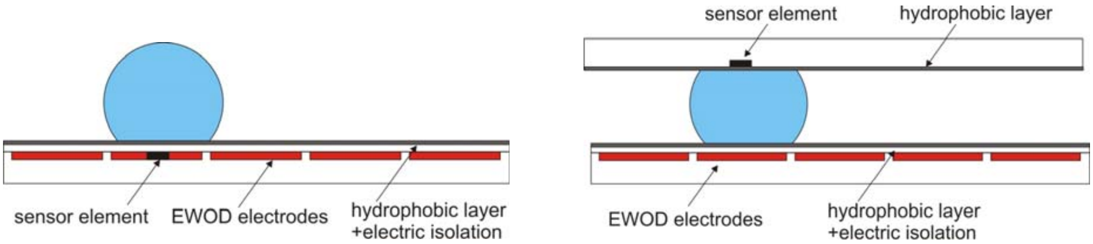

Quarz Crystal Microbalance

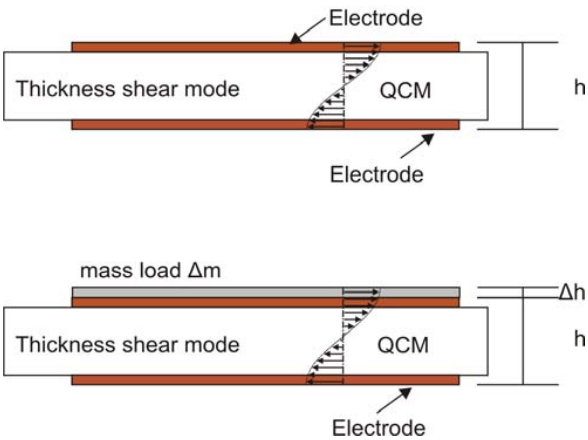

Sauerbrey Equation:

$$\Delta f = -2 f_0^2 \Delta m / \sqrt{\rho\mu}$$

Frequency shift dependent on the square of the fundamental resonance frequency f0

Resonance Condition: $f_0 = \frac{\sqrt{\mu / \rho}}{2h}$ → Thin Resonators !

QCM integration

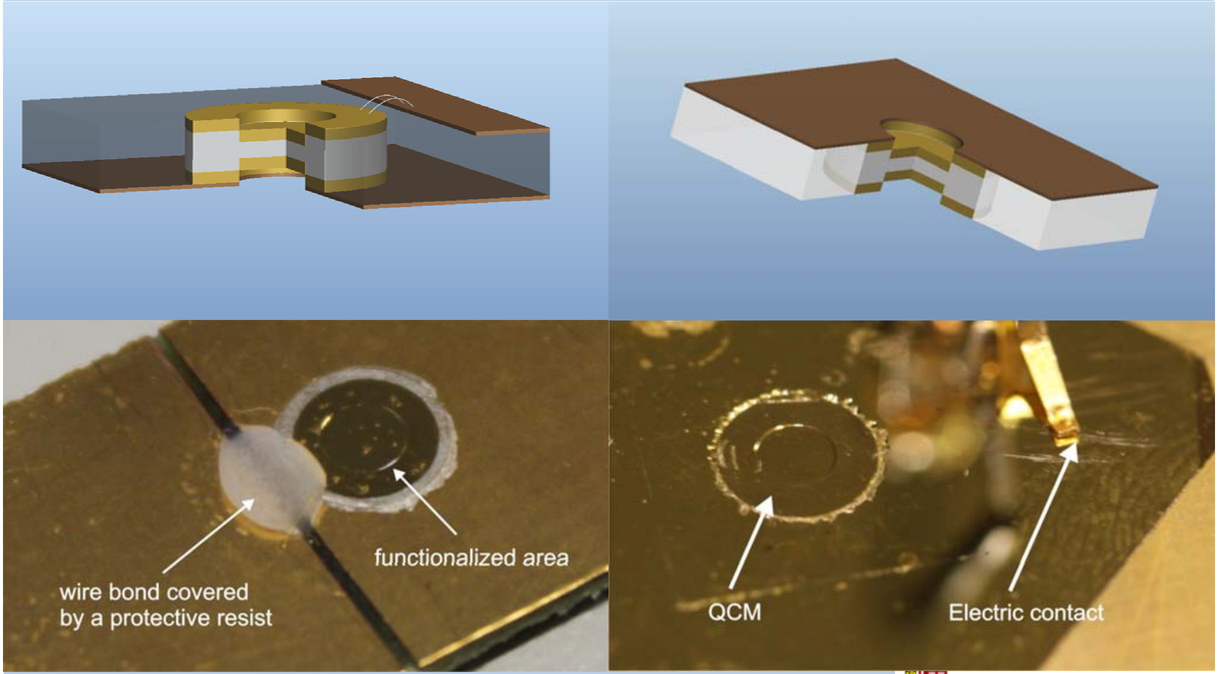

Possible Applications

- density/viscosity
- mass deposition (sedimentation)
- binding of molecules
  (unspecific/ specific)

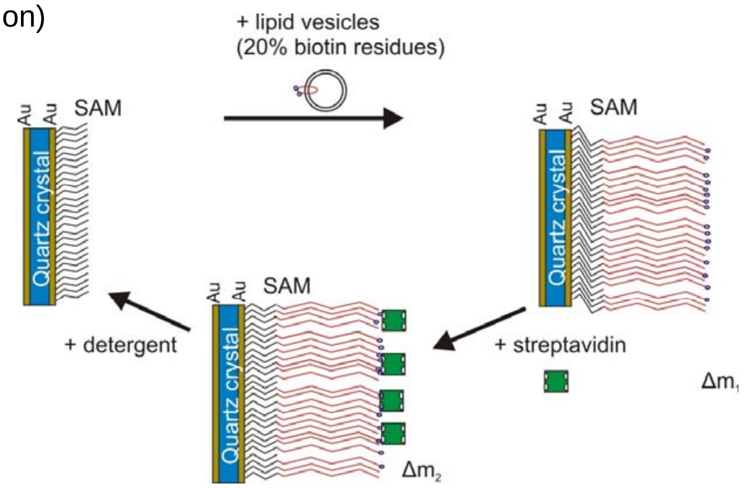

Detection of binding bio-molecules

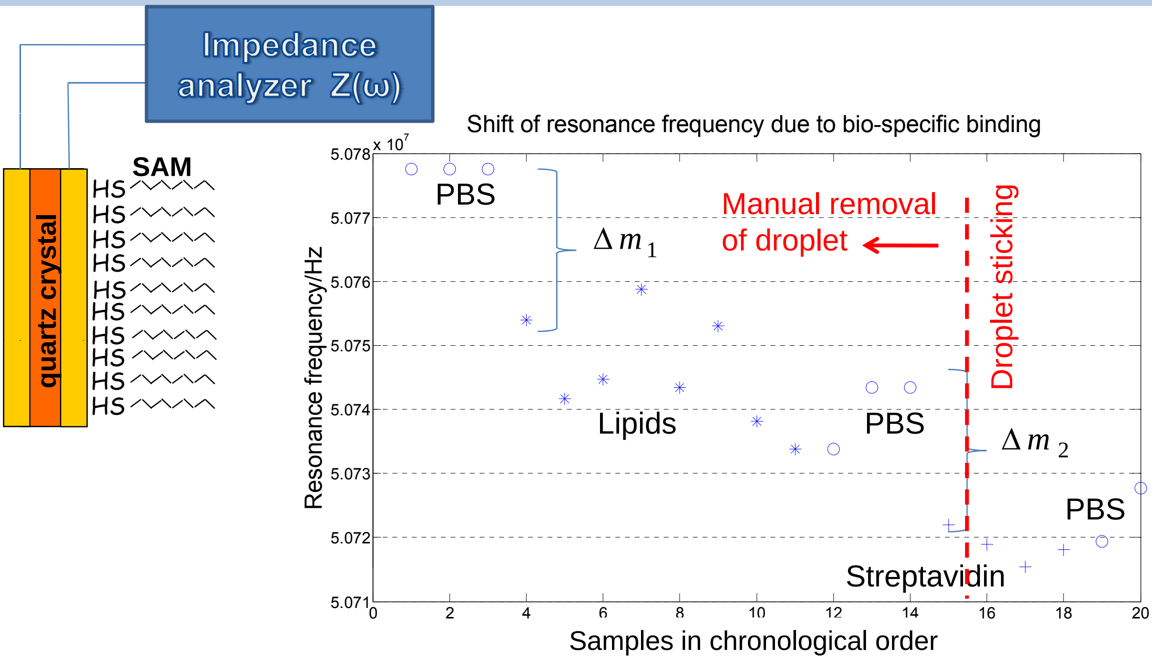

Optical measurement of the contact angle

→ Observed decrease of the contact angle du to specific binding on Bio-functionalized surface

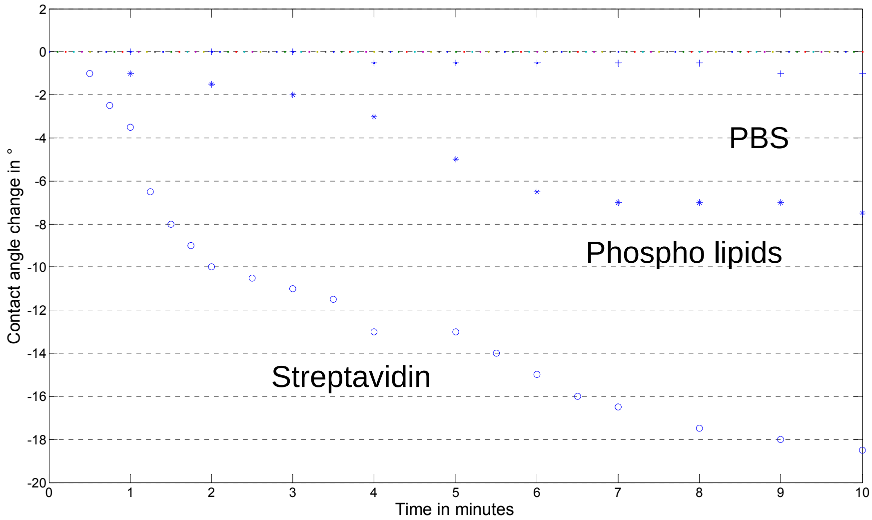

Discussion

- Detection of bio-molecules by measuring the shift of the resonance frequency
- Sticking problem due binding of the bio-molecules

Outlook

-Releasing the bio-molecules by washing with detergents

- Droplet pushing

Impedance Spectroscopy

Impedance function between two ports

$$Z(\omega) = Z'(\omega) + jZ''(\omega)$$

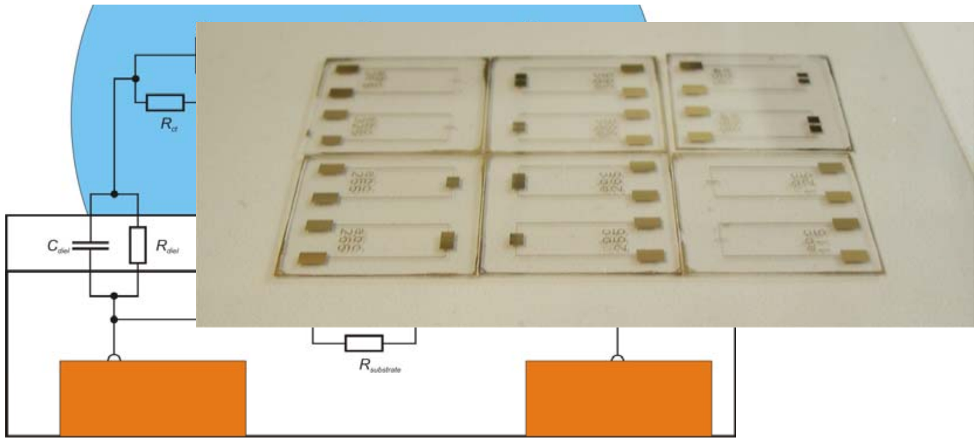

Material Selection

Bode plots of impedance of a DI-Water droplet onto dielectric materials

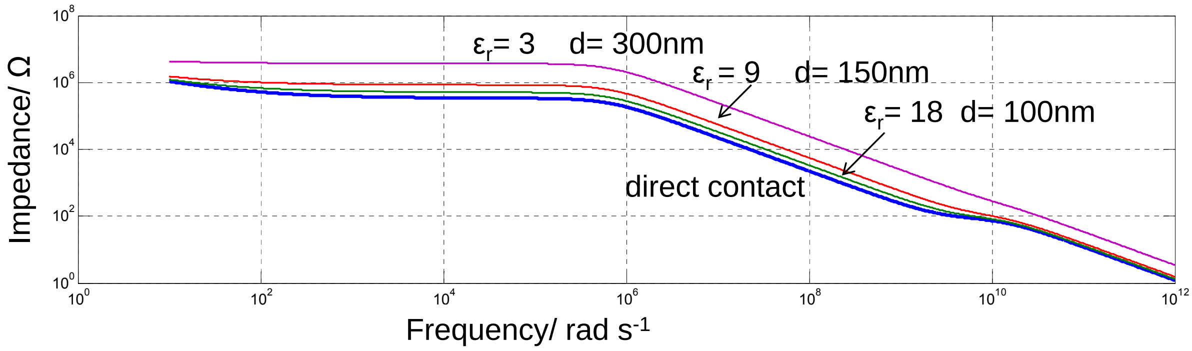

Measurement sequence

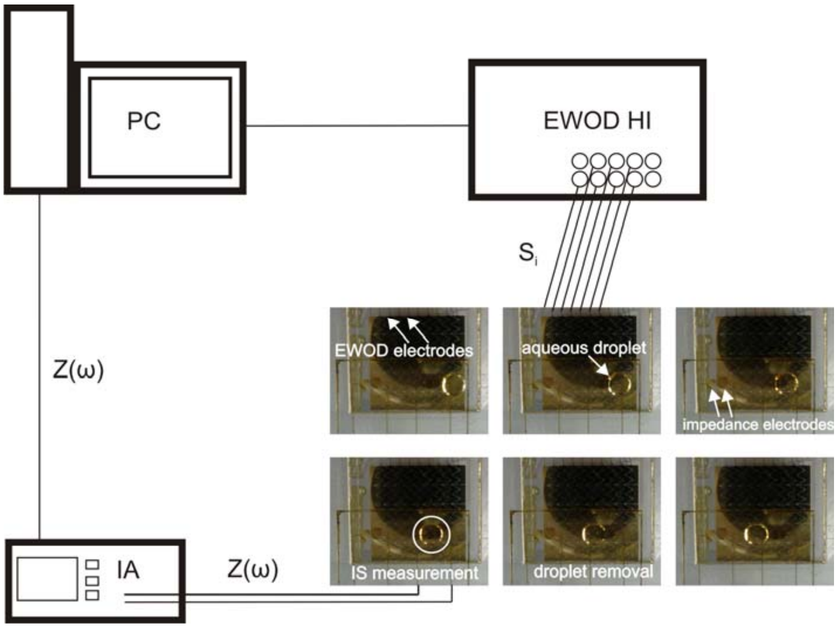

Measurement (Temperature)

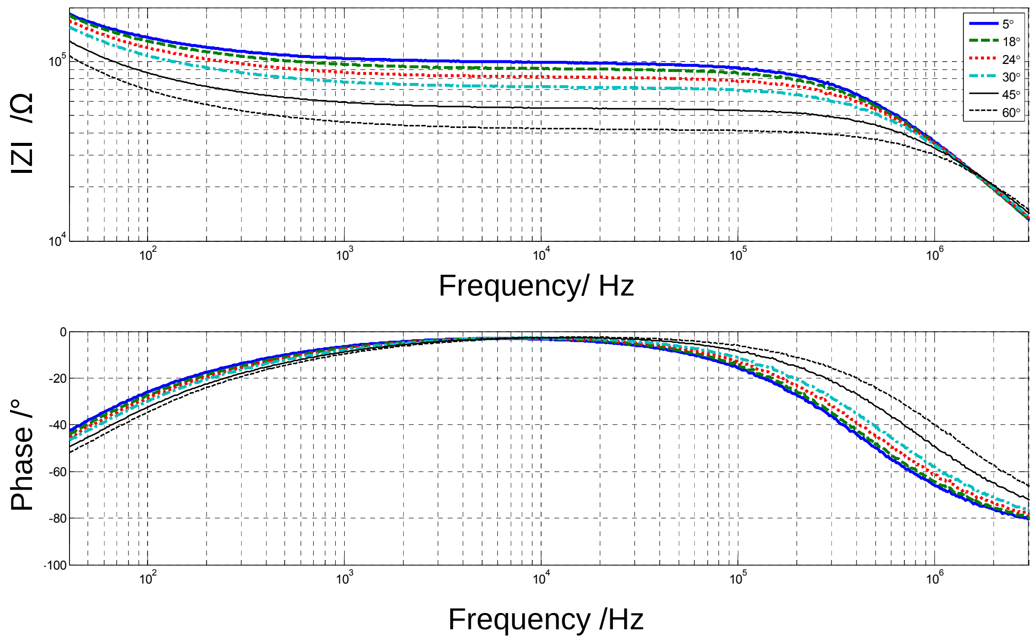

JOHANNES KEPLER UNIVERSITY LINZ | JKU

Measurement (Sedimentation)

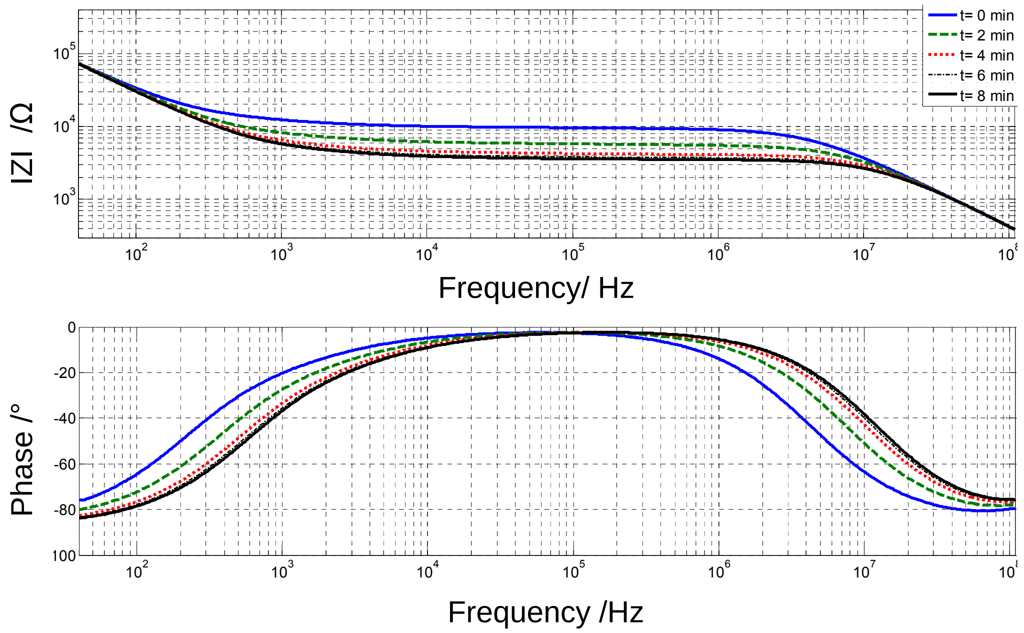

JOHANNES KEPLER UNIVERSITY LINZ | JKU

Measurement (Ion concentration)

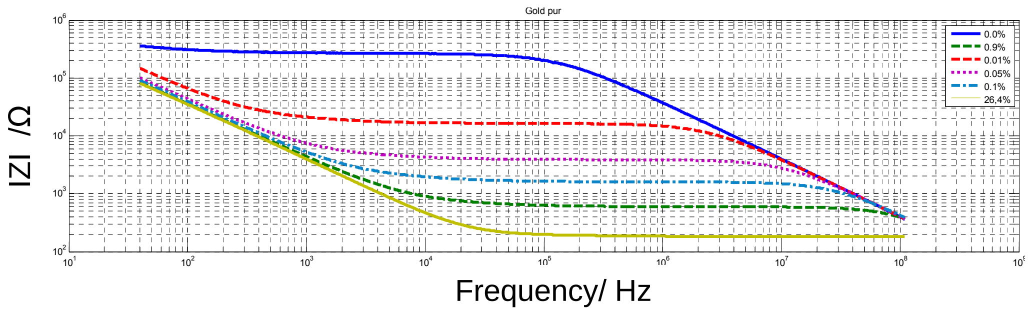

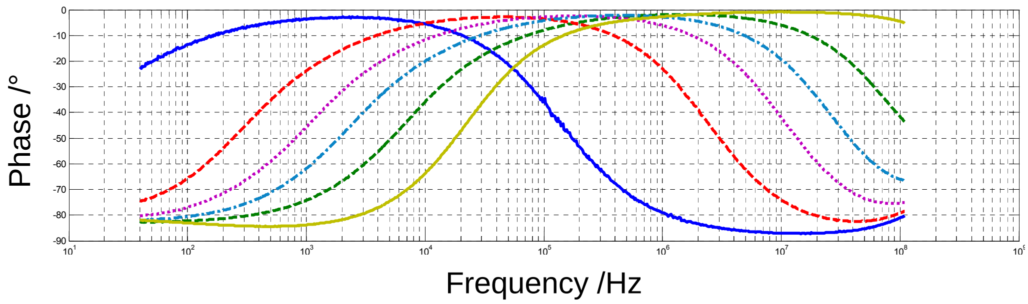

Discussion

- All electric measurement of various chemical and physical parameters
- Suitable for online-measurements of chemical reactions

Outlook

-Measurement on biologic samples

- Combination with RF-heating or with a dielectrophoretic concentration setup

Sensor Integration
in digital microfluidic systems

Thank You for Your Attention

JOHANNES KEPLER UNIVERSITY LINZ | JKU

TECHNISCHE UNIVERSITÄT WIEN Vienna University of Technology

isas

Label-Free Cell Analysis:
An Infrared Sensor for CH_2-stretch Ratio Determination

Sander van den Driesche
Institute of Sensor and Actuator Systems
Vienna University of Technology
driesche@tuwien.ac.at
ARGE Sensorik PhD Summit, 30. June 2011

TECHNISCHE UNIVERSITÄT WIEN Vienna University of Technology

- 2 -

isas

Overview

- Motivation and objectives
- Sensor design and realisation
- Label-free tumour screening
- Conclusions

01 July 2011 Sander van den Driesche

Motivation

Tumour screening: Biopsy

- **Labelling** and **staining** methods based on **morphological interpretation**
- High number of **false positives** and **false negatives**
- **Early detection** and **accurate staging** of the primary tumour will **increase** the **overall survival** rate tremendously

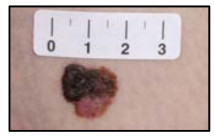

Objectives

1) to design a novel **tumour cell indicator** based on the cells **physical properties**

2) to design and realise a **sensor system**

Sensor design and realisation

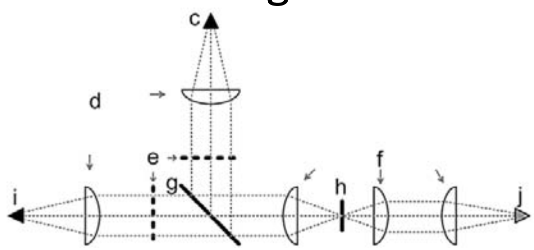

c: LED
d: plano convex lens
e: narrow band-pass filter
f: plano convex lens
g: beam-splitter
h: sample
i: LED
j: photodiode

S. van den Driesche, W. Witarski, S. Pastorekova, and M. J. Vellekoop, *Meas. Sci.Technol.*, vol. 20, pp. 124015, 2009 .

S. van den Driesche, W. Witarski, and M. J. Vellekoop, in *Proc of SPIE vol. 7362*, Dresden, Germany, May 2009, pp. 73 620Y–73 620Y–9.

S. van den Driesche, W. Witarski, C. Hafner, H. Kittler, and M. J. Vellekoop, in *Proc IEEE Sensors*, Christchurch, New-Zealand, Oct. 25-28, 2009, pp. 1562–1566.

S. van den Driesche and M. J. Vellekoop, Utility model, DE 20 2009 006 771.8, AT 11722(U1), 2009.

S. van den Driesche, C. Haiden, W. Witarski, and M. J. Vellekoop, in *Proc of SPIE vol. 8066*, Prague, Czech Republic, April 2011,pp. 80660E–80660E-8.

The CH_2-stretches

Infrared absorbance spectra comparison of **normal** and **tumour** cells (colorectal, breast, oesophagus, blood, melanocytes, and brain) show **differences** in the wavelength region between **3 and 4 µm**

- **Functional** infrared absorbance **bands**:

Wavelength (µm)	Function
3.42	CH_2-antisymmetric stretch
3.51	CH_2-symmetric stretch

The CH_2-stretch ratio

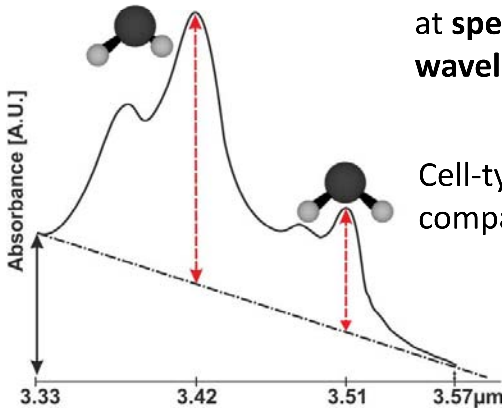

Record IR absorbance values at **specific functional wavelengths**

Cell-type discrimination by comparing **peak ratio's**
baseline correction required due to **water** content and **sample thickness**

Baseline correction

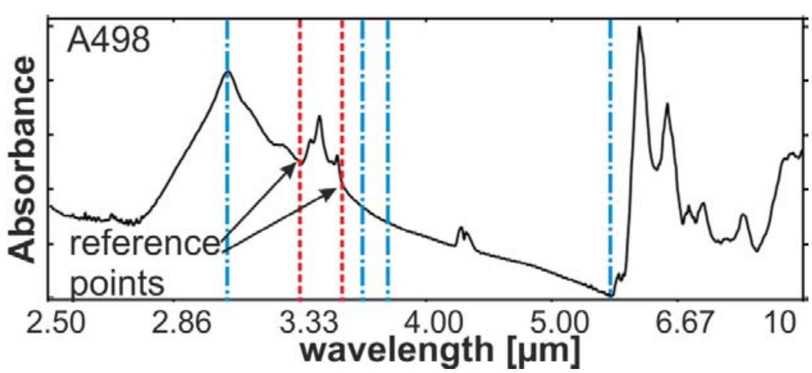

Different baseline procedures have a very small influence on the CH_2-stretch ratio

TECHNISCHE UNIVERSITÄT WIEN Vienna University of Technology

- 9 -

isas

Quadruple-wavelength sensor system

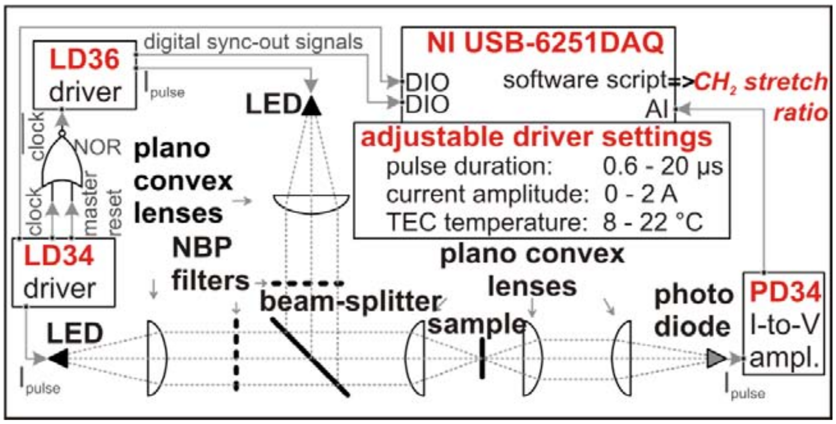

01 July 2011 Sander van den Driesche

TECHNISCHE UNIVERSITÄT WIEN Vienna University of Technology

- 10 -

isas

Quadruple-wavelength sensor system

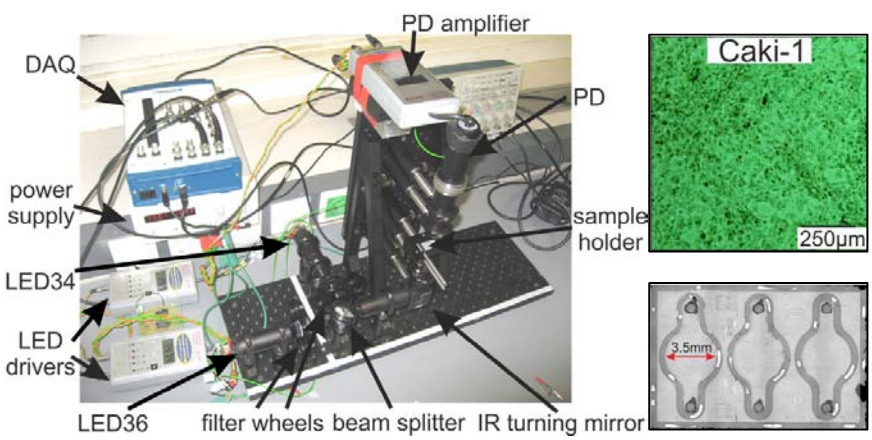

01 July 2011 Sander van den Driesche

CH_2-stretch ratio measurement

Four spots per cell line measured

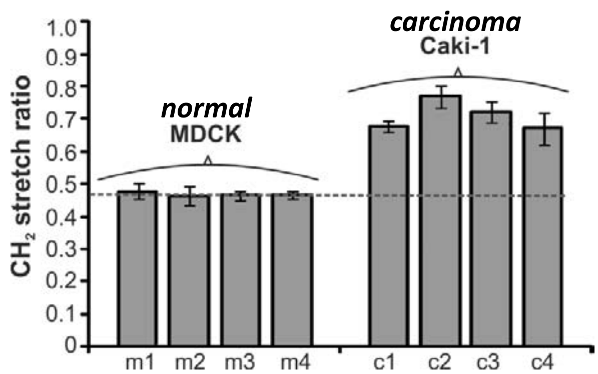

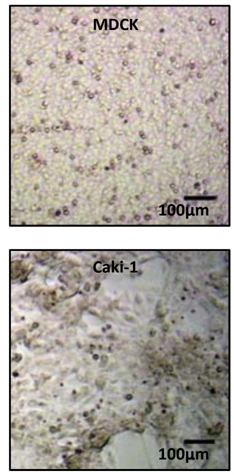

Label-free tumour screening

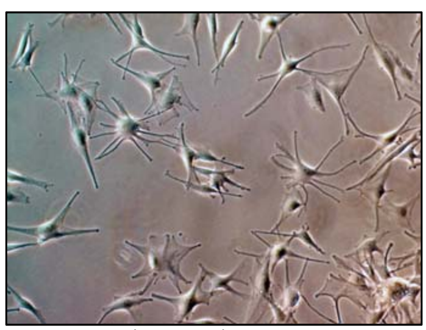

human melanocytes

S. van den Driesche, W. Witarski, and M. J. Vellekoop,
in *IFMBE Proceedings,* vol. 25/VIII, Munich, Germany, Sept. 2009 , pp. 15–18.

S. van den Driesche, W. Witarski, S. Pastorekova, H. Breiteneder, C. Hafner, and M. J. Vellekoop,
Analyst, 2011.

Epithelial kidney carcinoma

Investigation of normal and carcinoma kidney cell lines

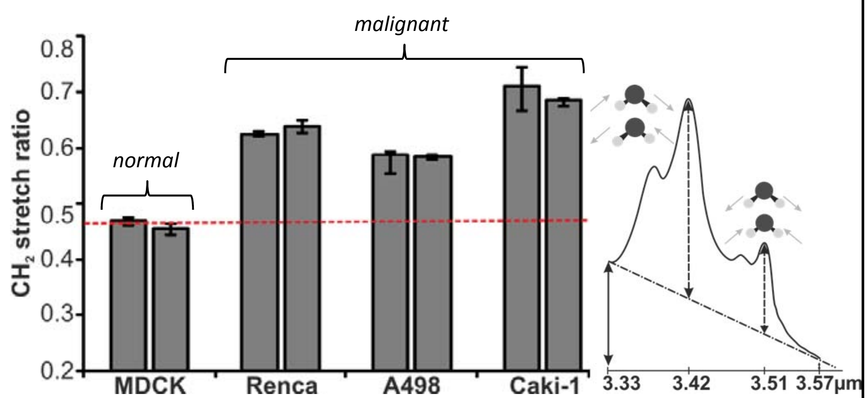

Melanoma

Investigation of melanocytes and melanoma cell lines

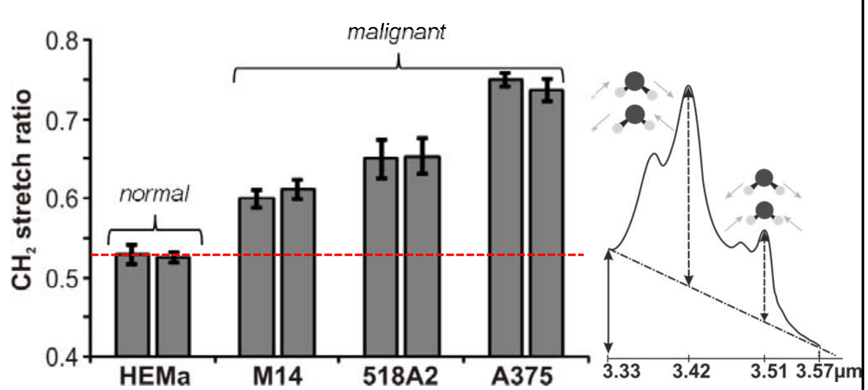

Mechanism investigation

Normal mammalian **plasma membranes** consist of about **20-25%** lipid mass **cholesterol**

A **decreased** concentration of **membrane stabilizing cholesterol** per area has been found for **malignant breast cells** and **melanocytes** compared to their normal cells

=> An **increase** in the **CH_2-stretch** ratio of normal cells is expected when **reducing** the **cholesterol concentration**

Mechanism investigation

Reducing the average plasma membrane cholesterol concentration yielded in a higher CH_2-stretch ratio

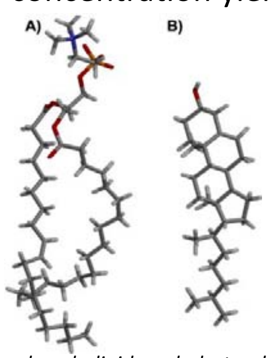

phospholipid *cholesterol*

Heller et al. 1993

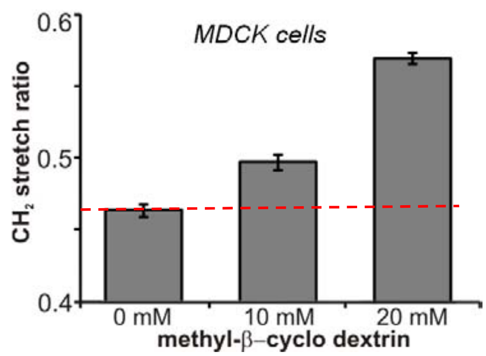

TECHNISCHE UNIVERSITÄT WIEN Vienna University of Technology

- 17 -

isas

Suspended melanoma cells

Investigation of in phosphate-buffered-saline melanoma cell lines

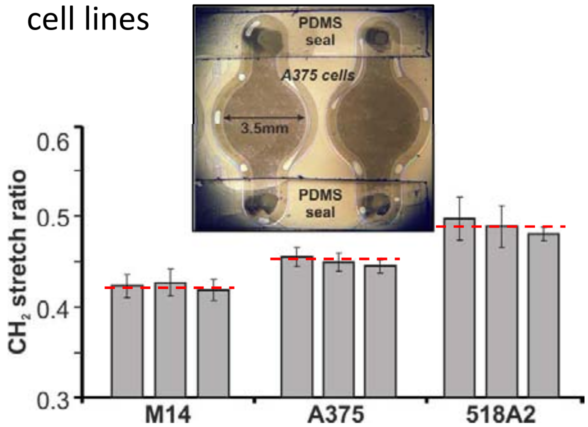

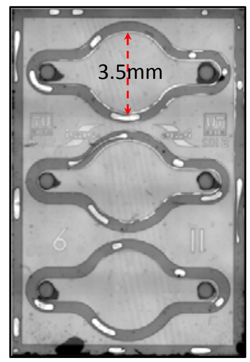

01 July 2011 Sander van den Driesche

TECHNISCHE UNIVERSITÄT WIEN Vienna University of Technology

- 18 -

isas

Conclusions

The realised **IR sensor system** was **successfully tested** for **normal** and various **malignant cell lines**, both in **dried** condition and in **suspension**

The **CH_2-stretch ratio** based **cell discrimination** method can aid physicians in the diagnosis of suspicious tissues

01 July 2011 Sander van den Driesche

TECHNISCHE UNIVERSITÄT WIEN Vienna University of Technology

- 19 -

isas

Acknowledgements

- Prof. Dr. Michael Vellekoop and Prof. Dr. Peter Verhaert
- Master students Dietmar Puchberger-Enengl, Vivek Rao, Christoph Haiden, and Helene Zirath
- Colleagues at the Institute of Sensor and Actuator Systems, TU Wien
- Group of S. Pastorekova, Institute of Virology, SAS Bratislava
- C. Hafner, Institute for Pathophysiology, Medical University of Vienna
- Group of B. Lendl, Analytical Biotechnology, TU Wien
- Colleagues of the CellCheck consortium
- The work was part of the EU Marie Curie Research Training Network, MRTN-CT-2006-035854, On-Chip Cell Handling and Analysis “CellCheck”

Thank you for your attention!

01 July 2011 Sander van den Driesche

Composition monitoring in a gas phase polymerization process

Institute for Microelectronics und Microsensors
Johannes Sell, Alexander Niedermayer, Bernhard Jakoby
Borealis Polyolefine GmbH
Sebastian Babik, Christian Paulik

Austrian Center of Competence in Mechatronics

Contents

- Problem/Motivation
- Density measurement
- IR
- Conclusion

Polymerization Process

Cooperation of ACCM and Borealis

Polymerization: Bonding of monomers to polymers

Monomers (e.g. propene)

Catalysts

Polymers

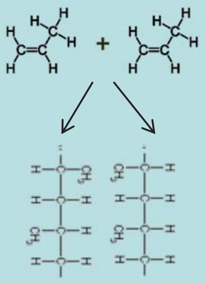

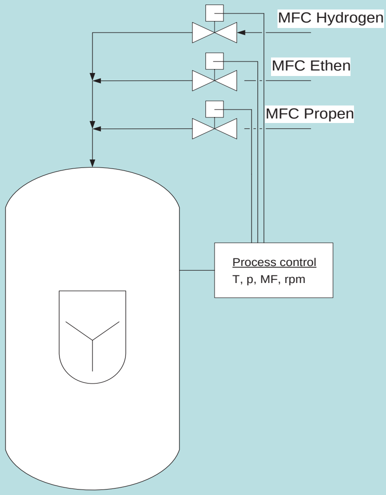

Typcial polymerization reactor

Austrian Center of Competence in Mechatronics
ACCM AUSTRIAN CENTER OF COMPETENCE IN MECHATRONICS

Polymerization Process

Problem

Different monomers are integrated into polymer chain with different probability.
=> Concentration ratio changes during reaction

Objective

Monitoring of the gas composition during the process
- Measurement time: < a few seconds
- Integration into the polymerization reactor

Approach

2 measurements to measure composition of a 3 component gas
- Density
- IR Absorption

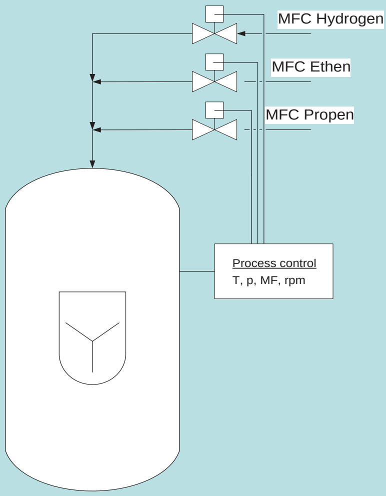

Typcial polymerization reactor

JKU JOHANNES KEPLER UNIVERSITÄT LINZ
LCM LINZ CENTER OF MECHATRONICS GMBH

Density measurement

Test system

- Pressure vessel
  - temperature
  - pressure

- Gases
  - propene
  - ethene
  - CF_4
  - N_2

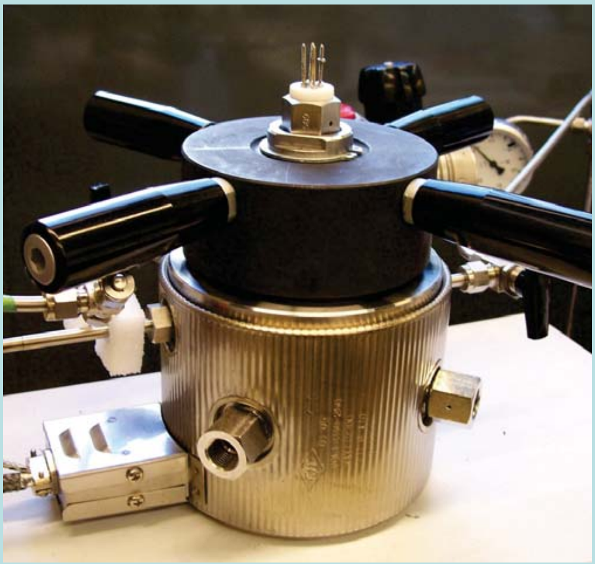

Austrian Center of Competence in Mechatronics

Density measurement

- Equivalent Circuit Model of a quartz tuning fork resonator [1]

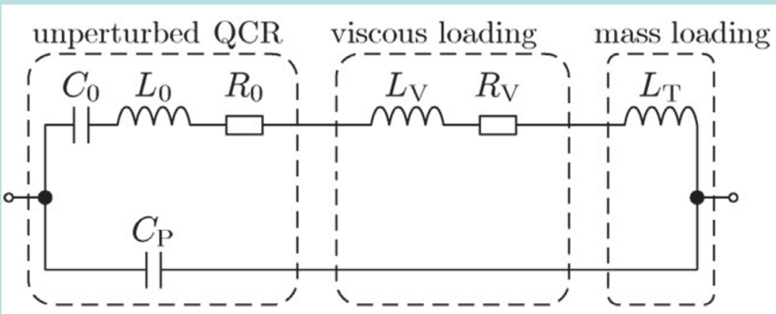

$$Z_m = R_0 + j(\omega L_0 - 1/(\omega C_0))$$
$$Z_V = B\sqrt{\rho\eta\omega}$$
$$Z_T = A\,\rho\omega$$

[1] L.F. Matsiev, *Proc. IEEE Ultrasonics Symposium* (2000), 427-434

Density measurement

- Measure frequency shift and motional resistance in dependence on pressure

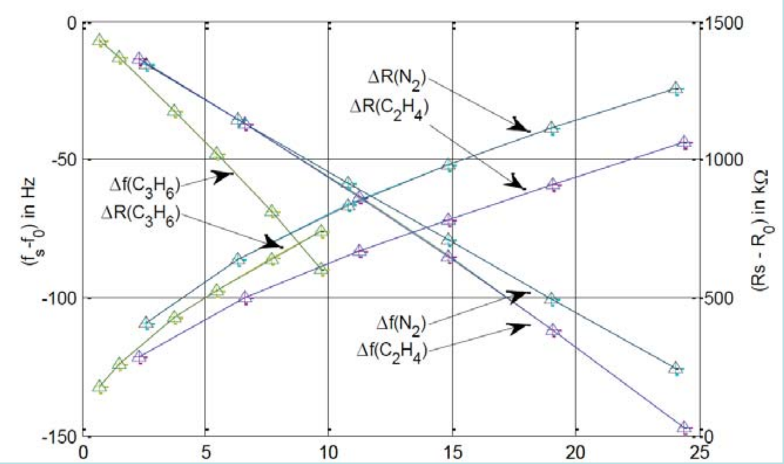

pressure in bar

Austrian Center of Competence in Mechatronics

Density measurement – Pressure Dependence

Remove viscosity dependence

$$L'C_0 = \frac{1}{\omega_s^2} = L_0C_0 + AC_0\rho + \frac{R-R_0}{\omega_s}$$

Measured resonance frequency of the motional branch

influence of viscous damping

$$\Rightarrow \frac{1}{\omega_{s,comp}^2} = \frac{1}{\omega_s^2} - \frac{R-R_0}{\omega_s}$$

$$= AC_0\rho + \frac{1}{\omega_0^2}$$

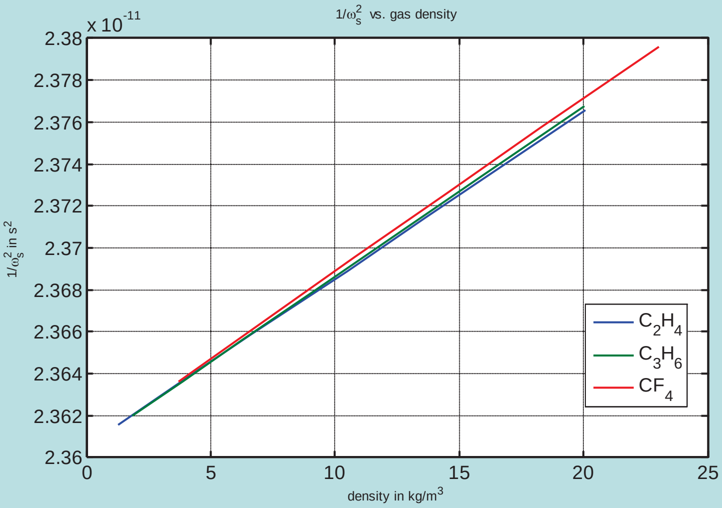

JKU JOHANNES KEPLER UNIVERSITÄT LINZ LCM LINZ CENTER OF MECHATRONICS GMBH

Density measurement – Pressure Dependence

Consider additional pressure dependent impedance

$$\Rightarrow \frac{1}{\omega_{s,comp}^2} = AC_0\rho + \frac{1}{\omega_0^2}$$

$$= \frac{1}{\omega_s^2} - \frac{R - R_0}{\omega_s} - \mathbf{Dp}/\boldsymbol{\omega_s}$$

Modeled by additional impedance $Z_p(p) = Dp$

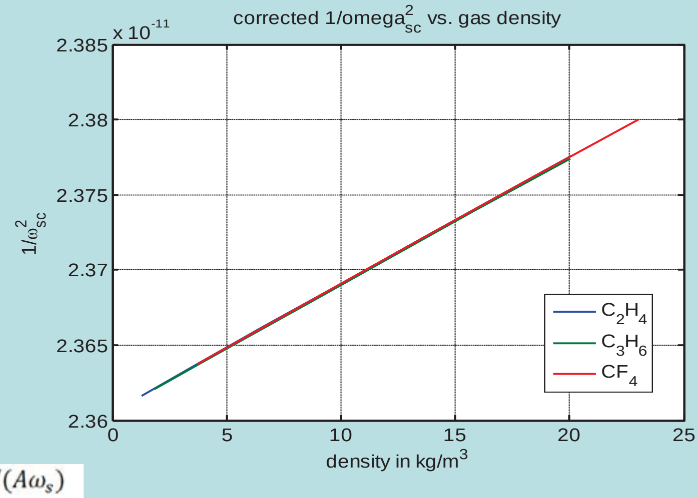

$$\rho = (1/(\omega_s C_1) - \omega_s L_1 - (Re(Z) - R_1 + Dp))/(A\omega_s)$$
$$\eta = ((Re(Z) - R_1)/B)^2/(\omega_s \rho),$$

By measurement of R_0, f_{sm0} and p, density and viscosity can be calculated

Austrian Center of Competence in Mechatronics

Determine f_s and R_1 by fitting the model to impedance spectra

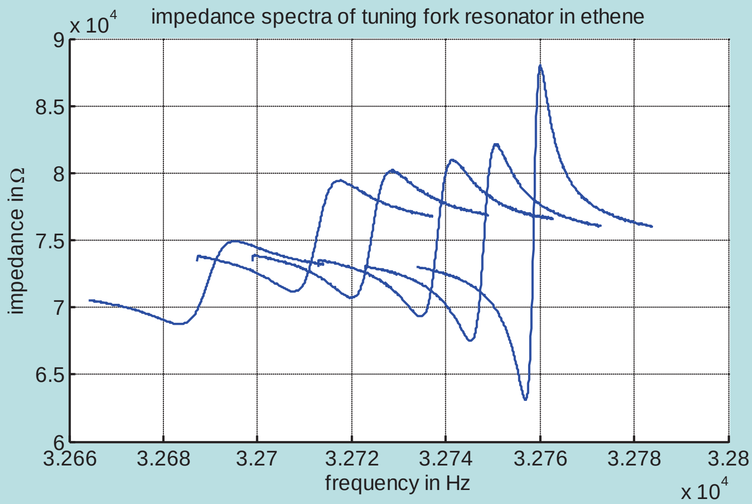

Long measurement time (about 1 min)

JKU JOHANNES KEPLER UNIVERSITÄT LINZ LCM LINZ CENTER OF MECHATRONICS GMBH

Measurement system

Frequency tracking system, based on Impedance Analyzer [2]

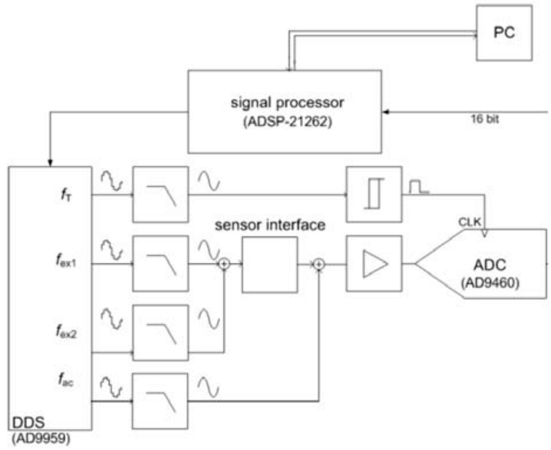

Fig. 2: Schematic description of the measurement system

- Normal operation: Continuous measurement of R_1 at f_s

⇒ Fast and accurate measurement

- Main components:
  - Digital signal processor
  - Direct Digital Synthesizer
  - Analog-To-Digital Converter
  - Serial Connection to PC
- Compensation techniques:
  - digital
  - Analog

[2] **A.O. Niedermayer, E.K. Reichel and B. Jakoby,** "Yet Another Precision Impedance Analyzer (YAPIA) For Resonating Sensors", Eurosensors 2008

Austrian Center of Competence in Mechatronics

ACCM AUSTRIAN CENTER OF COMPETENCE IN MECHATRONICS

Density measurement – Accuracy

Relative error in density measurement

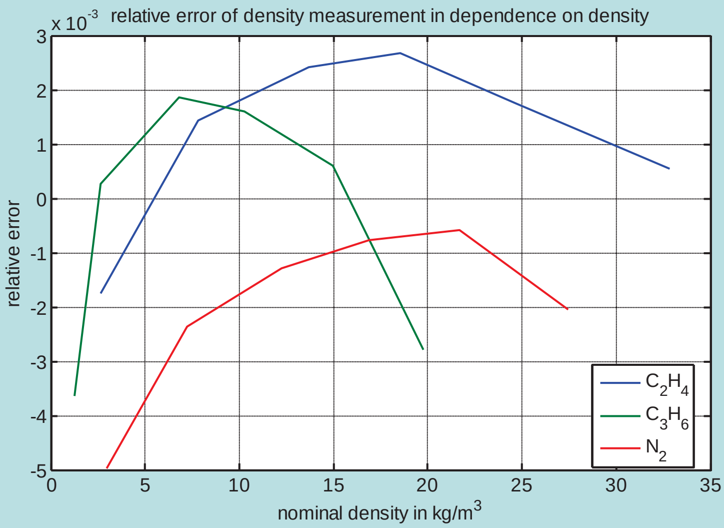

Viscosity measurement

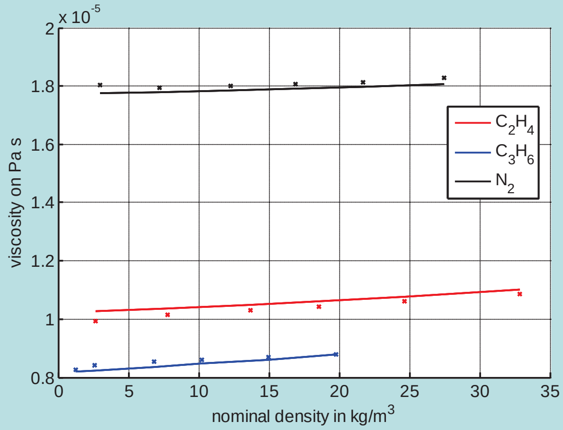

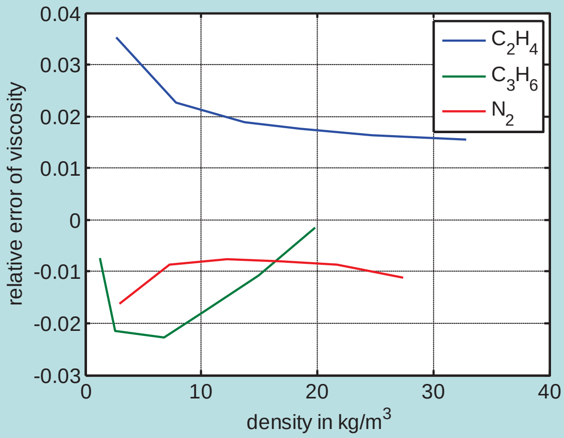

Accuracy is limited by reference data(viscosity: ≈ 5%, density 0.05%)

Austrian Center of Competence in Mechatronics
ACCM AUSTRIAN CENTER OF COMPETENCE IN MECHATRONICS

IR

- IR absorption of ethene and propene

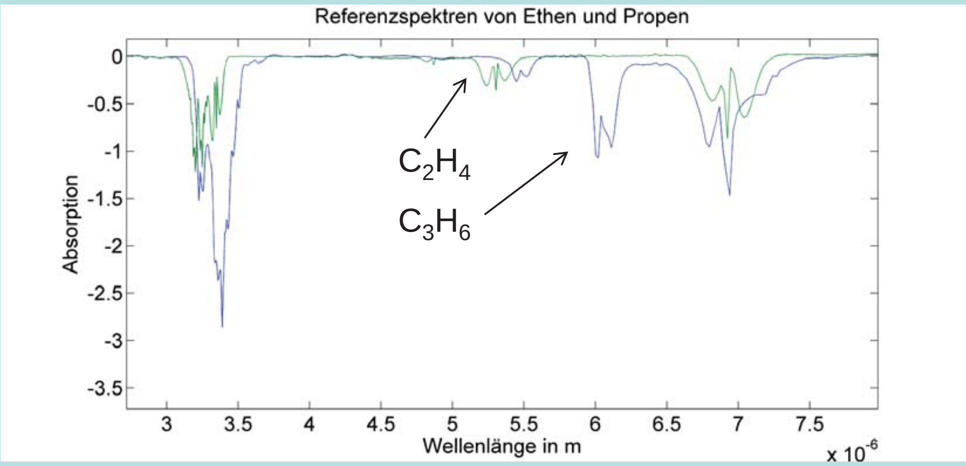

JKU JOHANNES KEPLER UNIVERSITÄT LINZ LCM LINZ CENTER OF MECHATRONICS GMBH

IR

Measurements with FTIR Spectrometer

Transmission path 0.75 mm

Measurement cell

- Integrated T-sensor
- Pressure sensor
- CaF_2 window
  (pressure tested to 50 bar)

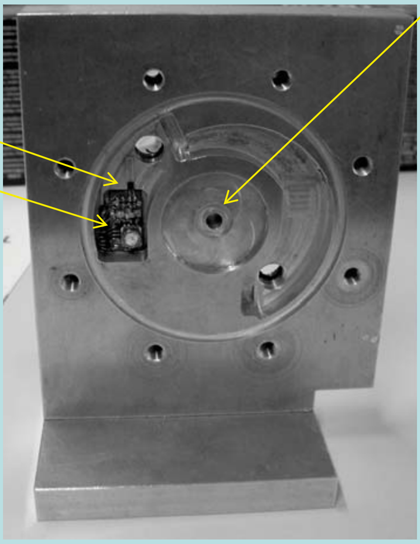

Can concentration be measured

- 1:1 mol sample provided by Borealis

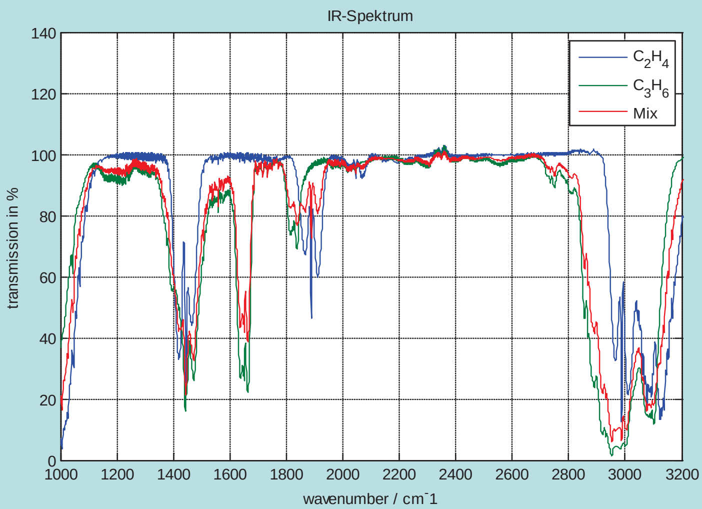

C_2H_4:	10.295 bar
C_3H_6:	7.80 bar
Mix:	ca. 9 bar

Can concentration be measured

Analysis

$$A(\nu) = \log\left(\frac{I(\nu)}{I_0(\nu)}\right) = \alpha_1(\nu)\rho_1 + \alpha_2(\nu)\rho_2$$

Solve:

$$l\begin{pmatrix}\alpha_{prop}(\nu_1) & \alpha_{eth}(\nu_1)\\ \vdots & \vdots \\ \alpha_{prop}(\nu_n) & \alpha_{eth}(\nu_n)\end{pmatrix}\begin{pmatrix}\rho_1\\ \rho_2\end{pmatrix} = \begin{pmatrix}A(\nu_1)\\ \vdots \\ A(\nu_n)\end{pmatrix}$$

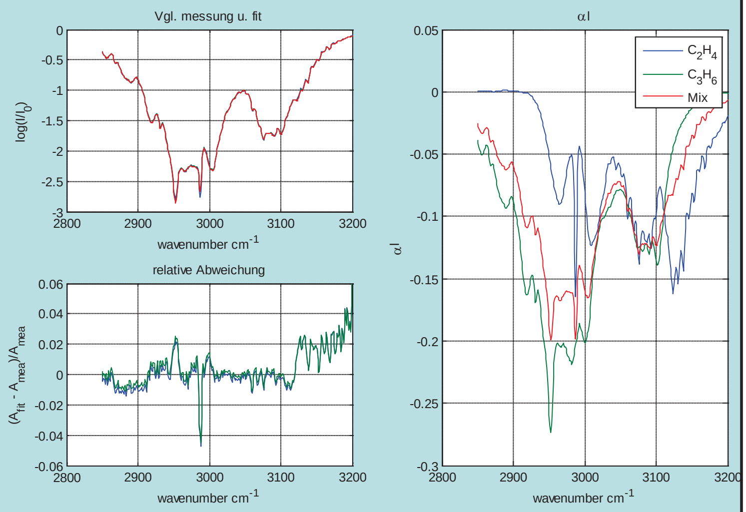

mol-ratio: 1.000 : 1.343 (Ethen - Propen)

density: ρ_{eth}=4.640 kg/m³, ρ_{prop}= 9.348 kg/m³

Austrian Center of Competence in Mechatronics

Can concentration be measured

Bande: 1620-1670 cm^{-1}

- $$l\begin{pmatrix}\alpha_{prop}(\nu_1)\\ \vdots \\ \alpha_{prop}(\nu_n)\end{pmatrix}\rho_1 = \begin{pmatrix}A(\nu_1)\\ \vdots \\ A(\nu_n)\end{pmatrix}$$

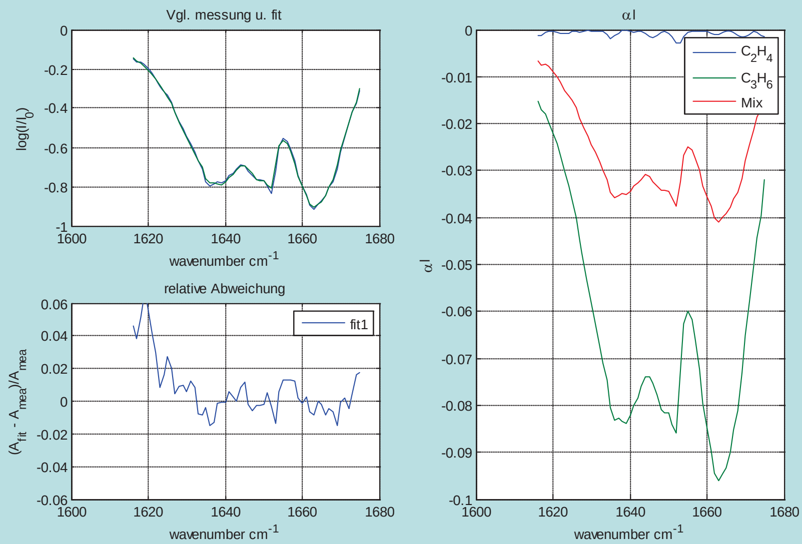

ρ_{prop} = 9.438 kg/m³

GC validation (Reference Method)

Validation of concentration with gas chromathograph

Obtained ratios:
1.51, 1.37, 1.35, 1.33

$\Rightarrow$ratio = (1.39 +- 0.08):1

IR & GC measurement agree

Reference Method is not very accurate

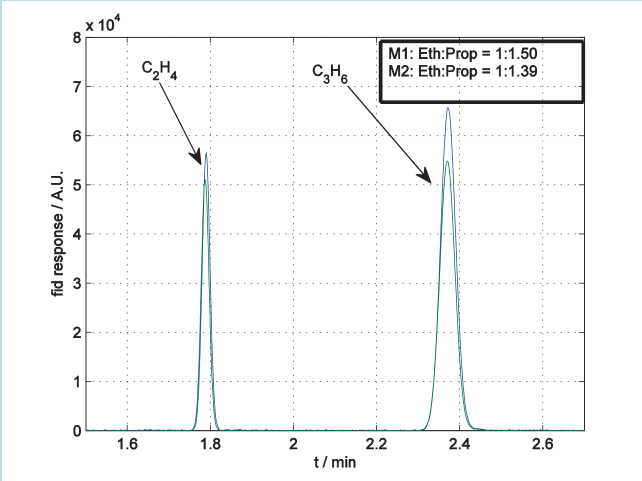

Austrian Center of Competence in Mechatronics

- 2^{nd} Mixture

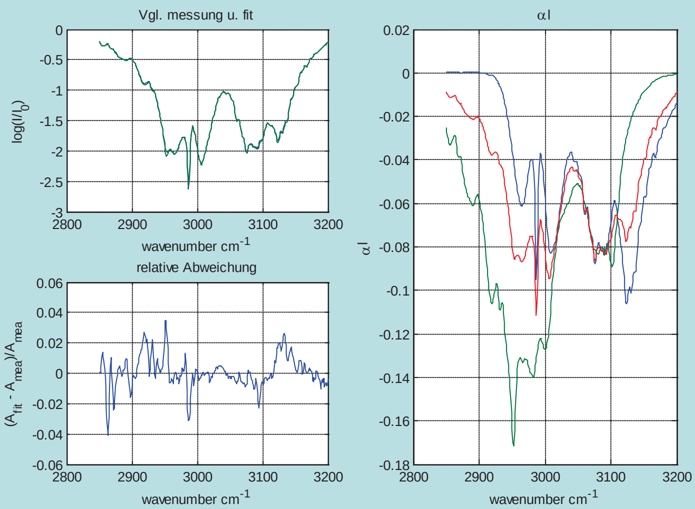

mol-ratio: 2.69:1(Ethene: Propene)
density: ρ_{eth} = 15.184 kg/m^3
ρ_{prop} = 8.479 kg/m^3

JKU JOHANNES KEPLER UNIVERSITÄT LINZ
LCM LINZ CENTER OF MECHATRONICS GMBH

- 2nd Mixture

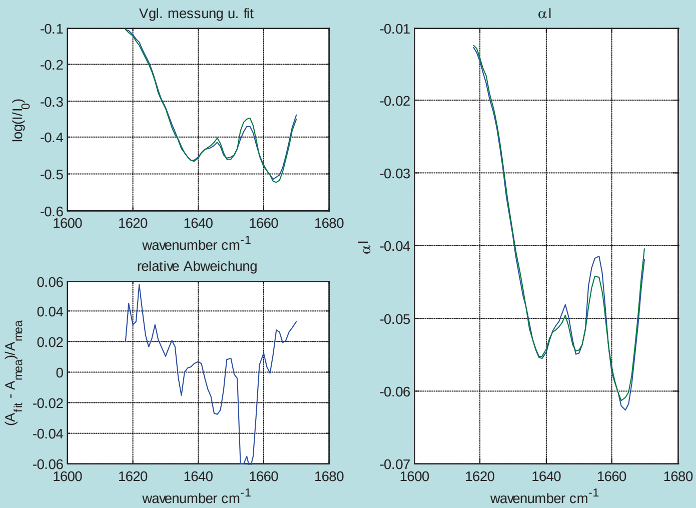

ρ_{prop} = 8.361 kg/m³

Austrian Center of Competence in Mechatronics

- GC measurement

- M1: r=3.05
- M2: r= 2.96

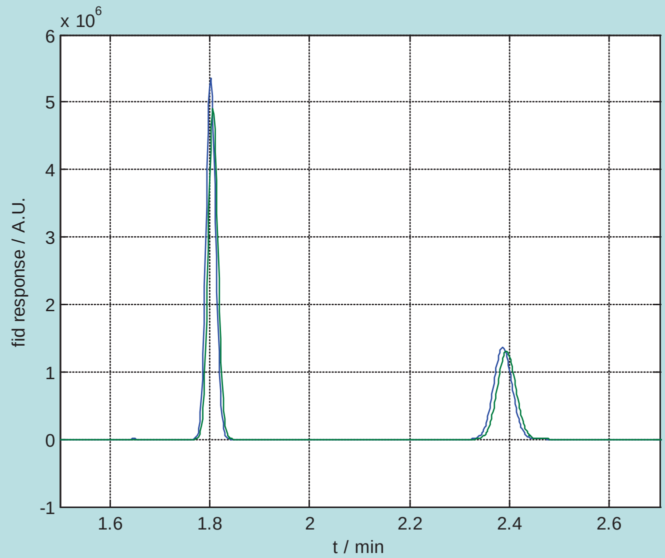

Questions

- Is GC accurate?
  - Measurement of more samples necessary for accurate value
- Is absorption coefficient proportional to total pressure? Does it depend on the partial pressures of the gas components?
  - Measurement of mixtures with exactly known concentration ratios.
  - due to limited accuracy of GC measurement many iterations are necessary
- Are specific wavenumbers suitable for concentration measurement without FTIR?
  - See above
  - PLS regression

Austrian Center of Competence in Mechatronics

Conclusion

- Density measurement with quartz tuning forks
  - continuous monitoring
  - accuracy: ~0.075 kg/m³ (~ 0.5 %)
  - Waiting for integration into polymerization reactor
- IR measurement
  - direct concentration of propene and/or ethene
  - More work needed….

JKU JOHANNES KEPLER UNIVERSITÄT LINZ LCM LINZ CENTER OF MECHATRONICS GMBH

Accelerated Statistical Inversion and Bayesian Calibration for Electrical Tomography

M. Neumayer

Institute of Electrical Measurement and Measurement Signal Processing,
Kopernikusgasse 24/4, A-8010 Graz, Graz University of Technology

30. 6. 2011

Outline

- Inverse Problems.
  - What are Inverse Problems
  - Statistical Inversion.
  - Model Errors.
- Computational methods.
  - Fast Computational Methods.
  - Approximation Techniques.
- Case Studies
  - Shape Reconstructions.
  - Gibbs Sampling.
  - Different Calibration Approaches

D. Watzenig, M. Neumayer and C. Fox 2011 *Accelerated Markov Chain Monte Carlo Sampling in Electrical Capacitance*

Inverse Problems

Determine $\boldsymbol{x}$ from

$$\tilde{\boldsymbol{d}} = P(\boldsymbol{x}) + \boldsymbol{v}, \tag{1}$$

Forward map (model) $F : \boldsymbol{x} \mapsto \boldsymbol{y}$.

$$\boldsymbol{y} = F(\boldsymbol{x}) \tag{2}$$

$$F(\boldsymbol{x}) = P(\boldsymbol{x}) \qquad \forall \boldsymbol{x}, \tag{3}$$

Where does the name come from:

$$\boldsymbol{x} = F^{-1}(\tilde{\boldsymbol{d}}), \tag{4}$$

Does not work as inverse problems are ill posed. $\rightarrow$ Use Regularization terms or Prior knowledge to stabilize $F^{-1}(\cdot)$

$$\mathscr{F}^{-1}(\tilde{\boldsymbol{d}}). \tag{5}$$

Statistical Inversion

Bayes Law:

$$\pi(\boldsymbol{x}|\tilde{\boldsymbol{d}}) = \frac{\pi(\tilde{\boldsymbol{d}}|\boldsymbol{x})\pi(\boldsymbol{x})}{\pi(\tilde{\boldsymbol{d}})} \propto \pi(\tilde{\boldsymbol{d}}|\boldsymbol{x})\pi(\boldsymbol{x}). \tag{6}$$

- The approach is applicable to any forward problem.
- No derivatives have to be computed.
- Available prior knowledge can be incorporated in a natural way.
- Information about the measurement noise can be added in the same natural way.
- The result is a probability density function. Hence, complete information about the uncertainty of the result is available.

Statistical Inversion 2

Meaningful point estimates:

$$\boldsymbol{x}_{ML} = \arg\max \pi(\tilde{\boldsymbol{d}}|\boldsymbol{x}), \tag{7}$$

$$\boldsymbol{x}_{MAP} = \arg\max \pi(\boldsymbol{x}|\tilde{\boldsymbol{d}}). \tag{8}$$

... can be formulated as optimization problem.

$$\boldsymbol{x}_{CM} = \int \boldsymbol{x}\pi(\boldsymbol{x}|\tilde{\boldsymbol{d}})d\boldsymbol{x}, \tag{9}$$

$\rightarrow$ high dimensional integral.

- Analytic solution is often not possible.
- Also not suitable for quadrature techniques.

Solution: Monte Carlo integration $\rightarrow$ support points are generated from the density itself.

Metropolis Hastings Algorithm

1. Pick the actual state $\boldsymbol{x} = \boldsymbol{X}_n$ from the Markov chain.
2. With proposal density $q(\boldsymbol{x}, \boldsymbol{x}')$ generate a new state $\boldsymbol{x}'$.
3. Compute the likelihood ratio $\alpha = \min\left[1, \frac{\pi(\boldsymbol{x}'|\tilde{\boldsymbol{d}})q(\boldsymbol{x}',\boldsymbol{x})}{\pi(\boldsymbol{x}|\tilde{\boldsymbol{d}})q(\boldsymbol{x},\boldsymbol{x}')}\right]$.
4. With probability α accept $\boldsymbol{x}'$ and $\boldsymbol{X}_{n+1} = \boldsymbol{x}'$, otherwise reject $\boldsymbol{x}'$ and set $\boldsymbol{X}_{n+1} = \boldsymbol{x}$.

- Slow as every proposal requires an evaluation of the forward map.
- Proposals can be rejected.
- Samples are highly correlated (large IACT τ_{int}).
- Problem with multi modal distributions.

Speedup possible with Delayed Acceptance MH (DAMH) algorithm ($F^*(\boldsymbol{x})$).

Gibbs Sampler

1. Pick the actual state $\boldsymbol{x} = \boldsymbol{X}_n$ from the Markov chain.
2. For every element i of the vector $\boldsymbol{x}$:
   1. Set x_i of $\boldsymbol{x}$ as independent variable, while all other elements are fixed.
   2. Calculate $\Phi_i(t) = \int_{-\infty}^{t} \pi(\boldsymbol{x}) dx_i$.
   3. Draw $u \propto \mathcal{U}([0,1])$ and set the i-th component of $\boldsymbol{x}$ as $x_i = \Phi_i^{-1}(u)$.
3. Set $\boldsymbol{X}_{n+1} = \boldsymbol{x}$.

- Every proposal is accepted.
- Evaluation of the conditional distribution is expensive.

Calibration and Model Errors

Useful approach to test the inversion algorithm

$$\mathscr{F}^{-1}(F(\boldsymbol{x}) + \boldsymbol{v}). \quad (10)$$

... is called Ïnverse Crime". Fine if everything also works directly with real data ... but sometimes it completely fails!
Reason

$$F(\boldsymbol{x}) \approx P(\boldsymbol{x}). \quad (11)$$

- Absolute imaging
- Differential imaging

Calibration of Computer Models 1

Approach:

$$P(\phi) \approx \rho F(\boldsymbol{x}) + \boldsymbol{c}. \tag{12}$$

Hyperparameter $\xi = \{\rho, \boldsymbol{c}\}$.

$$\pi(\boldsymbol{x}, \xi | \tilde{\boldsymbol{d}}, \boldsymbol{d}_c) = \pi(\tilde{\boldsymbol{d}}, \boldsymbol{d}_c | \boldsymbol{x}, \boldsymbol{x}_c, \xi) \pi(\boldsymbol{x}) \pi(\xi), \tag{13}$$

Product rule:

$$\pi(\boldsymbol{x}, \xi | \tilde{\boldsymbol{d}}, \boldsymbol{d}_c) = \pi(\boldsymbol{x} | \xi, \tilde{\boldsymbol{d}}, \boldsymbol{d}_c) \pi(\xi | \tilde{\boldsymbol{d}}, \boldsymbol{d}_c) \tag{14}$$

$\rightarrow \xi$ depends on the data!

Calibration of Computer Models 2

How to use calibration information

- Empirical Bayes: fix ξ

$$\xi = \arg \min_{\xi = \{\rho, \boldsymbol{c}\}} ||\rho F(\boldsymbol{x}_c) + \boldsymbol{c} - \boldsymbol{d}_c||_2^2 \tag{15}$$

- Mutual inference: treat also ξ as random variable.
- Bayesian Forward map:

$$\mathscr{Y} = \tilde{F}(\boldsymbol{x}) + \mathscr{D}(\cdot). \tag{16}$$

Say $\tilde{F}(\boldsymbol{x})$ is the best available forward map and build an inadequacy function $\mathscr{D}(\cdot)$ to incorporate error knowledge form calibration measurements.

Electrical Capacitance Tomography

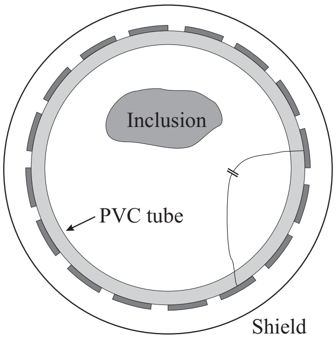

- Ω: whole domain
- Ω_{ROI}: interior of the pipe.
- $\partial\Omega_{ROI}$: interior of the pipe.

PDE:

$$\nabla \cdot (\varepsilon_0 \varepsilon_r \nabla V) = 0, \tag{17}$$

BC:

$$V_{\partial\Omega} = 0, \tag{18}$$
$$V_{\Gamma_j} = V_{\Gamma_j}, \tag{19}$$
$$V_{\Gamma_i} = 0 \quad \forall i \neq j, \tag{20}$$

Gauss law:

$$C_{i,j} = -\frac{1}{V_{\Gamma_j}} \oint_{\Gamma_i} \varepsilon_0 \varepsilon_r \nabla V_j \cdot \vec{\mathbf{n}} d\Gamma. \tag{21}$$

Gives a $N_{elec} \times N_{elec}$ matrix.

Standard Computations: $F : \varepsilon \mapsto \mathbf{C}$

Finite element system:

$$\mathbf{K} = \sum_{i=1}^{N_e} \varepsilon_i \mathbf{K}_{e,i}, \tag{22}$$

With BC:

$$\hat{\mathbf{K}} \mathbf{v} = \mathbf{r}. \tag{23}$$

Charge method:

$$Q_{elec} = \sum_{n_{elec}} (\mathbf{K}\mathbf{v})_{n_{elec}}, \tag{24}$$

Derivatives:

$$dC_{i,j} = \gamma_j^T \left[\left[\frac{\partial \mathbf{r}}{\partial \varepsilon_k} \right] - \left[\frac{\partial \hat{\mathbf{K}}}{\partial \varepsilon_k} \right] \mathbf{v}_i \right] d\varepsilon_k, \tag{25}$$

Solution with Greens Functions

PDE: $Lu = f$ solve by $u = L^{-1}f$ or $u = Gf$

- Jacobian operation $J : \varepsilon \mapsto \boldsymbol{Q}$:

$$d\boldsymbol{Q} = -\boldsymbol{G}_Q^T \hat{\boldsymbol{K}}_{d\varepsilon} \boldsymbol{G}_Q \quad (26)$$

$$d\boldsymbol{Q} = -\boldsymbol{G}_Q^T \left[\sum_l^p \boldsymbol{W}_l d\mathscr{E} \boldsymbol{W}_l^T \right] \boldsymbol{G}_Q. \quad (27)$$

- Jacobian transpose operation $J^T : \boldsymbol{Q} \mapsto \varepsilon$

$$\boldsymbol{J}^T \boldsymbol{q} = -\left(\sum_{l=1}^p \left(\boldsymbol{G}_Q^T \boldsymbol{W}_l\right)^T \otimes \left(\boldsymbol{Q}\boldsymbol{G}_Q^T \boldsymbol{W}_l\right) \right), \quad (28)$$

- Low rank updates

Neumayer and Fox 2011 Fast Forward Map Framework for Electrical Capacitance Tomography, submitted to IEEE Transactions

Low Rank Updates

How is $\boldsymbol{Q}$ effected when a low number of elements are updated?
Purpose: line search, conditional sampling
Woodburry Formula:

$$\boldsymbol{B}^{-1} = (\boldsymbol{A} + \boldsymbol{L}\boldsymbol{U})^{-1} = \boldsymbol{A}^{-1} - \underbrace{\boldsymbol{A}^{-1}\boldsymbol{L}\left(\boldsymbol{I} + \boldsymbol{U}\boldsymbol{A}^{-1}\boldsymbol{L}\right)^{-1} \boldsymbol{U}\boldsymbol{A}^{-1}}_{\text{update term}}, \quad (29)$$

How can we use this:

$$\boldsymbol{B} = \hat{\boldsymbol{K}}_{new} = \hat{\boldsymbol{K}}_{old} + \gamma \sum_{l=1}^p \boldsymbol{W}_l \Delta\mathscr{E} \boldsymbol{W}_l^T = \hat{\boldsymbol{K}}_{old} + \gamma \boldsymbol{L}\boldsymbol{U} \quad (30)$$

With $\boldsymbol{G}_Q$ to replace $\boldsymbol{A}^{-1} = \hat{\boldsymbol{K}}_{old}^{-1}$

$$\Delta\boldsymbol{Q} = -\gamma \boldsymbol{G}_Q^T \boldsymbol{L} \left(\boldsymbol{I} + \gamma \boldsymbol{U}_{:,C} \boldsymbol{G}_{C,C} \boldsymbol{L}_{C,:}\right)^{-1} \boldsymbol{U}\boldsymbol{G}_Q, \quad (31)$$

Neumayer and Fox 2011, to be published.

A Speed Comparison

Operation/Method	t_{mesh1}	t_{mesh2}
	ms	ms
Forward problem standard	96	640
Forward problem new	4.8	26
Standard material update	35.5	230
Fast material update	0.039	2
Matrix inversion	3.3	19
Jacobian by AVM	360	>2000
Jacobian op. $J : \varepsilon \mapsto \boldsymbol{Q}$	0.48	3.9
Jacobian transp. op. $J^T : \boldsymbol{Q} \mapsto \varepsilon$	3.3	15.5
Exact low rank update (1 elem.)	3.5	16.3
$\boldsymbol{wsw}^T$ Woodburry (1 elem.)	0.66	4.2
Exact low rank update (20 elem.)	11.6	55.4
$\boldsymbol{wsw}^T$ Woodburry (20 elem.)	2.7	14.1
Exact update 1 elem $\times$ 20	5.6	18
$\boldsymbol{wsw}^T$ Woodburry 1 elem $\times$ 20	1.1	3
Domain d. by Schur c.	23.8	66
Schur c. with Cho.	2.9	8
Woodb. for Schur c. with Chol.	0.895	17.1

Approximation Techniques $F^*(x)$

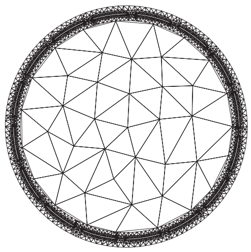

- First order approximation.

$$F(\boldsymbol{x}+\Delta\boldsymbol{x}) \approx F(\boldsymbol{x}) + \left.\frac{\partial F(\boldsymbol{x})}{\partial \boldsymbol{x}}\right|_{\boldsymbol{x}} \Delta\boldsymbol{x}, \quad (32)$$

- Polynomial approximation.

$$F(\boldsymbol{x}) \approx \boldsymbol{P}\tilde{\boldsymbol{x}}, \quad (33)$$

Adaptive version

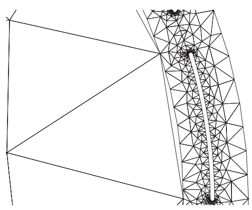

$$\boldsymbol{p}_{k+1} = \boldsymbol{p}_{k+1} + \mu(F(\boldsymbol{x}) - \boldsymbol{p}_k^T\tilde{\boldsymbol{x}})\tilde{\boldsymbol{x}}, \quad (34)$$

- Reduced physical model

Adaptive Error Learning within DAMH

How can the evaluation of $F(\cdot)$ be used:

$$\begin{aligned} \boldsymbol{e}_n &= F(\cdot) - F^*(\cdot) && (35)\\ \mu_{\boldsymbol{e},n} &= \frac{1}{n}\left((n-1)\mu_{\boldsymbol{e},n-1} + \boldsymbol{e}_n\right), && (36)\\ \boldsymbol{C}_{\boldsymbol{e},n} &= \boldsymbol{C}_{\boldsymbol{e},n-1} + \boldsymbol{e}_n\boldsymbol{e}_n^T, && (37)\\ \boldsymbol{\Sigma}_{\boldsymbol{e},n} &= \frac{1}{n-1}\left((n-1)\boldsymbol{C}_{\boldsymbol{e},n} - n\mu_{\boldsymbol{e},n}\mu_{\boldsymbol{e},n}^T\right). && (38) \end{aligned}$$

Likelihood function:

$$\pi_{\boldsymbol{x}^*}(\boldsymbol{x}|\tilde{\boldsymbol{d}}) = \exp\left\{-\frac{1}{2}\left(\boldsymbol{y}^* + \mu_{\boldsymbol{e},n} - \tilde{\boldsymbol{d}}\right)^T \left(\boldsymbol{\Sigma}_{\boldsymbol{v}} + \boldsymbol{\Sigma}_{\boldsymbol{e},n}\right)^{-1}\left(\boldsymbol{y}^* + \mu_{\boldsymbol{e},n} - \tilde{\boldsymbol{d}}\right)\right\}. \quad (39)$$

RBF Shape Model

Contour description by

$$f(\boldsymbol{z}) = \sum_{j}^{N} \lambda_i \phi(||\boldsymbol{z} - \boldsymbol{x}_j||) + P(\boldsymbol{z}), \quad (40)$$

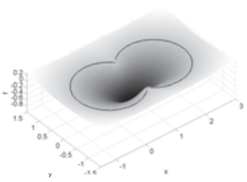

Thin plate RBF:

$$\phi(r) = r^2 \cdot \log(r), \quad (41)$$

Prior:

$$\pi(\boldsymbol{x}) = \exp\left(-\frac{1}{2\sigma_{pr}^2}\frac{c(\boldsymbol{x})}{\sqrt{\pi\Gamma(\boldsymbol{x})}}\right) I(\boldsymbol{x}), \quad (42)$$

Moves:

(a) Translation. (b) Rotation. (c) Scale. (d) Corner move.

Some DAMH Results

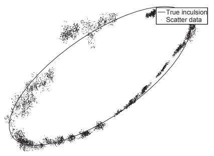

(e) Standard MH, $\varepsilon_r = 3.5$.

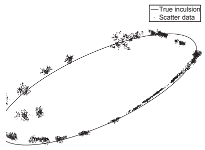

(f) Jacobian, $\varepsilon_r = 3.5$

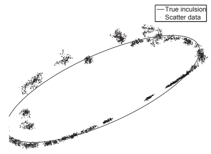

(g) Affine map, $\varepsilon_r = 3.5$.

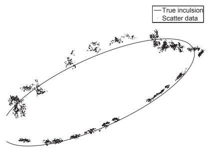

(h) Adapt. affine map, $\varepsilon_r = 3.5$.

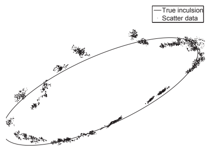

(i) Red. model, $\varepsilon_r = 3.5$.

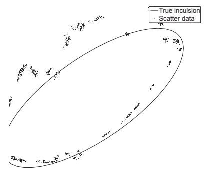

(j) Standard MH, $\varepsilon_r = 80$.

Gibbs Sampler for ECT

$$\pi(\boldsymbol{x}|\tilde{\boldsymbol{d}}) \propto \exp\left(-\frac{1}{2}\boldsymbol{e}^T\boldsymbol{\Sigma}_v^{-1}\boldsymbol{e}\right)\exp\left(-\frac{1}{2}\alpha\boldsymbol{x}^T\boldsymbol{L}^T\boldsymbol{L}\boldsymbol{x}\right) I(\boldsymbol{x}) \qquad (43)$$

- Bimodal Distributions
- Arbitrary Distributions: requires some support points of the conditional distribution.

→ low rank updates mandatory for efficient sampling.

IACT: $\tau_{int} = 1$!

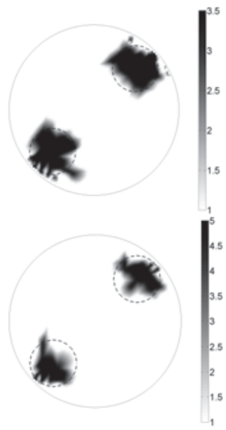

Neumayer and Fox 2011 to be published

Incorporation of Calibration Information

Observations:

- Low level representations cover most calibration effects.
- Shape determination suffers for inclusions with high permittivities.

How to find a better set of calibration parameters ξ?

Or is there another way to incorporate calibration information?

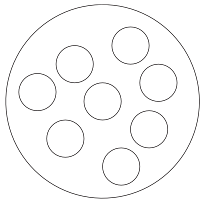

Mutual Inference Approaches

$$\pi(\tilde{\boldsymbol{d}}, \boldsymbol{d}_c^{(N)} | \boldsymbol{x}, \xi, \boldsymbol{x}_c^{(N)}) \propto \exp\left\{-\frac{1}{2}\left(\rho \boldsymbol{y} + \boldsymbol{c} - \tilde{\boldsymbol{d}}\right)^T \boldsymbol{\Sigma}_v^{-1}\left(\rho \boldsymbol{y} + \boldsymbol{c} - \tilde{\boldsymbol{d}}\right) - \frac{1}{2}\sum_{i=1}^{N_c}\left(\rho \boldsymbol{y}_{c,i} + \boldsymbol{c} - \boldsymbol{d}_{c,i}\right)^T \boldsymbol{\Sigma}_c^{-1}\left(\rho \boldsymbol{y}_{c,i} + \boldsymbol{c} - \boldsymbol{d}_{c,i}\right)\right\}. \tag{44}$$

Implementation: sample from ξ with a Gibbs sampler.

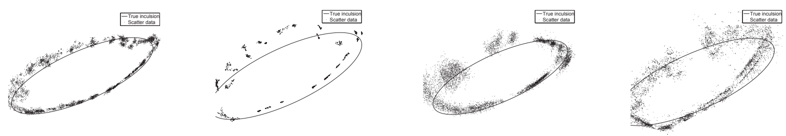

(k) $\varepsilon_r = 3.5$. (l) $\varepsilon_r = 80$. (m) $\varepsilon_r = 3.5$. (n) $\varepsilon_r = 80$.

Decreased IACT but the gain in quality is comparatively low.

Bayesian Forward Map

Use calibration measurements to build

$$\mathscr{Y} = \tilde{F}(\boldsymbol{x}) + \mathscr{G}\mathscr{P}_{\mathscr{D}_e}(\cdot). \quad (45)$$

$$\begin{bmatrix} \boldsymbol{e}_c \\ \boldsymbol{e} \end{bmatrix} = \mathscr{N}\left(\boldsymbol{0}, \begin{bmatrix} \boldsymbol{\Sigma}(\boldsymbol{x}_{c,r}, \boldsymbol{x}_{c,r}) & \boldsymbol{\Sigma}(\boldsymbol{x}_{c,r}, \boldsymbol{x}_r) \\ \boldsymbol{\Sigma}(\boldsymbol{x}_r, \boldsymbol{x}_{c,r}) & \boldsymbol{\Sigma}(\boldsymbol{x}_r, \boldsymbol{x}_r) \end{bmatrix}\right), \quad (46)$$

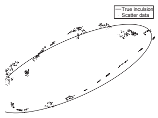

(o) No Bayesian Forward Map (Extreme high IACT).

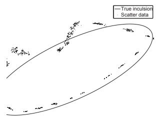

(p) With Bayesian Forward Map (Low IACT).

Neumayer and Fox 2011 to be published

Institute of Electrical Measurement and Measurement Signal Processing
www.emt.tugraz.at

Thank you for your attention!

Yet another precision impedance analyzer

Readout electronics for resonating sensors

Alexander O. Niedermayer

Institute for Microelectronics and Microsensors,
Johannes Kepler University, Linz

Institute for Microelectronics and Microsensors

ACCM

JKU JOHANNES KEPLER UNIVERSITY LINZ

Modeling

penetration depth $\delta = \sqrt{\frac{2\eta}{\rho\omega}}$

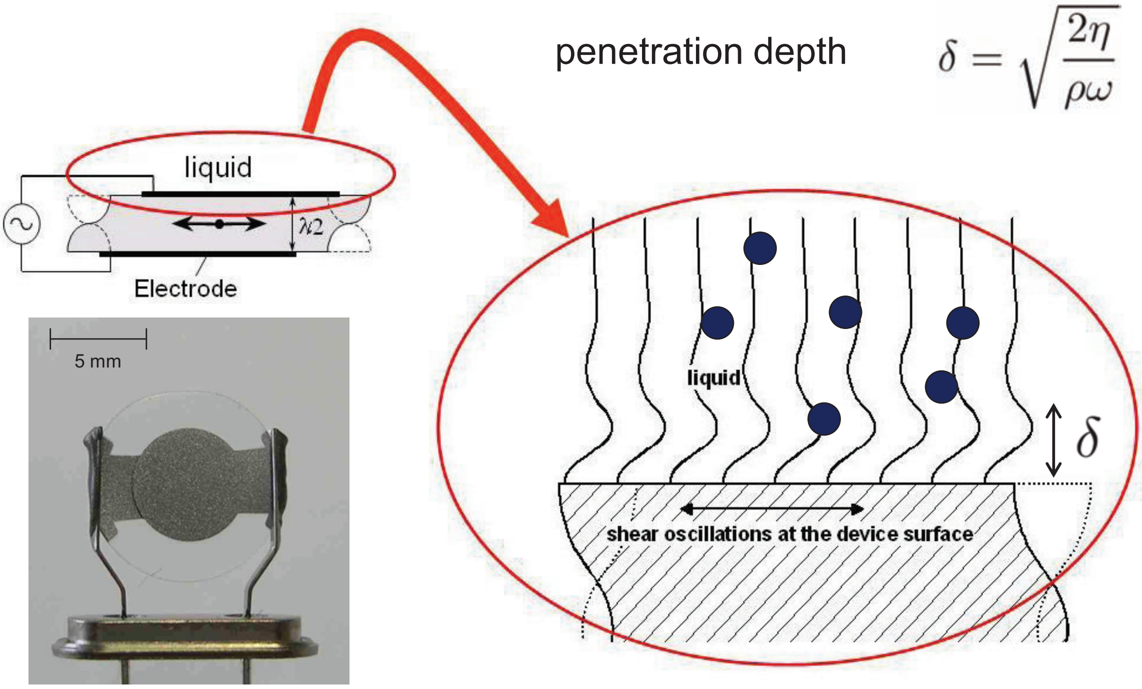

Institute for Microelectronics and Microsensors

ACCM

JKU JOHANNES KEPLER UNIVERSITY LINZ

Modeling

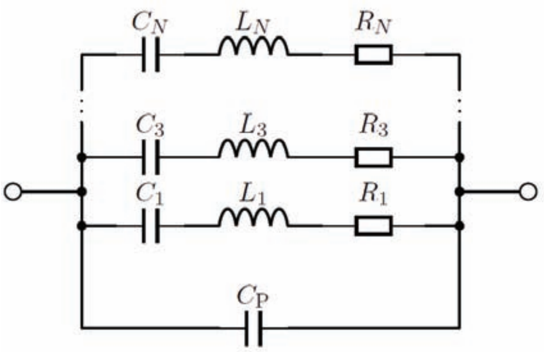

motional branch resistance
of harmonic number N:

sensor admittance

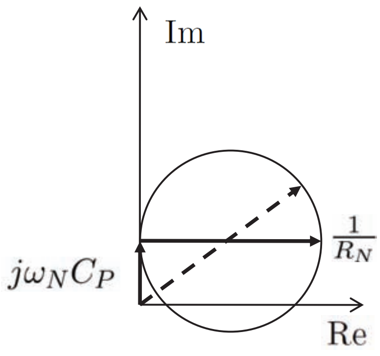

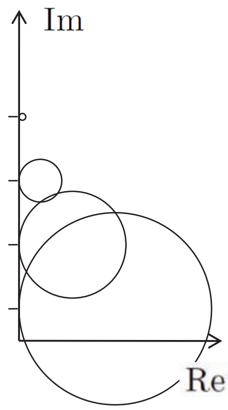

$$R_N = R_{N1} + R_{N2} = R_{11} \cdot N^2 + R_{12} \cdot N$$

unloaded resonator (R_{N1}) — viscous loading (R_{N2})

[S. Martin '94]

Circuit Concept

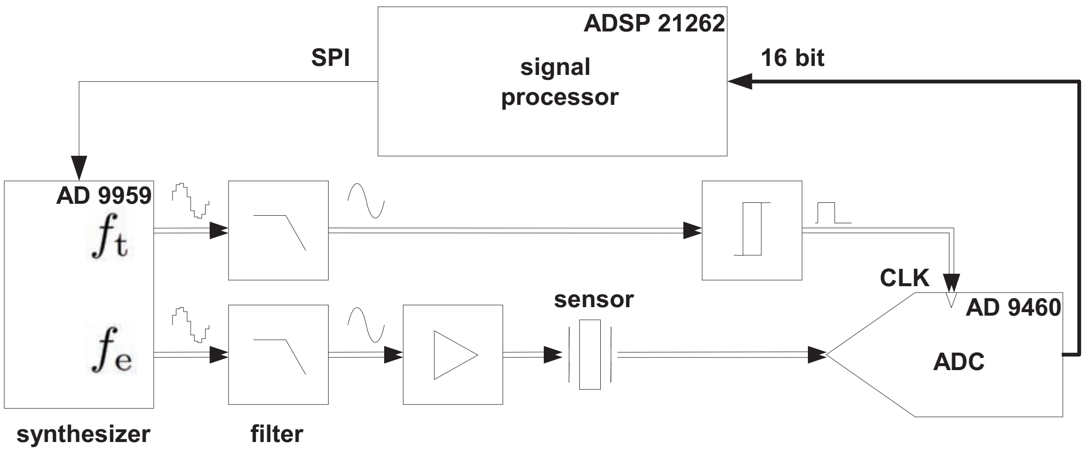

Synchronous subsampling

$$f_t = f_e \cdot \frac{n}{n-m}$$

n samples per m periods

Demodulation

$$Y(f) = \sum_{k=0}^{N-1} \left(x[k] \cdot \cos\left(\frac{2\pi f\ k}{N}\right) + j\ x[k] \cdot \sin\left(\frac{2\pi f\ k}{N}\right) \right)$$

Synchronous sampling

$$f_{\mathrm{t}} = f_{\mathrm{e}} \cdot \frac{n}{n-m}$$

n samples per m periods

Goertzel Algorithm

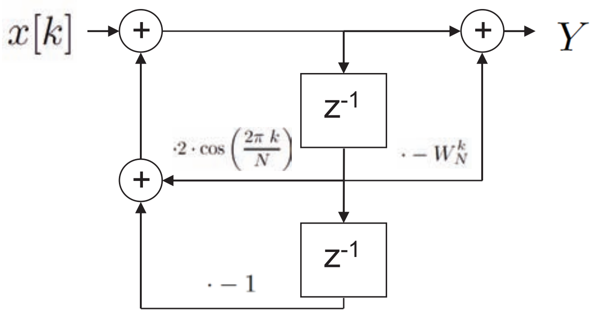

Sensor admittance

AT-cut QCR, f_1 = 1.8432 MHz, N=3, in Isopropanol

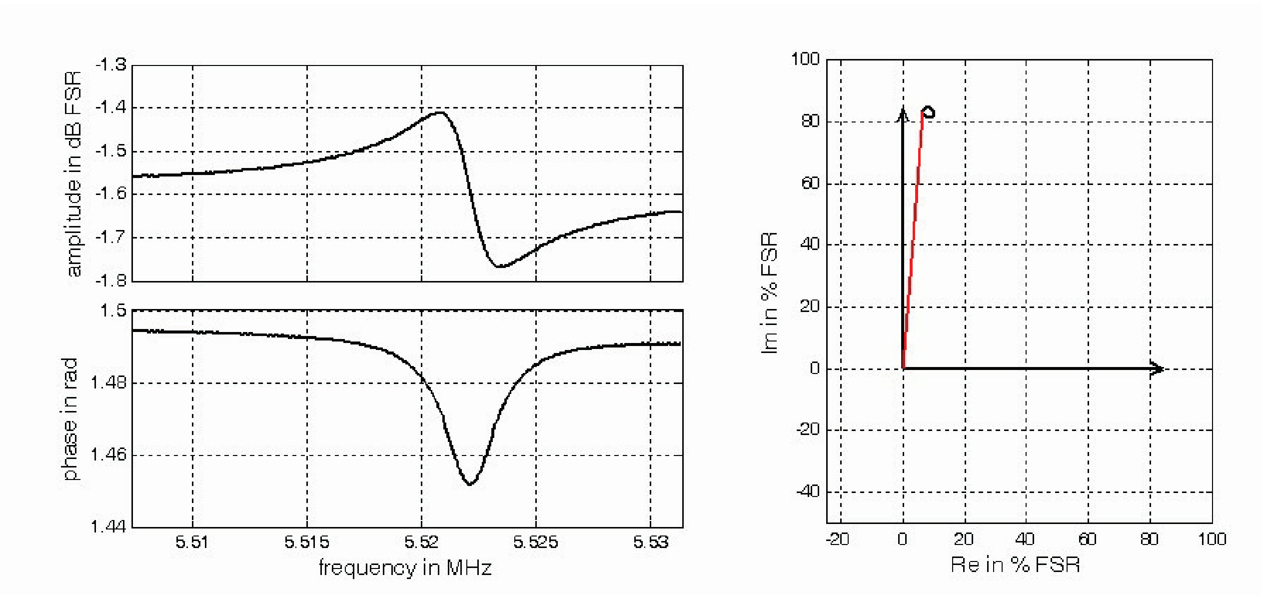

Institute for Microelectronics and Microsensors
ACCM
JKU JOHANNES KEPLER UNIVERSITY LINZ

Circuit Concept

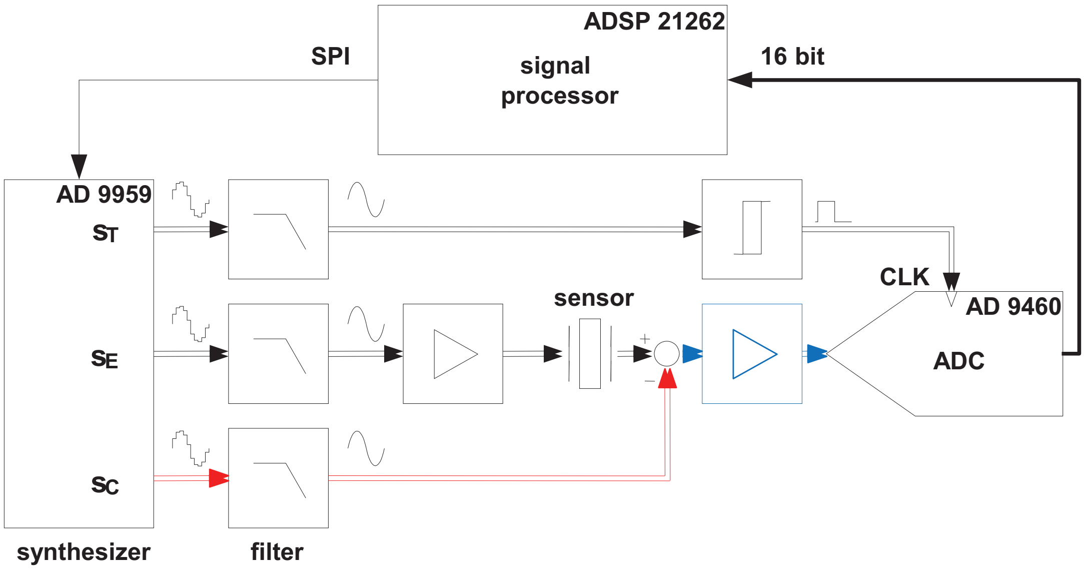

Sensor admittance

AT-cut QCR, f_1 = 1.8432 MHz, N=3, in Isopropanol, t = 12 s

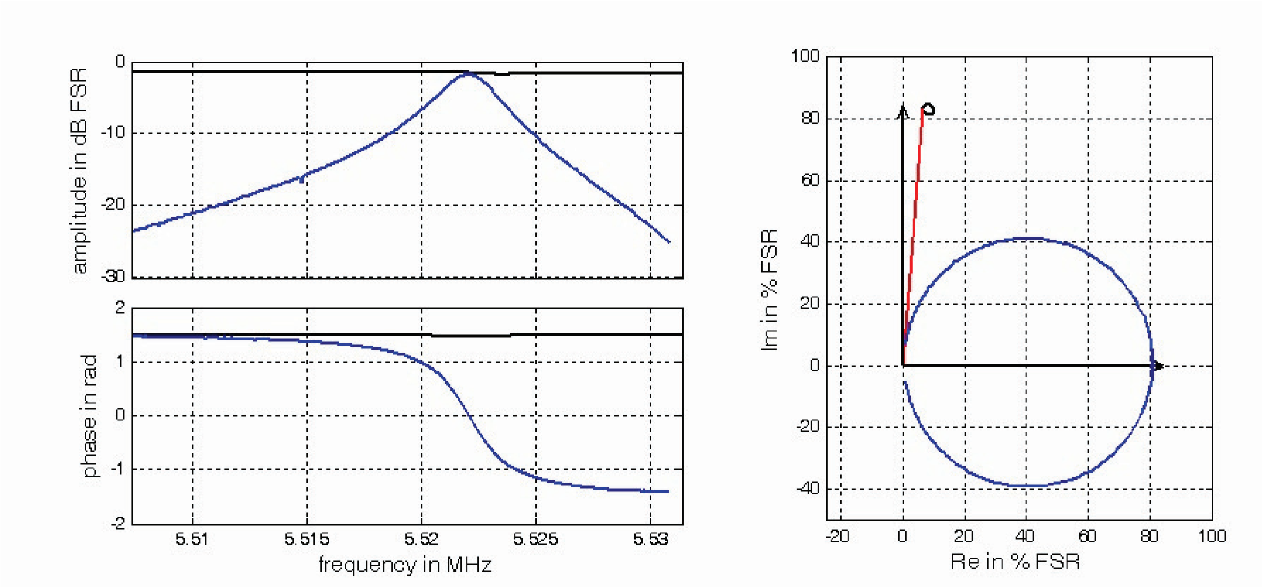

Institute for
Microelectronics and
Microsensors
ACCM
JKU
JOHANNES KEPLER UNIVERSITY LINZ

Applying compensation signal

AT-cut QCR, f_1 = 1.8432 MHz, N=3, in Isopropanol, t = 12 s

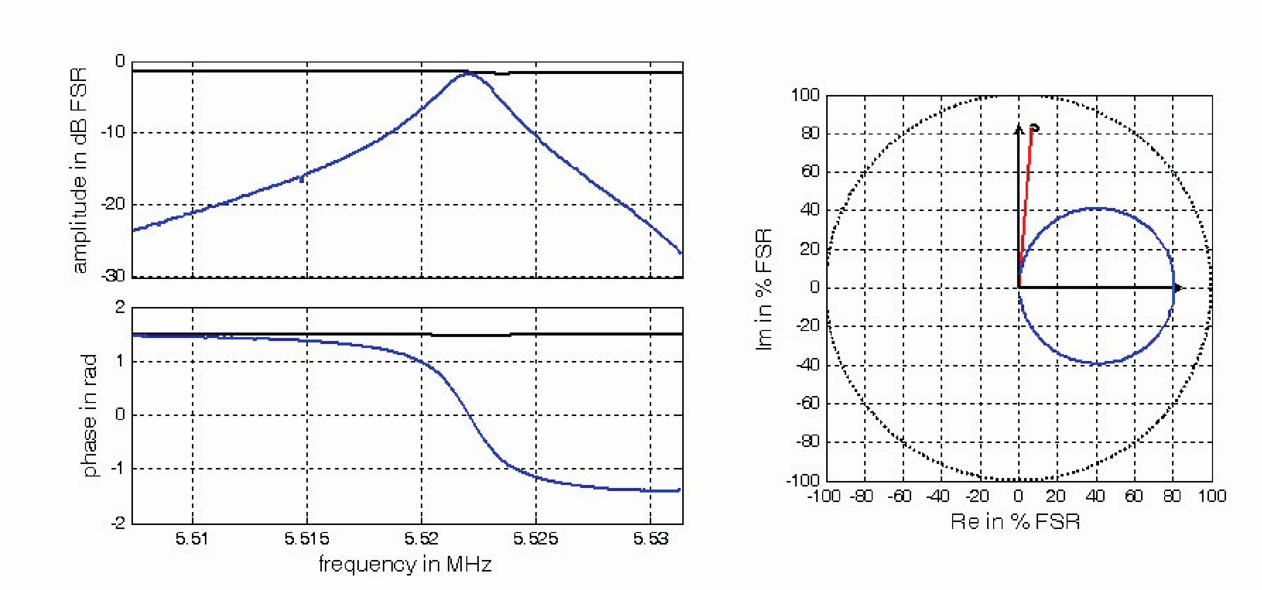

Conclusion

- phase resolution is very important
- wide frequency range (subsampling)
- handle higher harmonics
- various types of resonating sensors
- very compact design

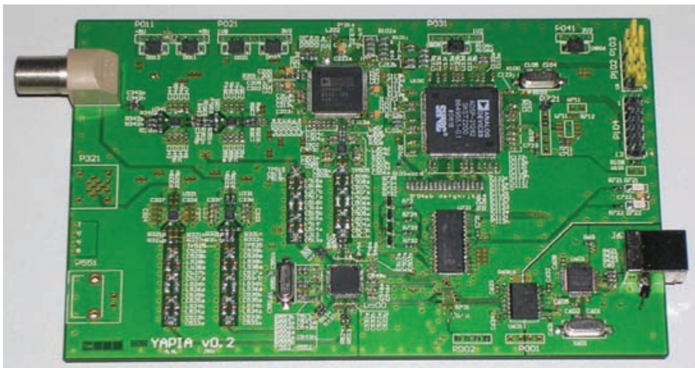

Institute for
Microelectronics and
Microsensors
ACCM
JKU
JOHANNES KEPLER
UNIVERSITY LINZ